

University of Windsor

## Scholarship at UWindor

---

Electronic Theses and Dissertations

Theses, Dissertations, and Major Papers

---

2013

# Automated Classification of Medical Percussion Signals for the Diagnosis of Pulmonary Injuries

Bhuiyan Md Moinuddin  
*University of Windsor*

Follow this and additional works at: <https://scholar.uwindsor.ca/etd>

---

### Recommended Citation

Md Moinuddin, Bhuiyan, "Automated Classification of Medical Percussion Signals for the Diagnosis of Pulmonary Injuries" (2013). *Electronic Theses and Dissertations*. 4941.  
<https://scholar.uwindsor.ca/etd/4941>

This online database contains the full-text of PhD dissertations and Masters' theses of University of Windsor students from 1954 forward. These documents are made available for personal study and research purposes only, in accordance with the Canadian Copyright Act and the Creative Commons license—CC BY-NC-ND (Attribution, Non-Commercial, No Derivative Works). Under this license, works must always be attributed to the copyright holder (original author), cannot be used for any commercial purposes, and may not be altered. Any other use would require the permission of the copyright holder. Students may inquire about withdrawing their dissertation and/or thesis from this database. For additional inquiries, please contact the repository administrator via email ([scholarship@uwindsor.ca](mailto:scholarship@uwindsor.ca)) or by telephone at 519-253-3000ext. 3208.

# Automated Classification of Medical Percussion Signals for the Diagnosis of Pulmonary Injuries

By

Md Moinuddin Bhuiyan

A Dissertation

Submitted to the Faculty of Graduate Studies through  
the Department of Electrical and Computer Engineering  
in Partial Fulfillment of the Requirements for  
the Degree of Doctor of Philosophy at the  
University of Windsor

Windsor, Ontario, Canada

2013

© 2013, Md Moinuddin Bhuiyan

All Rights Reserved. No part of this document may be reproduced, stored or otherwise retained in a retrieval system or transmitted in any form, on any medium by any means without prior written permission of the author.

Automated Classification of Medical Percussion Signals for the Diagnosis of  
Pulmonary Injuries

By

Md Moinddin Bhuiyan

Approved By:

---

Dr. J. Saniie, External examiner  
Illinois Institute of Technology, USA

---

Dr. W. Kedzierski  
Department of Physics

---

Dr. M. Ahmadi  
Department of Electrical and Computer Engineering

---

Dr. Mitra Mirhassani  
Department of Electrical and Computer Engineering

---

Dr. Roman Gr. Maev, Advisor  
Department of Electrical and Computer Engineering, Physics

August 22, 2013

---

## Declaration of Co-Authorship / Previous Publication

---

### 1. Co-Authorship Declaration

I hereby declare that this thesis incorporates material that is result of joint research with Professor Dr. Roman Gr. Maev, Malyarenko E V, Pantea M A, and Baylor A. E. I am aware of the University of Windsor Senate Policy on Authorship and I certify that I have properly acknowledged the contribution of other researchers to my thesis, and have obtained written permission from each of the co-author(s) to include the above material(s) in my thesis. In all cases, the key ideas, primary contributions, experimental designs, data analysis, and interpretation were performed by the author, and contribution of the co-authors was primarily through the provision of data collection, formatting and display.

I certify that this thesis, and the research to which it refers, is the product of my own work.

### 2. Declaration of Previous Publication

This thesis includes four original papers that have been previously published/submitted for publication in peer reviewed journals and conferences, as follows:

Thesis Chapter	Publication title/full citation	Publication status*
Chapter 6,9	Bhuiyan M, Malyarenko E V, Pantea M A, Maev R G, Baylor A E." Estimating the parameters of audible clinical percussion signals by fitting exponentially damped harmonics" Journal of Acoustical Society of America (JASA), J Acoust Soc Am. 2012 Jun;131(6):4690-8. doi: 10.1121/1.4712018.	Published

Chapter 4, 7	M. Bhuiyan, E.V. Malyarenko, M. A. Pantea, F. Seviaryn, and R. Gr. Maev, "Advantages and limitations of using Matrix Pencil Method for the modal analysis of medical percussion signals," IEEE Trans Biomed Eng. Vol.60(2), pp. 417-26, 2013.	Published
Chapter 8	Bhuiyan M, Malyarenko, E.V. ; Pantea, M.A. ; Seviaryn, F.M. ; Maev, R.G. "Time-Frequency analysis of clinical percussion signals using Matrix Pencil Method" submitted to Med Eng. and physics.-ELSEVIER	Submitted
Chapter 8	Bhuiyan M, Malyrenko E, Pantea M and Roman Maev" Time-frequency analysis of multi-component, non-stationary signals using matrix pencil method" 11 <sup>th</sup> International Conference of Upcoming Engineers 2012 (ICUE'12), IEEE Toronto Chapter Ryerson University, Toronto, ON, Canada	Published

I certify that I have obtained a written permission from the copyright owner(s) to include the above-published material(s) in my thesis. I certify that the above material describes work completed during my registration as graduate student at the University of Windsor.

I declare that, to the best of my knowledge, my thesis does not infringe upon anyone's copyright nor violate any proprietary rights and that any ideas, techniques or any other material from the work of other people included in my dissertation, published or otherwise, are fully acknowledged in accordance with the standard referencing practices.

Furthermore, to the extent that I have included copyrighted material that surpasses the bounds of fair dealing within the meaning of the Canada Copyright Act, I certify that I have obtained a written permission from the copyright owner(s) to include such material(s) in my thesis.

I declare that this is a true copy of my thesis, including any final revisions, as approved by my thesis committee and the Graduate Studies office, and that this thesis has not been submitted for a higher degree to any other University or Institution.

## ABSTRACT

---

Used for centuries in the clinical practice, audible percussion is a method of eliciting sounds by areas of the human body either by finger tips or by a percussion hammer. Despite its advantages, pulmonary diagnostics by percussion is still highly subjective, depends on the physician's skills, and requires quiet surroundings. Automation of this well-established technique could help amplify its existing merits while removing the above drawbacks. In this study, an attempt is made to automatically decompose clinical percussion signals into a sum of Exponentially Damped Sinusoids (EDS) using Matrix Pencil Method, which in this case form a more natural basis than Fourier harmonics and thus allow for a more robust representation of the signal in the parametric space. It is found that some EDS represent transient oscillation modes of the thorax/abdomen excited by the percussion event, while others are associated with the noise. It is demonstrated that relatively few EDS are usually enough to accurately reconstruct the original signal. It is shown that combining the frequency and damping parameters of these most significant EDS allows for efficient classification of percussion signals into the two main types historically known as "resonant" and "tympanic". This classification ability can provide a basis for the automated objective diagnostics of various pulmonary pathologies including pneumothorax.

## **Dedicated to**

I would like to dedicate this Doctoral dissertation to my late father, who inspired me to reach this goal.

Mom, you did scarifies so many years without seeing me, thank you for your love, support and encouragements

To my wife and my son, without whom I would most certainly be lost, thank you.

## ACKNOWLEDGEMENTS

---

I would like to express my sincere appreciation to Professor Dr. Roman Maev, my advisor, for his excellent guidance and invaluable support, which helped me accomplish the doctorate degree and prepared me to achieve more life goals in the future. His total support of my dissertation and countless contributions to my technical and professional development made for a truly enjoyable and fruitful experience. Special thanks are dedicated for the discussions we had on almost every working day during my research period and for reviewing my dissertation. I would also like to thank Dr. Eugene Malyarenko, Research Scientist at Tessonics Corp, for his invaluable guidance and involvement throughout the course of this research. I am also grateful to Dr. Mircea Pantea, who helped me in various stage of my research work. I consider it is an honour to work with them. My work would also not have been possible without the assistance of the rest of the pulmonary project group.

I would also like to acknowledge my fellow colleagues for the wealth of knowledge they shared, particularly Jeff Sadler for his expertise in MATLAB programming, Ms. Sarah Beneteau for assistance proof reading and administrative issues, and Ms Sabina for her help to get schedule on time with my supervisor.

I would also like to extend a very special thanks to my committee, Dr. Majid Ahmadi, Dr. Mitra Mirhassani, Dr. Wladislaw Kedzierski and Dr. Jafar Saniie for their feedback during my seminars and in the process of writing this dissertation.

The author also expresses sincere gratitude to the personnel of Tessonics Corp., the Institute for Diagnostic Imaging Research, the Detroit Medical Center, and Departments of

Electrical & Computer Engineering and Physics at the University of Windsor. The authors also thank Dr. Alfred Baylor, Detroit Medical Center, for his methodological advises.

My deepest gratitude goes to my wonderful family for their encouragement, support and providing a loving environment throughout my life. Finally, and most important, I cannot find words to express my gratitude to my wife and my son. Without their encouragement, sacrifice, and compassion I would not have finished the degree.

# Contents

Declaration of Co-Authorship / Previous Publication	iv	
Abstract	vii	
Dedication	viii	
Acknowledgements	ix	
List of Tables	xvii	
List of Figures	xviii	
List of Abbreviations	xxiii	
Chapter 1	Medical Percussion	1
1.1	Introduction	1
1.2	Historical background	2
1.3	Acoustical properties of human body	5
1.4	Percussion sound & clinical significance	6
1.4.1	Percussion sounds	7
1.4.2	Clinical significance	8
1.5	The physics of percussion	8
1.6	Thesis study outline	10
1.6.1	Research motivation and hypothesis	10
1.6.2	Goals and Objectives	11
1.6.2.1	Portable Pulmonary Injury Diagnostic Device(PPIDD) concept	11
1.6.2.2	Pneumothorax condition	11

	1.6.3 Medical percussion for detecting Pneumothorax condition	13
	1.7 Review of percussion signals analysis literature.	13
	1.7.1 Clinical percussion signals recordings	13
	1.7.2 Properties of the clinical percussion signals.	15
	1.7.3 Research review on medical percussion signals.	15
	1.8. Thesis organization and contribution	19
	1.9 Summary	22
Chapter 2	Materials and mathematical model of the clinical percussion signals	23
	2.1 .Signal collection procedures	23
	2.2.Clinical percussion signal collection challenges	26
	2.3. The proposed model for the clinical percussion signals	27
	2.4. Summary	29
Chapter 3	Primary research focus	31
	3.1 Cross correlation	31
	3.1.1 Maximum frequency correlation	33
	3.1.2 Minimum damping correlation	34
	3.1.3 Verification of damping and frequency value measured using cross-correlation procedure	36
	3.1.4 Tympanic signal reconstruction	39
	3.2 Hilbert transform	40
	3.2.1 Analytic signal	40
	3.2.2. Damping value calculation using signal envelope	41
	3.3 Summary	43

Chapter 4	Analysis of noise in clinical percussion signals	45
	4.1 Introduction	45
	4.2 Noise in clinical percussion signals	46
	4.2.1 Noise spectrum of clinical percussion signal	47
	4.3 Signal preparation	49
	4.4 Noise cancellation procedures	51
	4.4.1 Signal conditioning	51
	4.5. Configure decimation filter	52
	4.6 Percussion signal noise cancellation technique using Singular Value Decomposition (SVD).	56
	4.6.1 Introduction	56
	4.6.2 SVD background	57
	4.6.3 Square Hankel matrix issue	58
	4.6.4 Reduced rank approximation	58
	4.6.5 SVD Theory	59
	4.6.6 Threshold value	61
	4.6.7 Experimental analysis of threshold value	63
	4.6.7.1 Synthetic signal	63
	4.6.7.2 SVD operation on medical percussion signals	67
	4.6.8. Percussion signal SNR measurement	69
	4.6.9 Singular values energy distribution	70
	4.7 Summary	71
Chapter 5	Matrix Pencil Method	73

	5.1 Introduction	73
	5.2 Matrix Pencil Method theory	75
	5.3 Summary	81
Chapter 6	Estimating the parameters of clinical percussion signals	82
	6.1 Introduction	82
	6.2 Clinical percussion signals decomposition using matrix Pencil method	83
	6.3 Decomposition results and analysis	85
	6.4 Reconstruction analysis	94
	6.4.1 Reconstruction error analysis	96
	6.4.1.1 Theory	96
	6.4.1.2 Reconstruction performance analysis	98
	6.5 Summary	100
Chapter 7	Super-resolution Modal analysis of medical percussion signals	102
	7.1 Introduction	102
	7.2 Drawbacks of Fourier spectral analysis	103
	7.3 Super resolution spectral analysis	105
	7.4 Results and analysis	106
	7.4.1 Comparison of the spectral and MPM analysis using a simulated signal	106
	7.4.2 Comparison of the MPM and DFT analysis of clinical percussion signals.	109
	7.4.3 Analysis of the fine structure of the spectral peaks	112

	7.5 Summary	119
Chapter 8	Time-frequency analysis of medical percussion signals	121
	8.1 Introduction	121
	8.2 Motivation for Time-frequency analysis of Medical Percussion signal	122
	8.2.1 Inherent Causes	122
	8.2.2 Methodological causes	123
	8.3 Review of existing TFDs	124
	8.4 Proposed TFD Techniques	125
	8.5 Proposed TFDs	127
	8.5.1 First approach: MPMWV distribution	127
	8.5.1.1 MPMWV distribution performance analysis	129
	8.5.2 Second approach: MPM based TFD	133
	8.5.2.1 performance analysis	134
	8.6. MPM TFR of Medical percussion signals	135
	8.7 Using MPM TFR to detect changes in physical condition	141
	8.8 Summary	143
Chapter 9	Medical Percussion Signals Classification and Recognition	145
	9.1 Introduction	145
	9.2 Minimum number of pole modeling techniques	146
	9.2.1 Medical percussion signals classification.	150
	9.3 Medical Percussion signal classification based on Quality factor (Q factor)	153

	9.4 Classification based on Dominant frequency	156
	9.5 Summary	158
Chapter 10	Conclusions and contributions	160
	10.1 Conclusions	160
	10.2 Contributions	166
	Bibliography	167
	Vita Auctoris	180

## List of Tables

Table1.1 Classification of percussion sounds by several sources	7
Table 3.1: Simulated signal parameters	33
Table 3.2: Simulated signal parameters	35
Table4.1 Decimator filter [H (z)] design data	54
Table 4.2 EDS simulated signal parameters	63
Table 4.3 Simulated signal SVD values and identifying threshold criteria.	64
Table 5.1: Signal and noise subspaces	80
Table-6.1 MPM decomposition results for the resonant signal from Figure 6.1.a	85
Table-6.2 MPM decomposition results for the tympanic signal from Figure 1.b	86
Table 7.1: Parameters of six EDS in the simulated signal	107
Table 7.2: Frequency and $\frac{A}{a}$ values for 10 strongest EDS found in percussion signals shown in Fig. 1(a, b)	110
Table 7.3: Five most significant EDS produced by the MPM for the chest signals acquired before and after carbonated drink consumption	118
Table 8.1 Parameters of 6 EDS in the simulated signal	134
Table 8.2 parameters of all EDS extracted by MPM from resonant signal	137
Table 8.3 parameters of all EDS extracted by MPM from resonant signal	137
Table 9.1 Percussion signals poles	147

# List of Figures

Figure 1.1: Medical percussion technique	1
Figure 1.2 Medical Percussion technique using neurological hammer and pleximeter	4
Figure 1.3 Percussion resonance and dullness of posterior regions (Piorry) (b) Showing areas of percussion resonance and dullness of front of the chest (Piorry)[7]	6
Figure 1.4 (a) Pneumothorax condition. [12] (b) Transverse sections of the chest in normal	12
Figure 1.5 Sound pressure waveforms for three main types of percussion signals	14
Figure 2.1 Percussion points location. Twelve percussion points used during the healthy volunteer study are marked with black circle.	24
Figure 2.2 Medical percussion signals	25
Figure 3.1 Maximum frequency correlation searching algorithm	34
Figure 3.2 Algorithm for minimum correlated damping factor	35
Figure 3.3 Tympanic signal spectrum	37
Figure 3.4 Optimal cross-correlated frequency and dominant frequency from the spectral analysis. The grey bar is for the frequency from spectrum analysis and dark bar for the analysis.	37
Figure 3.5 Tympanic signal damping values measured by cross correlation and Hilbert transform.	38

Figure 3.6 Reconstructed tympanic signal and original tympanic	39
Figure 3.7 Block diagram of Hilbert transform envelope creation and damping calculation	42
Figure 3.8 Envelope of a percussion signal (Tympanic)	42
Figure 3.9 Tympanic signal-damping values	43
Figure 4.1. Amplitude spectrum of a resonant signal before and after subtracting the noise spectrum, which is shown as well.	48
Figure 4.2 Signal preparation flow diagram	50
Figure 4.3 Percussion signals conditioning steps	52
Figure 4.4 Multi-rate processing of percussion signals	53
Figure 4.5 Percussion signals before and after conditioning	55
Figure 4.6 Flow diagram of SVD based threshold technique to separate noise space and the signal space.	62
Figure 4.7 Synthesis signal	64
Figure 4.8 Threshold value plot after SVD operation on simulated noisy signal	65
Figure 4.9 Energy calculation of different singular values	66
Figure 4.10 Percussion signal singular value plot	67
Figure 4.11 threshold value indications after SVD	68
Figure 4.12 Medical Percussion signals SNR	70
Figure 4.13 Energy distributions between different singular values in clinical percussion signals	71
Figure 6.1: Two examples of audible percussion signals collected from healthy volunteers: (a) – signal collected over the left subclavicular area (“resonant”	84

character); (b) – signal collected over the left abdominal area (“tympanic” character)

Figure 6.2 Resonant signal EDSs	88
Figure 6.3 Tympanic Signal EDS	89
Figure 6.4 Reconstruction of medical Percussion signals (a)resonant and (b)Tympanic signal	93
Figure6.5 (a): Reconstruction of the original resonant signal from the increasing number of EDS components sorted by the amplitude	95
Figure 6. 5 (b) Reconstruction of the original tympanic signal from the increasing number of EDS components sorted by the amplitude	95
Figure 6.6 Reconstruction performance analyses for Resonant and Tympanic signals	99
Figure 7.1 Examples of clinical percussion signals from (a) chest and (b) abdomen.	105
Fig. 7.2 Simulated signal waveform (no noise case)	107
Fig. 7.3 Discrete-Discrete-Fourier Transform and Matrix Pencil Method spectra of the simulated signal shown in Fig. 7.2 (rescaled)	108
Fig.7.4a Spectrum of the resonant percussion signal shown in Fig.7. 1.a. Normalized EDS are shown as well to illustrate matching	111
Fig.7.4 b Spectrum of the tympanic percussion signal shown in Fig. 7.1.b. Normalized EDS are shown as well to illustrate matching.	111
Fig.7.5.a. Frequency histogram of the spectral peaks of the upper chest signals from 30 volunteers using the DFT method (the frequency bin was set to 5 Hz).	114
Fig.7.5b. Frequency histogram of the main EDS for the upper chest signals from 30	114

volunteers decomposed by the MPM [the frequency bin was set to 5 Hz]	
Fig.7.6 EDS frequencies of chest (white), right abdominal (black) and stomach (hatched) percussion signals from 30 volunteers (for some volunteers the data were taken more than once)	116
Fig.7.7. Frequency spectrum of the percussion signals for the subject with no gas in the abdominal cavity. (Black squares – chest, open circles – stomach, black triangles – abdomen)	117
Fig.7.8. Frequency spectrum of the percussion signals from the subject with gas in the abdominal cavity. (black squares – chest, open triangles – abdomen).	117
Figure 8.1 MPMWV algorithm diagram	127
Figure 8.2 (a) Simulated signal generated by adding four exponentially damped sinusoidal (b) Spectrum of the simulated signal	129
Figure 8.3 Time-frequency representation of the simulated multicomponent signal by (a) WVD (c) CWD (c) MAPWV .	131
Figure 8.4 MPMWV TFD's for two close frequencies	133
Figure 8.5 Time-frequency representation of noise free analytical signal based on MPM	134
Figure 8.6 Medical Percussion signals (a) Resonant (left) (b) Tympanic (right) and their Spectrums	135
Figure 8.7 : Time frequency representation of medical percussion signals based on (a) WVD (b) CWD (C) MPM TFR	138
Figure 8.8 MPM TFR of percussion signals from a normal volunteer before and after intake of a carbonated drink. The percussion signals were recorded both	142

over the abdomen and the chest.

Fig.9.1. Percussion signals (a) Resonant collected from chest (b) Tympanic 147

collected from abdomen

Figure 9.2 Pole structure of resonant and tympanic signal. The real part represents 148

the damping and the imaginary part represents the frequency.

Figure 9.3 Resonant and Tympanic signal pole/residue relationship. The real part 149

represents the damping and the imaginary part represents the frequency.

Figure 9.4 PRD curve for the resonant and tympanic signals 152

Figure 9.5 Number of EDS required getting saturation region for 28 healthy 153

volunteer's percussion signals.

Figure 9.6 Percussion signal classification based on Q-factor 154

Fig 9.7: Distribution of the Q of the dominant EDS for resonant and tympanic 155

signals

Fig 9.8 Frequency distribution of the dominant EDS for the resonant and typanic 156

signals

## **List of Abbreviations**

PPIDD	Portable Pulmonary Injury Diagnostic device
OPT	Objective Percussion Technology
FFT	Fast Fourier Transform
SVD	Singular Value Decomposition
EDS	Exponential Damped Sinusoidal
MPM	Matrix Pencil Method
MP	Matrix Pencil
TFR	Time Frequency Representation
MSE	Mean Square Error
HT	Hilbert Transform
SNR	Signal to Noise Ratio
PCA	Principle Component Analysis
NNMF	Non Negative Matrix Factorization
FIR	Finite Impulse Response
DFT	Discrete Fourier Transform
TFD	Time Frequency Distribution
TF	Time Frequency
KT	Kumaresan— Tufts
MUSIC	Multiple Signal Classification

ESPRIT	Estimation of Signal of Signal Parameters Via Rotational Invariance Technique
STFT	Short Term Fourier Transform
WVD	Wigner-Vile Distribution
CWD	Choi-Williams Distributions
MPMWW	Matrix Pencil Method Wigner vile
PRD	Percentage Root Mean square difference
ROI	Reason of Interest

# Chapter 1

## Medical percussion

---

### 1.1 Introduction

Clinical percussion - a method of eliciting sounds by striking body parts with fingertips or a neurological hammer - has been used for centuries as a physical diagnostics technique [1-5]. Percussion mainly involved the tapping of the areas of the body by the fingers of the physicians-either directly with two fingers or indirectly, where one hand is placed over the skin and other is used to tap the middle fingers of the first hand (Figure 1.1) [4,7,18,20]. It is a centuries-old technique used by physicians to assess the condition of the thorax and abdomen [1, 3, and 7]. Using this physical diagnostic technique, the physicians investigate the primary signs of the disease [1, 7].

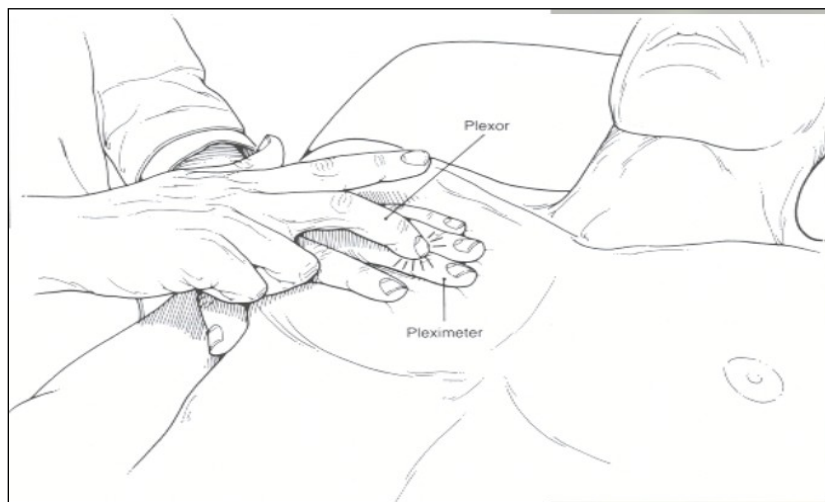


Figure 1.1: Medical percussion technique [6]

By interpreting the audible percussion sounds, a skilled physician can determine the location and dimensions of the underlying body organs in norm and pathology as well as find out

whether the underlying tissues contain air or fluid inclusions, density anomalies or anatomical defects [3, 10, 14]. This physical diagnostic technique also provides qualitative information to physician about the size, consistency, and borders of the vital organ or pathology under the percussed area [9,11,13]. It is non-invasive and can be used anywhere, since no tools are required. This approach also offers several potential advantages including simplicity, availability, prompt result and no cost making it useful to physicians for centuries [8]. However, patient cooperation is required for doing the physical examination. Sometimes in rural areas access to experienced doctors and modern services is limited. In that situation, poor people can easily access this physical diagnostic procedure from the health care workers such as nurses and doctors. Despite all its advantages, the percussion technique has declined in popularity with the advent of modern diagnostic techniques [8]. Even though percussion is still used by physician for early detection of diseases in the chest and abdomen, nowadays physician does not consider the percussion a reliable method of diagnosis disease [8].

## **1.2 Historical background**

Joseph Leopold Auenbrugger (1761), the founder of percussion, was born in 1722 in Graz (Austria) in the inn called "Zum schwarzen Mohren"[1,4,8,10,14,16,18]. It was there that Auenbrugger saw his father striking wine barrels in order to determine the level of the liquid inside [4]. The bright boy latter studied medicine and treated his patients like beer barrels [23]. This led to his great discovery, which he started to use as a diagnostic tool for assessing the condition of patients [3, 4, 23]. It was observed that when percussing a healthy man's thorax, the sound is "resonant", and recognized three other categories of sound such as "tympanic", "dull" and of indistinct quality [1, 4, 7]. Swiss veterinarians used to percuss the heads of the cattle to detect cysticerci. Unfortunately, Auenbrugger's work was not taken

seriously by physicians of this time [3, 7, 22]. Later Tissot (1782), Corvisat (1787), and Laennec (1826) propagated percussion as a diagnostic tool in medical science [4, 9, and 18]. Corvisart believed that the physician's sense organs, education and exercise were essential components of a good bedside physician [18]. He also used percussion technique for discovering and localization of many diseases. He added the use of palmar surface of extended and approximated fingers to percuss regions of the chest [3, 18]. He introduced the technique to his students of whom Rene' Laennec was one. Laennec described two kinds of percussion sounds as clear and dull [4, 10, 21]. He felt that percussion on its own was insufficient for diagnosing diseases of the chest, and he invented the technique of auscultation, which led to his discovery of the stethoscope [21]. It was a book by Forbes (1824), which introduced the techniques of percussion and auscultation into the english literature [1, 4]. It could be painful in case of pleural inflammation, and the sound elucidating from a large area may miss to give the exact status of small area [24]. Piorry (1828), William Stokes and James introduced indirect percussion and implemented pleximeter as a solid body placed on the human chest and struck by the right index finger (figure 1.2) [7,20]. Piorry felt direct percussion is inadequate as it may cause pain when patient suffers from inflammation of the pleura. Later, two of his students, William Stokes and James Hope, tried to simplify the technique by using left middle finger and still using the method in that way [20]. Although Piorry disliked this simplification, it was accepted by the Skoda - a well known physician who became the advocate of percussion in Europe. Skoda (1839) also classified the various sounds obtained with percussion despite dislike by Piorry at that time [1, 4, 10,]. "Skoda's resonance" is an important diagnostic sign [4, 20].

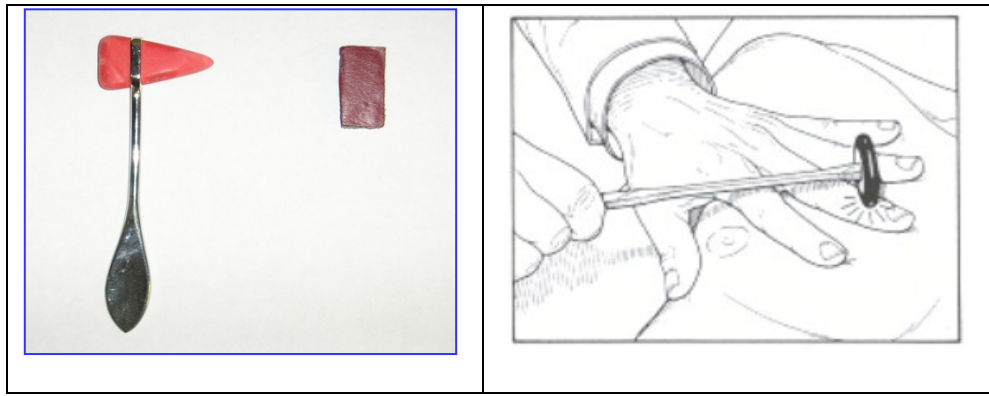


Figure 1.2 Medical Percussion technique using neurological hammer and pleximeter

Some physicians replaced the striking finger by a percussion hammer [7]. Following Skoda's work, percussion at last gained general acceptance as a diagnostic procedure. Skoda mentioned four types of percussion notes such as full-empty, clear-dull, tympanic-nontympanic and high-low [4]. Woilliez (1855) described the characteristics of percussion notes in terms of intensity and tone, which can be normal, low or high, and also the thoracic elasticity, which is perceived by the percussion finger [4]. According to the author, the percussion note may vary from tympanic to flat depending on the area where the percussion was applied [4]. Stomach full of gas produces tympanic sound whereas solid organs, such as liver, produce dull percussion note [1, 4, 10 and 24]. In case of emphysema, pneumothorax or large cavities, the hyperresonant or tympanic note was heard [4, 6, 9]. Letulle (1876) and Osler (1892) improved the classification of percussion tone. In 1900's, little development has been done of percussion method itself, but different people described classification of percussion sound in different ways. An improved method of lung percussion was shown in 1924 [9]. Delph and Manning (1968) claimed that percussion can detect lesions up to 50 mm deep and 20-30 mm in diameter and Roberts (1966) emphasis his idea on percussion can reveal more than radiography [1]. Percussion is a well-known physical diagnostic technique for long centuries, and the description of the percussion sound has varied greatly over the

time. Starting from Auenbrugger description of percussion sound such as tympanic, dull and indistinct to Skoda's full, empty, clear-dull, tympanic-nontympanic and high-low [1, 10, 14]. Next section will discuss the acoustical properties of human body under percussion.

### **1.3 Acoustical properties of human body**

The sounds produced by percussion are not always directly related to the organ lying immediately beneath. Sound may be conveyed across the chest. It is also remembered that whole chest is an acoustic box - all the internal organs can modify the sound [3, 10, 14, 20]. For example, one can usually observe a line of pulmonary resonance at the base of the left lung in front, and the transition from resonance of the lung to flatness of the liver on the right side and diminished intensity of the sound in the right inframammary region [7, 10,21]. The suprasternal region gives tubular resonance. In the upper sternal region the sound is of a somewhat mixed characteristic [7]. Indeed, the percussed human body represents a passive viscoelastic system with multiple degrees of freedom [10]. A percussion impact excites several such degrees at once, and then the oscillations fade out with their respective rates [7, 13]. If the impact is weak, the transient response can be considered linear, and the damping of all normal modes – exponential [13, 20]. The map of percussion sounds from different parts of the human body is shown in figure 1.3. This sound map is very old and various researchers produced different types of such maps. In pathological cases, the percussion notes may vary from tympanic (like the note, which is perceived over the stomach gas bubble) to flat (like the note perceived over the liver) [7, 20, 21]. The suprasternal region gives tubular resonance [1,7,11,15].

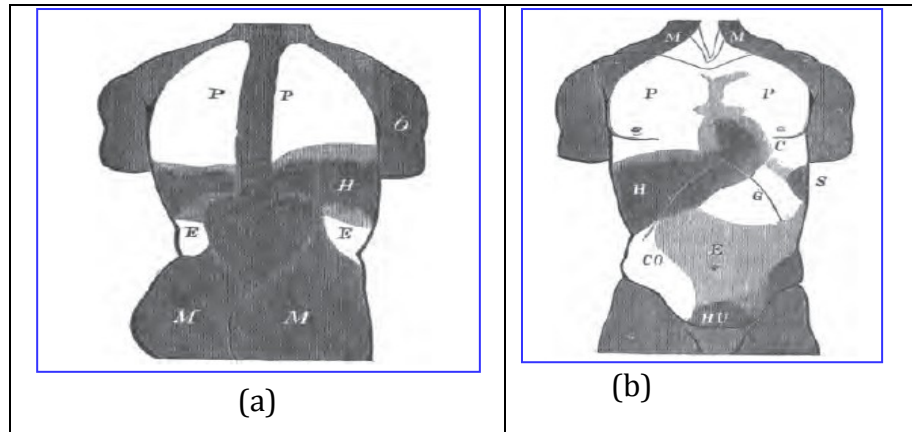


Figure 1.3 Percussion resonance and dullness of posterior regions (Piorry) (b) Showing areas of percussion resonance and dullness of front of the chest (Piorry)[7]

In the upper sternal region the sound is of some kind of mixed characteristics, and also lower sternal region, where stomach may further modify the sound[7,15]. over the trachea and large bronchial tubes the percussion sound is tubular in quality, its intensity is full, owing partly to the contained air and partly to the walls of the tube themselves[7,9,13,20]. The posterior thoracic regions do not give the pulmonary sound as well as anterior regions because of the thickness of the dorsal muscles [7]. The sound over the stomach is tympanic and over the intestines, whether they are empty, full of feces, or distended with gas, varies from tonelessness to typanitic resonance[7,15].

The percussion sound quality and properties are different over different parts of the body [7]. On the impact of percussion, the physician listens the sound and tries to differentiate the sound in the categories of normal and abnormal. In the next section we will discuss the clinical significance of the percussion sound.

## 1.4 Percussion sound & clinical significance

According to Hudson and Piorry, different body parts produce different percussion sounds [7]. It is generally accepted that the sound of conventional percussion of the chest results

from the vibration of the air-filled thorax and its contents [13]. It is stated in medical literature that there are three main kinds of percussion sound/tone, commonly named as “resonant”, “tympanic” and “dull” [1,7,20]. The vibration of the air-filled thorax and its contents are superimposed on the sound of impact of the percussion finger upon the pleximeter finger to produce resonant note [7,13, 15]. It is also noted that the replacement of air filled parenchyma by a solid mass gives dull sound [10,13]. The resonance of the lung shows in the area between the 2<sup>nd</sup> and 5<sup>th</sup> intercostals spaces, the dull sound can be produced on the liver side from 6<sup>th</sup> to 8<sup>th</sup> intercostals spaces, tympanic sounds are usually produced over the abdomen [1,4,25,].

### 1.4.1 Percussion sounds

- *Resonant sounds:* The resonance is a low-pitched, loud intensity, long duration (approx. 15 ms) and hollow sound heard over normal lung [1, 20]. The lungs are normally 99% full of air and produce the “resonant” sound [10, 20].

Table1.1 Classification of percussion sounds by several sources [1]

Source	Normal Lung “resonance”	Liver or heart underlying lung ‘Decreased resonance,	Below-lung margin No resonance
Auenbrugger (1761)	Sonus clarior	Sonus Obturior	
Forbes (1824)	Sonorous	Mprbid	
Laennec (1826)	Clear		
Flint (1876)	Resonant	Dull	Ull
Cabot (1906)	Vesicular resonance	Dull	Flat
Major and delph (1956)	Resonance	Dull	Flat
Appleton and simon (1958)	Resonant	Less resonant	Flat
Lewis (1966)	Resonant	Impaired	Dull
Macleod(1967)	Resonant	Impaired	Dull
Delp and Manning (1968)	Resonant	Dull	Flat

- *Flat or extremely dull sounds:* The dull sound is medium, high pitched and short duration. Dull sound heard over the solid areas such as bones. Liver, and heart [7,10,20]
- *Tympanic:* Tympanic quality results from an unusual amount of air contained within a cavity with elastic walls. Tympanic sounds are higher intensity, even longer duration (> 40 ms) high-pitch and drum-like sounds [1]. The sound is drum-like. Typical tympanic sound occurs in pneumothorax and is heard over the stomach [4, 7].

### **1.4.2 Clinical significance**

Different percussion sound produces from different parts of the body [7]. Resonant sound usually heard over the normal lung [1, 7, 10]. A decrease in sound amplitude is usually the sign of lung abnormality [10,13,17]. Dullness may result from pneumonia, tumor, infarction, or fluid collections [1,7,20]. Typical tympanic sound produced over the chest in case of pneumothorax, emphysema or large superficial cavities, whereas in case of massive pleural effusion compressing the underlying lower part of the lung [4,7]. Lung noises provide anatomic advice such as adventitious expiring air in asthma, crackles secretions in bronchitis, and other subtleties like crackles air in emphysema [19, 25]. Abnormal lungs may be hyper-resonant, dull, or stony dull. It is expected to hear tympanic sound over the stomach but dullness may be produced by the intra-abdominal tumors or masses. In addition, shifting dullness may indicate the presence of ascites [7]. An expanded area of dullness around the heart may indicate cardiomegaly or pericardial effusion [10, 11].

### **1.5 The physics of percussion**

Transmission properties of respiratory system are very important for considering the impact of percussion of the thorax subsystem [4, 21, and 22]. The transmission properties of

respiratory system depend on the properties of the coupled systems of the lung and chest wall placed in series [4]. When the chest wall is percussed, it vibrates and “rings” as a resonant cavity partially damped by the thoracic contents [20]. In normal conditions, the vibrations of percussion are underdamped, as a consequence of large acoustic mismatch observed between the chest wall and underlying lung parenchyma [3,4,21]. Such mismatch is due to the fact that the acoustic impedance of the semi rigid chest wall is quite dissimilar to that of the chest parenchyma, a structure that behaves like gas and tissue [4,22]. If the acoustical impedance of the medium is  $Z$ , then  $Z$  can be defined as

$$Z = \text{Density of the medium} \times \text{Sound velocity}$$

Also, If  $Z_1$  and  $Z_2$  are the acoustical impedance of the two media, then the transmission coefficient  $T$  is defined as

$$T = \frac{4Z_1Z_2}{(Z_1+Z_2)^2} \quad (1.1)$$

The proportion of the sound energy transmitted across the boundary of the two medias is a function of acoustic impedance of the two media shown in equation 1.1 [4]. A large portion of the vibration energy of percussion is reflected at the gas-tissue interface, yielding a clear and long lasting sound described as “resonant”[4,7,10,20]. If the underlying lung parenchyma is replaced by air, as pneumothorax, the acoustic mismatch is maximal, so that under damping is more pronounced [4]. The result is a sound of greater amplitude and duration called “tympanic” [1, 7, 8]. Finally, when the acoustic mismatch between the chest wall and the underlying tissue is minimal, because the acoustic impedances of the two the structure are similar, percussion vibrations are over damped [3, 4]. They propagate away from the surface very rapidly and vanish quickly, resulting in a sound of low amplitude and short duration describes as “dull” [7, 8, and 25].

## **1.6 Thesis study outline**

### **1.6.1 Research motivation and hypothesis**

Although medical percussion is a simple and quick physical diagnostic technique, presently its diagnostic capability and reliability depends on different subjective factors. All current implementations of this methodology hinge on the experience of the doctor, natural limitations of the human ear, and on the need of quiet surroundings. Despite many advantages of the traditional percussion technique, most physicians no longer rely on the percussion as diagnostic tool because of the lack of a permanent record. In addition, there is an overall lack of success in bringing it to the modern digital-age technology in order to increase objectivity.

The analysis of percussion signal characteristics by advanced signal processing methods might show promising results that could assist in clinical diagnostics while removing the limitations of conventional approach. Using digital signal processing techniques to extract information from percussion sound might help recover the former popularity of this diagnostic method and advance its clinical utility beyond the traditional scope. In this respect, automated analysis and computerized representation of percussion findings might help determine the pathological condition in a more objective and standardized way.

The use of digital signal processing techniques to extract diagnostic information from percussion sounds would comprise a major step towards advancing the utility of medical percussion beyond its traditional scope. The step of advancing the percussion method can be implemented in a handheld device equipped with an embedded microcomputer to perform

data acquisition and classification of the signals in a standardized and reliable manner. These considerations lead to a concept of a Portable Pulmonary Injury Diagnostic Device (PPIDD).

## **1.6.2. Goals and objectives**

### **1.6.2.1 Portable Pulmonary Injury Diagnostic Device(PPIDD)**

#### **concept**

The acoustical methods of lung diagnosis offer many advantages including ease of administration, no reliance on bulky equipment, low cost, and ability to acquire a large amount of information about the both physical nature and functionality of the repository system. Fast and accurate diagnosis is needed for various types of battlefield trauma , even in the absence of the doctor. The aim of such PPIDD is to create an electro-acoustical device for pulmonary assessment that takes advantage of inherent advantages of the methods, while removing its limitations.

The objective of the PPIDD is to create a device enabling the applications of the percussion diagnosis methodology to pulmonary injury detecting quickly and under variety conditions. The detection of trauma and/ or disease in the human would be based on the principle of Objective Percussion Technology (OPT). It is obvious that many of the lung traumas can be successfully treated if they are detected in timely manner. It would also significantly impact the mortality rate if pulmonary traumas could be identified on site and rapidly. This new development would facilitate the diagnostic facilities as well as successful treatment plan without the necessary of the standard diagnostic procedure such as CT, MRI and ultrasound.

#### **1.6.2.2 Pneumothorax condition**

Pneumothorax is a collapsed lung condition. It is a potential medical emergency caused by accumulation of air or gas between the parietal and visceral pleurae, occurring either as a

result of disease or injury, or spontaneously [27,28, 30]. Pneumothorax is a life-threatening condition that occurs when the lung's outer membrane is injured by a sharp object, and the air leaks into the thoracic or chest cavity [29]. The air can then build up inside the chest cavity, compress the heart and lungs and deprive the victim of oxygen (figure 1.4) [26,29]. The most common types of pneumothorax are spontaneous, tension, and traumatic [24, 28]. Traumatic pneumothorax resulting from either a blunt trauma to the chest wall or from an open chest wound may lead to the lung collapse [19,29]. It can be stated based on the reviewed literature that conventional percussion over pneumothorax (collapsed lung) produces sounds of tympanic character [7, 19].

On the other hand, the normal lung absorbs the sound energy rapidly [28, 29]. In case of collapsed lung condition (Pneumothorax), the pleural cavity is filled with air and the sound energy cannot penetrate it as easily as a healthy lung because of high impedance mismatch at the border with the air [4].

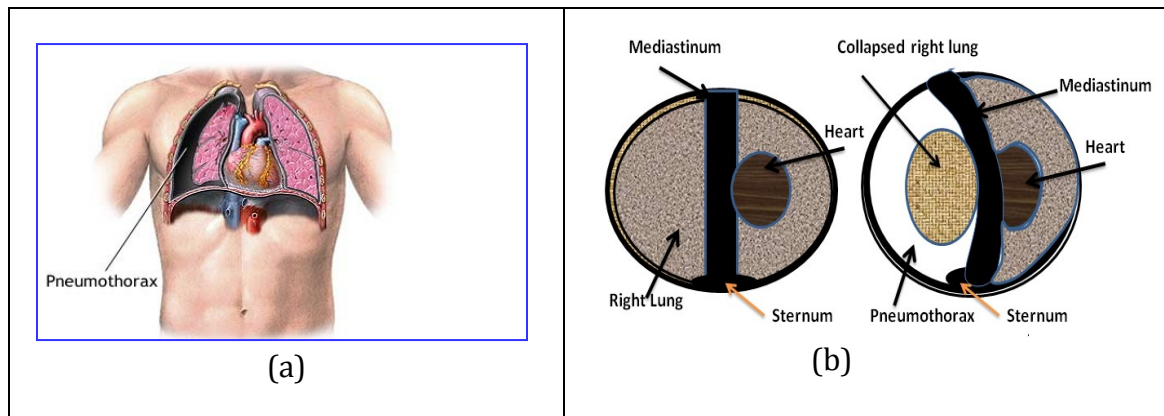


Figure 1.4 (a) Pneumothorax condition. [12] (b) Transverse sections of the chest in normal

condition (Left) and under a pneumothorax condition (Right). The white space represents the air accumulation into the pleural space. These two medium causes the acoustical impedance mismatch

### **1.6.3 Medical percussion for detecting pneumothorax condition**

The large acoustical impedances mismatch at the boundary of the air cavity forms a virtually impenetrable barrier to the percussion wave and reduction in amplitude of the incident wave [29]. The greater the acoustic mismatch, the greater the percentage of acoustical signal reflected and the less transmitted [4, 29]. Percussion response from the chest at this situation would change due to impedance mismatch at the air cavity boundary [26, 28, 29]. As a result, the rate of acoustical energy transfer decreases and leads to lower amplitude decay over time [29]. The imposed air cavity will generate tympanic-like sound [29]. The hypothesis is that we can detect this effect using objective percussion methods, not just the ear of the doctor.

## **1.7 Review of percussion signals analysis literature.**

### **1.7.1 Clinical percussion signals recordings**

Early attempts to record percussion sound waveforms were made by Castex (1895) and Selling (1907) [1,3]. Castex used a manometer flame modulated by percussion sounds. The capsule in the manometer tube was placed in contact with the trachea or in the mouth of the patient to be percussed [1]. The sound waveforms recorded on photographic plates mounted on a moving carriage and pulled by hand in front of the flame [1]. Selling recorded sound on gramophone disc and playback, the vibrations were transmitted through a system of compound levers and marked the waveforms on the smoked paper of a kymograph using a simple microphone and a galvanometer [1, 3]. In his recordings, the duration of percussion signals was 42 ms for resonance and 28 ms for dullness. A modern textbook on clinical diagnosis (Delp and Manning, 1968) still includes Selling's original waveform. In 1955, McKusic employed condenser-type microphones and recorded the resulting electrical signals

on the magnetic disc [21]. The variable filter was used each time and scanning was done at different frequency. The corresponding signal strength of each frequency band was then translated into proportionate level of light intensity, and the data thus recorded on light-sensitive paper [21].

Murray and Neilson developed a system for recording percussion sounds (Figure 1.5) in 1975 [1]. They used a crystal microphone connected with high impedance amplifier for obtaining low frequency cutoff [1]. The amplifier was connected to an FM tape recorder. They processed all the recordings by playing back the tape and used averaging for noise cancellation. To facilitate the recording of short percussion waveforms on a chart recorder, it was switched for a predetermined period of time with a special advance trigger. This advance trigger signal also triggered a Grammascope pulse height analyzer modified as a transient averager [1].

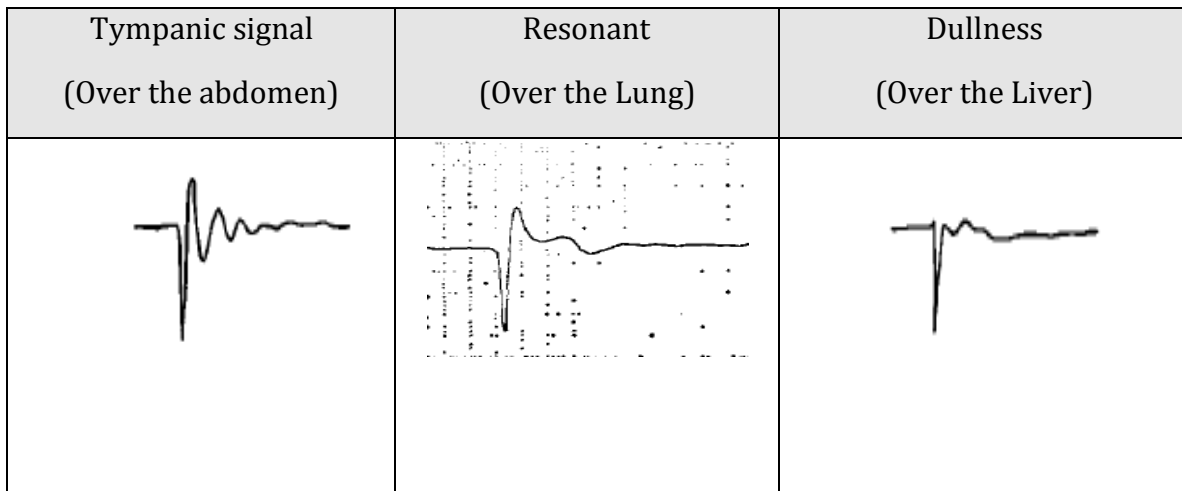


Figure 1.5 Sound pressure waveforms for three main types of percussion signals (Source: A. Murray and Neilson [1])

The microphone was usually placed at a distance of 150 mm from the chest. The tape was played back at low speed for bringing the high frequency cut off at 25 Hz and so making the signals suitable for chart recording [1]. The bandwidth of the system was chosen between 3 Hz and 1.5 KHz for minimizing the waveform distortion. The doors were closed for

minimizing external high frequency noise and large low frequency variations. A headphone was used for the listening test and a IBM 360/70 computer was used for frequency analysis [1].

### **1.7.2 Properties of the clinical percussion signals.**

As mentioned earlier, the three main percussion sound types are commonly referred in the clinical practice as “resonant”, “dull”, and “tympanic”. All of them contain sharp initial rarefaction pressure peak [1,2,10]. The “resonant” signal is approximately 15 ms long and has a large rarefaction and two compression peaks signal. The “dull” signal is relatively short, (sometimes as short as 3 ms), and has a rarefaction pressure spike only [1,3,10]. The tympanic signal is usually longer than 40 ms and shows similarity with a damped sinusoidal signal, so that it has a more definite pitch compared to other percussion sounds [1,10]. By percussing different parts of the body, it is possible to produce many different waveforms including the three main types and their intermediate gradations [7].

### **1.7.3 Research review on medical percussion signals.**

The majority of previous work involving the objective analysis of the pulmonary percussion sound signals is based on the Fourier transform [1-3, 21, 26, and 28]. In 1876, Gerhardt took initiative to measure the fundamental frequency of the percussion sound first by the natural sense of pitch, and then by comparing it with the sounds of tuning forks and Helmholtz resonators [1]. One then had to wait until the 1955s to observe the development of modern methods of recording and signal processing, which allowed objective studies of lung sounds in time and frequency domain. McKusick et al. (1955) has made use of sound spectroscopy

that is used for analysis sound into spectrogram [28]. In 1961, Casteleijn studied the percussion signals using Fourier analysis [1].

The qualitative and quantitative analysis has been provided by Murray and Neilson (1975) who suggested computational algorithms to differentiate between three main types of percussion sound defined as resonant, tympanic and dull [1]. In particular, computerized Fourier analysis of percussion signals was used in this work to determine the frequency components of signals obtained from the averaged printout. No real discretization was done in this work. In the time domain, the resonant signals showed two main peaks while the tympanic signals showed many peaks, and dull signals showed poorly defined variations of sharpness. In spectral domain, the tympanic signals showed only one peak (at 280 Hz in the analyzed case and in the range of 200 to 600 Hz in general) [1]. The resonant sounds contained a far greater proportion of their energy in the lower frequency band than dull sounds. The conclusion was made that the tympanic signals exhibit a single dominant frequency and that the resonant and dull signals are perceived to have low and high-frequency component with respect to each other.

In 1975, the second article of Murray and Neilson proposed a four-parameter quantitative model describing the percussion sound signal [2]. A piecewise linear approximation of the signal based on four distinctive parameters (2 parameters for time, and 2 parameters for pressure) were used. Artificial percussion sounds were synthesized based on the four-parameter model and then compared to the experimental signals to validate the model. Tape recordings of “resonant” “impaired resonant” and “dull” sounds of both real and simulated types were produced. A number of physicians and non physicians were asked to identify the types of sound irrespective of its being real or simulated. They observed that simulation contained adequate information to describe and correctly identify various sounds. Later on,

Murray and Neilson (1978) investigated the relationship between the motion of the chest wall and the sounds produced [3]. The chest wall was percussed and its motion was simultaneously recorded with an accelerometer [3]. A single rebound peak was observed at 4 to 5 ms after the percussion impact on the underlying rib [4]. The accompanying sound pressure waveform reflects this motion, but showed an additional wave with its first peak arriving later, around 9 -10ms [3]. The existence of this additional peak was attributed to the motion (also measured with an accelerometer) of the rib adjacent to the percussed rib [3]. No further signal processing attempts was mentioned in that study. In 1989, the transmission of sound generated by sternal percussion was studied [31]. The authors indirectly determined the transmission path of sound generated by sternal percussion in five healthy subjects. This study was mainly concerned with the factors affecting sound transmission through the chest by investigating the influence of the lung volume and gas density variation on the characteristics of sound generated by sternal percussion. Lung sounds were measured in three lung volumes such as at Functional Residual Capacity (FRC), total Lung Capacity (TLC), and Residual Volume (RV) both with the lungs filled with air and with an 80% He-20% O<sub>2</sub> (heliox) gas mixtures [31].

The authors focused on the three acoustic indexes such peak to peak amplitude, the peak frequency, and mid power frequency. It was observed that the average values of all indexes tended to be greater in the upper than in the ipsilateral lower lung zones. In the upper zones, peak-to-peak amplitude was greater at total lung capacity and residual volume than at functional residual capacity [31]. It was also found in this research that replacing air with heliox did not change these results. The frequency analysis was done by FFT. Detection of air in the abdominal cavity (pneumoperitoneum) was studied in [26]. The main goal of this study was the detection of changes in the abdominal percussion sound caused by the

alteration of the abdominal structure due to pneumoperitoneum. This study also used FFT for finding the dominant frequency of the percussion signal. In addition to the listed above, there are several other articles based on the Fourier analysis of the body sounds recorded with contact microphones. However, all of them study passive auscultation signals, while the focus of this review is on clinical percussion signals (active excitation).

Some researchers have already attempted to address the problem of diagnosing pneumothorax by acoustical methods such as auscultation [10, 11]. The signal processing approach used by these authors was based on the Fourier analysis. In 1999, Winter and Smethurst have successfully tried percussion as a rapid and simple acoustical method to diagnose pneumothorax [27]. The sternal percussion was done while simultaneously auscultating the anterior chest on the side of the suspected pneumothorax [9]. The authors commented that the simple methods of percussion auscultation were a good way to confirm the presence of pneumothorax. Again, there was no signal processing analysis involved in this research. In [28], pneumothorax detection was done on sedated mongrel dogs by sending acoustical sounds into the respiratory system via endotracheal tube, and measuring the acoustic signal transmitted through the lung at the chest wall surface. Using the FFT, the spectra of apodized chest wall sounds were calculated and analyzed. A method of finding air cavities in the body by sending low frequency vibroacoustic waves into the body and collecting the signal at a second location on the body was claimed in [32]. Resonance and anti resonance peaks in the received FFT spectra indicate the presence of gas cavity. The same authors investigated the effects of pneumothorax on breath sounds and evaluated their use for pneumothorax diagnosis [29]. Both papers are not related to the conventional percussion method and build on the spectral analysis using FFT. Despite all the advantages of conventional percussion, the literature on quantitative pneumothorax diagnostics with this

simple, quick, and efficient technique is very scarce and difficult to find. From the above discussion, it can be concluded that the majority of preceding work attempting the objective classification of percussion sounds is based on the Fourier analysis.

## 1.8 Thesis organization and contributions

The rest of this dissertation is organized as follows: A detailed summary of the contents and contribution of each subsequent thesis chapter is provided below. In the beginning of every chapter, there is an introductory section with a more detailed outline.

- **Chapter 2:** This chapter begins with the discussion of percussion signal collection from healthy volunteers. The percussion signals collection procedures, challenges and physician feedback are discussed. Two medical percussion signals, which are historically known as “resonant” and “tympanic”, are introduced in this chapter. The author’s first contribution is to assign a mathematical model to medical percussion signals is presented in this chapter. This model is the key point that led us to start our research in various ways. Finally, all mathematical formulas supporting the model are provided.
- **Chapter 3:** begins with the description of the initial research conducted before the proposed model based solution was identified. In the beginning of the project we explored several alternative signal classification approaches in order to find the most logical and optimal one. In one of the early attempts, we tried to match the original percussion signal to a model one using cross correlation procedure. Here we measured the frequency and damping using cross correlation method, then we tried to generate the percussion signal based on these two parameters while keeping other two parameter fixed. As a result, a close match between the original signal and the simulated signals was achieved, although at the expenses of slow convergence and difficulty to fully automate

the algorithm. Another attempt involved verification of the frequency and damping parameters using a spectral and Hilbert Transform procedure. This effort yielded quick characterization of the percussion signal without going into detailed analysis. However we cannot rely on this type of solution, as the percussion signals are very short and their characteristics do vary considerably. As a result, we were not done and kept searching for a reliable, robust and accurate solution that would provide satisfactory recognition of medical percussion signals.

- **Chapter 4:** Several methods of reducing the noise associated with medical percussion signals are discussed in this chapter. One of them is a denoising technique prior to decomposing the medical signal with a super resolution approach. A hybrid noise filtering technique is introduced here, which is the combination of bandpass filtering and Hankel SVD methods. The problem of detecting the initial point of the digitized percussion signal is also discussed in this chapter along with the signal truncation techniques. We have designed and analyzed a BP-Hankel SVD-based hybrid noise cancellation technique. This hybrid noise cancellation technique for the medical percussion signals is also a original contribution by the author.
- **Chapter 5:** introduces a model based signal decomposition technique that was applied to medical percussion signals. The decomposition technique based on the Matrix Pencil Method (MPM). Although the core method was not modified, its application was adapted to the specifics of clinical percussion signals and their classification needs. In this chapter, the MPM steps are analyzed in detail and the advantages and disadvantages of the method are described. The finding of suitable decomposition method for medical percussion signal is a contribution by the author.

- **In chapter 6:** In this chapter, a technique for estimating parameters of percussion signals using MP method is introduced. The Matrix Pencil Method decomposes given percussion signal into a number of EDS based on the chosen signal model. Each EDS is defined by 4 parameters, such as frequency, amplitude, damping and initial phase angle. The EDS decomposition and parameter extraction are realized using MPM. The resulting EDS are shown for each type of percussion signals. The reconstruction of the original signal was done by adding all the EDS is described in this chapter. We were able to get back the percussion signals with minimum reconstruction errors. The analysis of the reconstruction error is another contribution by the author.
- **Chapter 7:** Percussion technique has been in use for centuries. However, the modern percussion signal analysis for the medical percussion signals is Fourier transform. Despite its advantages, Fourier method contains many drawbacks. In case of damped percussion signal, the closely spectral peaks are difficult or impossible to resolve. This happens due to the damping of the signal. In addition, the close spectral peaks are not easily resolved using traditional spectral analysis. We have introduced a super resolution spectral analysis based on the Matrix Pencil Method (MPM) where we were able to identify all natural oscillation frequencies in the signal. The suggested method is able to separate closely spaced frequencies. The addition of a super resolution technique for modal analysis for the percussion signals is a contribution to signal processing.
- **Chapter 8:** discusses a Time-Frequency Representation (TFR) of a multi-component signal based on the MPM, while the conventional techniques are not able to provide a practically useful time frequency representation. The conventional techniques introduce cross terms, have low resolution at least in one of the two domains, and suffer from masking of the lower energy components by higher energy ones. The proposed time-

frequency representation technique based on MPM is shown to overcome the common problem of conventional TFR and provide a practically useful time-frequency representation of clinical percussion signals. The time-frequency analysis and classification of real percussion signals are discussed as well. This new TFR of highly damped medical percussion signals is also a contribution by the author.

- **Chapter 9:** One of the practical goals of the work described in this thesis is the development of a method for recognizing tympanic signal among the normally resonant chest signals, which would signal about possible pneumothorax. It is mentioned in the medical literature that tympanic sound/ signal is produced over the chest percussion in the case of pneumothorax condition [4, 7, 8]. We presented two methods for recognising and classifying medical percussion signals. We have introduced PRD and Q-factor methodology for doing this.
- **Chapter 10: Contributions and Recommendations:** We have listed the contributions to the medical percussion signal analysis using a contribution tree. We have shown the existing literature and previous efforts on the analysis of medical percussion signals and added our contribution to this tree. At last, several open questions raised in this thesis are also summarized. Recommendations are also provided regarding possible further enhancements of the percussion signal analysis presented this chapter.

## 1.9 Summary

We have discussed the historical background of the percussion signals in this chapter. The previous research findings on medical percussion signals using digital signal processing techniques are also discussed in the chapter. The research motivations, objectives and goals are discussed in this chapter. The remaining parts of the dissertation are also highlighted at the end of the chapter.

# Chapter 2

## Materials and mathematical model of the clinical percussion signals

---

We have illustrated the various percussion sound characteristics, signal collection procedures and graphs of the previous researchers in chapter 1. We noticed that Murray and Neilson documented the percussion signals waveform in 1975 [1]. In the latest attempt, we have collected percussion signals in hospital settings placed in this chapter. The percussion signals were collected from the healthy volunteers and will be compared with the previously documented percussion signals described in [1]. We proposed a model for the percussion signal, which will also be discussed in this chapter.

### 2.1 Signal collection procedures

The collection of percussion signals from normal volunteers was conducted in clinical (hospital) condition at Wayne State University - Detroit Receiving Hospital under the supervision of trained medical personnel. The study-involved collection of percussion signals over 30 normal individuals using three different methods. Out of total 30 volunteers tested, 26 were mostly young and middle-aged males, the remaining 4 volunteers were females. The purpose of the investigation was to identify the different percussion signals from different parts of the body and classifying the signals characteristics. The manual percussion was performed three times for each (out of 12) body areas for 24 volunteers. One round of testing was conducted for the first six volunteers. The different locations of the body areas where the percussion signals were collected are shown in Fig 2.1. The trained medical personnel

administered the percussion in different parts of the body. The physician confirmed the different character of the audible sounds, like resonant, tympanic and dull before saving the digital signals into the computer. Each volunteer had to sign a consent form prior to the percussion event.

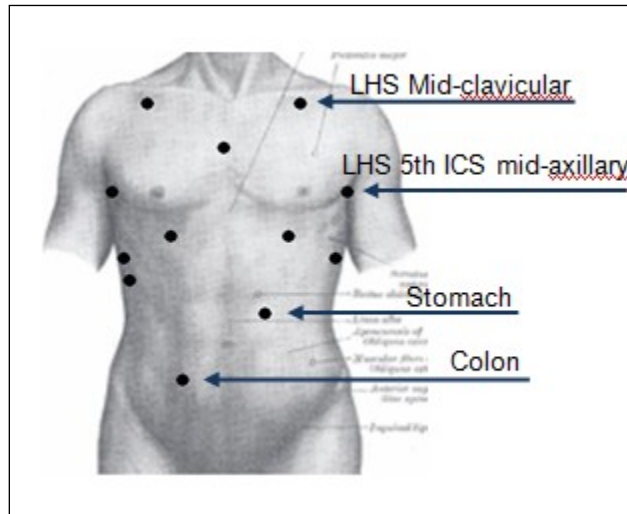
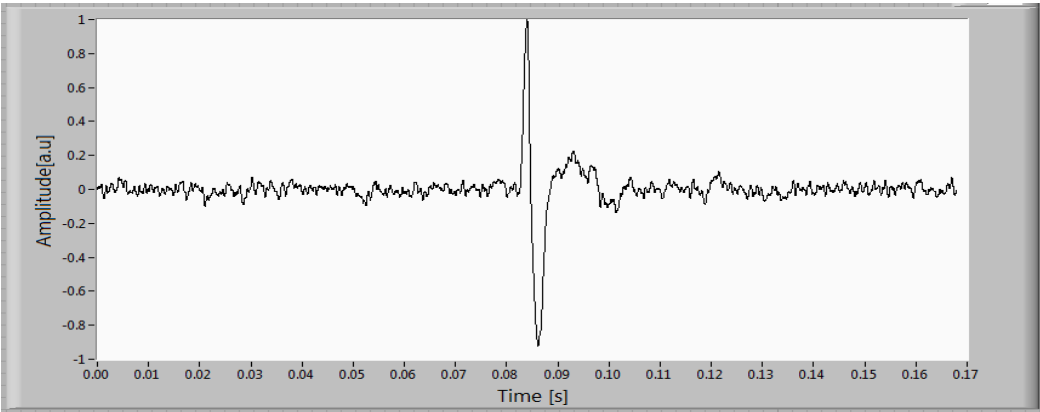


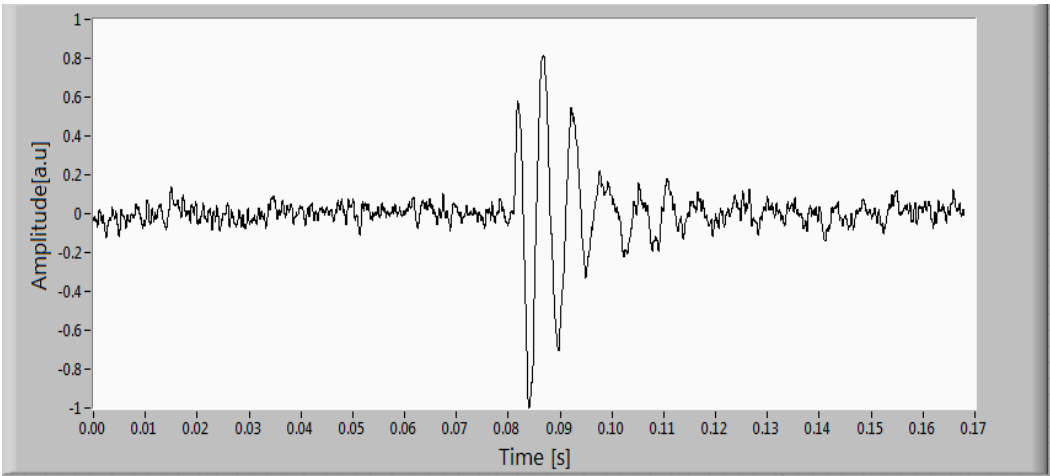
Figure 2.1 Percussion points location. Twelve percussion points used during the healthy volunteer study are marked with black circle.

The volunteers were tapped over the chest and abdominal areas with a neurosurgical hammer and the signals were collected with an omnidirectional electret condenser air microphone. The microphone was placed 150-300 mm away from the percussion spot. Then the signals were amplified and digitized at 48 KHz sampling rate using a 16-bit computer sound card. The tapping was applied through a multi-layered pad (plessimeter) pressed against the skin. Three rounds of percussion were performed where the conditions allowed. Two examples of typical medical percussion signals are shown in Figure 2.2. The resonant signal in Figure 2.2a acquired over the subclavicular area, and the tympanic signal in figure 2.2b collected over the left portion of the abdomen. Both signals represent transient responses of the human body to the percussion impact. Their amplitude is highest at the onset and then rapidly fades out below the noise level. The respective duration of the signals

in Figures 2.2.a and 2.2.b is approximately 0.17s. For instance, percussion of the LHS mid-clavicular region of the volunteers typically produced well-defined resonant signals 2.2(a).



(a) Resonant Signal



(b) Tympanic signal

Figure 2.2 Medical percussion signals

The percussion signal collected from the abdomen shown in figure 2.2(b) is historically known as tympanic signal. Notably, the signals recorded in our experiments are similar in shape to those recorded by Murray and Neilson in 1975 [1].

## 2.2 Clinical percussion signal collection challenges

There are some challenges arose at the time of percussion signal collection. Normally, all the chest signals should be identified as resonant. However, in some cases the chest signals showed weak tympanic behavior. This could be explained by certain corruption of the signal quality that took place when the percussion was done through clothing, e.g. gown, shirt, or even a sweater. The abdomen signals identified as non-tympanic can be attributed to cases when there was no air in the stomach or colon. Visual inspection of these signals (waveforms) confirms that they do not have fully tympanic character but rather resonant or weak tympanic.

On the other hand, percussion of certain abdominal areas is known to often provide a response of tympanic nature. As an example of tympanic signal, we used the percussion responses from the right vertical segment of the colon and from the stomach. These tympanic signals (when present) sound similar to the percussion of a chest pneumothorax condition, as confirmed by medical doctors. Percussion signals were also collected over intermediate areas of the body around the heart and in the liver area. The signals in these areas are reportedly characterized as “dull”. Very often, however, depending on the patient’s position, anatomy, and presence of the air in the abdomen, the signal in these border areas could be a mixture of tympanic, dull, and sometimes even resonant signals. Analysis of the recorded data allows us to refine the automatic classification algorithms and demonstrate the validity of the principles of the Objective Percussion Technology (OPT). The other challenges came at the time of percussion even are listed below:

- To collect a significant amount of data from normal (healthy) volunteers
- To confirm that the chest signals are of a resonant nature for an extended set of volunteers.

- To confirm that the stomach signals are of a tympanic nature for an extended set of volunteers.
- To collect the percussion signals in quite hospital environment

We let medical personnel use the equipment and provide feedback for immediate and future improvements.

## **2.3 The proposed model for the clinical percussion signals**

The proposed model for the percussion signal comes from the physical reasons, as tympanic signal represents a slowly decaying oscillation and often allows for a direct fit with a single exponentially damped sinusoid (EDS). Therefore, the shape of a purely “tympanic” abdominal signal inspires the model presented here. We further hypothesize that chest (resonant) signals can also be approximated by a small number of EDS, as they are also comprised of several damped harmonic oscillation modes. We also noticed from the other authors, such as in [1], these signals exhibit damped sinusoidal character. The cause is that the propagation of a wave through a coupled system is attenuated due to acoustical mismatch [4]. As the sound speed is inversely proportional to the square root of gas density in free gas, but not in porous media, the acoustic mismatch is maximal when the underlying lung is full of air [33]. This acoustical mismatch causes the damping characteristic of abdominal percussion signal.

Through extended experimentation with chest and abdominal percussion signals has done, we found out that the slowly decaying oscillations of abdominal (tympanic) percussion signals allow for direct fit with a single complex exponential function. This shape can be explained by the oscillation of air cavities with elastic walls. Although the shape of the “resonant” chest percussion signal does not readily resemble a damped sine wave, the physical model of the oscillating chest wall and other thoracic subsystems suggests the same

damped harmonic character of the transient response to percussion. According to this model, the percussion event usually excites oscillations of several anatomical subsystems at once, and superposition of these oscillations results in a more complex shape of the “resonant” signal [34]. The promising preliminary results stimulated our further attempts to automate the decomposition process in which we seek to approximate given percussion signal by a sum of Exponentially Damped Sinusoidal (EDS) waves according to the parametric model widely studied in literature [47-71].

The underlying signal model for the EDS method consists of exponentially-damped sinusoids (where the sinusoidal signal part consists of the fundamental and all of its harmonic and inter harmonic components). Each component can be described by the amplitude, the angular frequency, the initial phase, and damping factor. We proposed that the percussion signal is multi-component, and all its components are decaying as complex exponentials. According to our assumption, we also assume percussion signals contain some additive noise:

$$y(t) = x(t) + n(t) \tag{2.1}$$

$y(t)$  = observed time response of percussion signal,  $x(t)$ = signal without noise, and  $n(t)$  is the noise associated with the observation.

Experimentally recorded audible percussion signals contain noise originating from the measurement equipment and the environment. The most significant sources of noise in our data were the microphone/tripod shaking due to vibration of the hospital building (moving elevators etc), the ambient noise in the room, and the 60 Hz AC component from the computer power supply. The noise from other electronic components (pre-amplifier, analog-to-digital conversion etc.) was relatively weak compared to the above. The characteristics of percussion signal’s noise and noise reduction procedures will be discussed in chapter 4.

$$y(t) = \sum_{i=1}^M R_i \exp(s_i t) + n(t) \quad 0 \leq t \leq T \quad (2.2)$$

$R_i$  = residues or complex amplitudes (related to amplitude and phase),  $M$  is number of EDS in the signals. Here  $S_i$  is a complex quantity and can be written as follows:

$$s_i = -d_i + j\omega_i \quad (2.3)$$

$\omega_i$  = angular frequencies =  $(2\pi f_i)$ , and  $d_i$  = Damping factors

Therefore, one can write the sampled signals as,

$$y(kT_s) = x(kT_s) + n(kT_s) \cong \sum_{i=1}^M R_i e^{s_i k T_s} + n(kT_s), \quad \text{for } k = 0, 1, 2, \dots, N-1 \quad (2.4)$$

Here  $N$  is the total number of samples and  $T_s$  is sampling interval.

$$y(kT_s) = \sum_{i=1}^M R_i z_i^k + n(kT_s) \quad (2.5)$$

Where  $z_i = e^{s_i T_s} = e^{(-d_i + j\omega_i) T_s}$  where for  $i=1, 2, \dots, M$ .

Therefore, it is clear from the model that the EDS model contains four parameters such as amplitude, frequency, damping factor and initial Phase. The research focus is to best estimation of these four parameters from the noisy contaminated percussion signals.

## 2.4 Summary

In this chapter, we have discussed the percussion signal collection procedures and introduced the EDS-based mathematical model. The proposed exponentially damped sinusoidal model presented in this chapter naturally fits the signals of tympanic type. As discussed, however, the resonant signal can be represented by this model as well. We will show the representation in the subsequent chapters. We have presented the various equations for the model. The goal of our analysis is to find the best estimate of the residue  $R_i$

and the poles  $z_i$  by using the signal  $y(kT_s)$ . The percussion signals analysis and results will be discussed in two ways (a) The initial effort that we took for representing the percussion signals. This effort was discarded later on as the method doesn't suit with the proposed model. (b) In the second approach, super resolution signal decomposition's method will be discussed. This second method will lead the enter dissertation completion. We will discuss both procedures in the following chapters. Next chapter, we will present a preliminary research focus that explored at the beginning of our research.

# Chapter 3

## Primary research focus

---

We have discussed the percussion signals model in the previous chapter. In this chapter, an attempt is made to find out the two parameters (frequency and damping) of the EDS model. Approximating a simple tympanic signals with a single damped sinusoid where our primarily focus was to find out its frequency and damping. These two parameters are the most influential parameter in the EDS model. To find out these tow parameters based on EDS model, we used a cross correlation methodology. Initially, we kept the amplitude and initial phase constant and produced synthetic trial EDS that correlated with the original percussion signal. We will discuss the procedures, findings, and analysis in detail in this chapter.

### 3.1 Cross correlation

Cross correlation describes the relationship between multiple processes. It is most frequently used to identify the time delay at which two signals "line up", or are "most similar. Correlation determines the degree of similarity between two signals [35]. The observations of one series are correlated with the observations of another series at various parameters such as damping, frequency and phase angle. It is possible to identify variable using Cross-correlations, how much one variable is predicted to change in relation the other variable [35,36]. Here the method is performed between two sequences, one is kept stationary while the other is shifted. If the two processes are similar, there will be at least one maximum where the shift equals. The cross correlation  $R_{xy}(t)$  of the input signals  $x(t)$  and  $y(t)$  is defined by the following equation [35]:

$$R_{xy}(t) = x(t) \otimes y(t) = \int_{-\infty}^{\infty} x^*(t) \cdot y(t + \tau) d\tau \quad (3.1)$$

Where, the symbol  $\otimes$  denotes correlation. The discrete representation is a sequence whose indexing can be negative. Let  $N$  be the number of elements in the input sequence  $X$ , let  $M$  be the number of elements in the sequence  $Y$ , and assume that the indexed elements of  $X$  and  $Y$  that lie outside their range are equal to zero, such as  $x_p = 0, P < 0$  or  $P \geq N$  and  $y_p = 0, P < 0$  or  $P \geq M$ . Then the cross correlation can be rewritten as follows:

$$h_p = \sum_{k=0}^{N-1} x_k^* \cdot y_{p+k} \quad (3.2)$$

for,  $p = -(N - 1), -(N - 2), \dots, -1, 0, 1, \dots, (M - 2), (M - 1)$ . The elements of the output sequence  $R_{xy}$  are related to the elements in the sequence  $h$  by

$$R_{xy(i)} = h_{i-(N-1)}, \text{ for } i = 0, 1, 2, \dots, N + M - 2 \quad (3.3)$$

Matching the four parameters of the EDS model with the existing percussion signals is a challenging task. It is difficult to achieve a reasonably good fit of a real resonant percussion signal with only one single EDS. Therefore, we began with the simplest case and picked a weakly damped tympanic signal for doing cross correlation with the single component EDS. As such, we tried to find out the optimal frequency and damping values using cross correlation methodology. The amplitude was fixed to 1 and initial phase value was taken to 0. According to the cross correlation methodology, if the signals are identical, then the correlation coefficient is 1, if they are totally different, the correlation coefficient is 0, and if they are identical except that the phase is shifted by exactly  $180^\circ$ , then the correlation coefficient is -1.

### 3.1.1 Maximum frequency correlation

As the cross-correlation between two signals is a standard approach to feature detection, we picked EDS model based arbitrary signal to correlate with the tympanic signal. According to the equation (2.5), four parameters are needed to generate the signal. At first, we started to find out the optimal frequency value for the arbitrary EDS signal by keeping the damping factor to fixed (zero). Therefore, the four parameters of the arbitrary EDS signal are listed below:

Table 3.1: Simulated signal parameters

<i>SL</i>	<i>Parameters</i>	<i>Values</i>
1	Frequency	Variable
2	Amplitude	1
3	Initial Phase	0
4	Damping	0

The block diagram of cross-correlation procedure is shown in figure 3.1. Here the frequency value increases 1 Hz at every iteration. The cross-correlation function is maximized when the two signals have similar frequency content and are in phase with one another. In this experiment, our target is to get the frequency at which the two signals have maximum correlation. We kept the damping and initial phase fixed to zero (0) for all iterations in this experiment. At some point, we got the frequency value where the two signals have maximum correlation. After calculating the cross-correlation between the two signals, we have collected the frequency at the maximum correlation point. The maximum of the cross-correlation function indicates the point in time where the signals are best aligned. According to the algorithm 3.1 shown here, we can get only the frequency value as we expected.

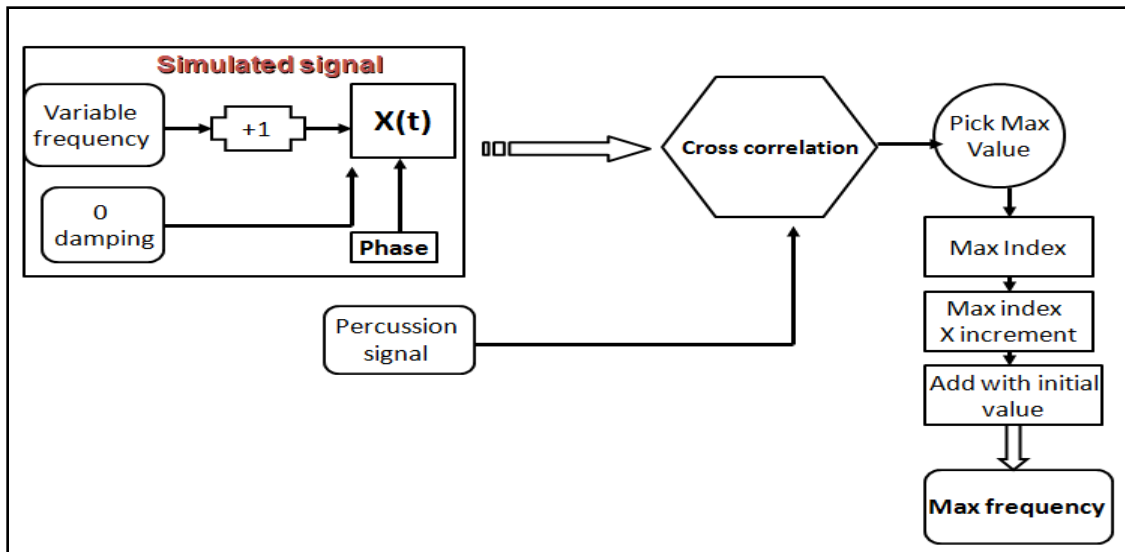


Figure 3.1 Maximum frequency correlation searching algorithm

The recorded maximum frequency is only for the tympanic signal. The arbitrary EDS was our model signal where the model signal are best match with the original signal for this frequency. After measuring the maximum correlated frequency, the next target was to get the damping factor.

### 3.1.2 Minimum damping correlation

The minimum damping value was calculated using cross correlation method. Here we cross correlate the arbitrary EDS signal with a tympanic signal as before. But the parameters selection is different as our target to find out the damping factor. We have the maximum correlated frequency from the previous section and the other two parameters are constant as before (shown in Table 3.2). Now the target is to measure the minimum damping factor based on the cross correlation procedure. We used MSE (Mean Squared Error) method to compare the damping factors of the both signals. MSE is the average squared difference between a reference signal and the real signal. Our reference signal is simulated model signal and the real signal is the tympanic signal.

Table 3.2: Simulated signal parameters

SL	Parameters	Values
1	Frequency	Fixed (maximally matched between the two signals).
2	Amplitude	1
3	Initial Phase	0
4	Damping	Variable: Starts from 5 and increased by 0.2

MSE between the two signals can be calculated using the formula 3.4.

$$MSE = \frac{1}{N} \sum_{i=0}^{N-1} (x_i - y_i)^2 \quad (3.4)$$

Here  $x_i$  is the simulated signal and  $y_i$  are the percussion signals and “N” is the number of sample values. The differences between the two signals are always positive. Therefore, who is first does not matter. The algorithm for finding minimum damping values is shown in figure 3.2.

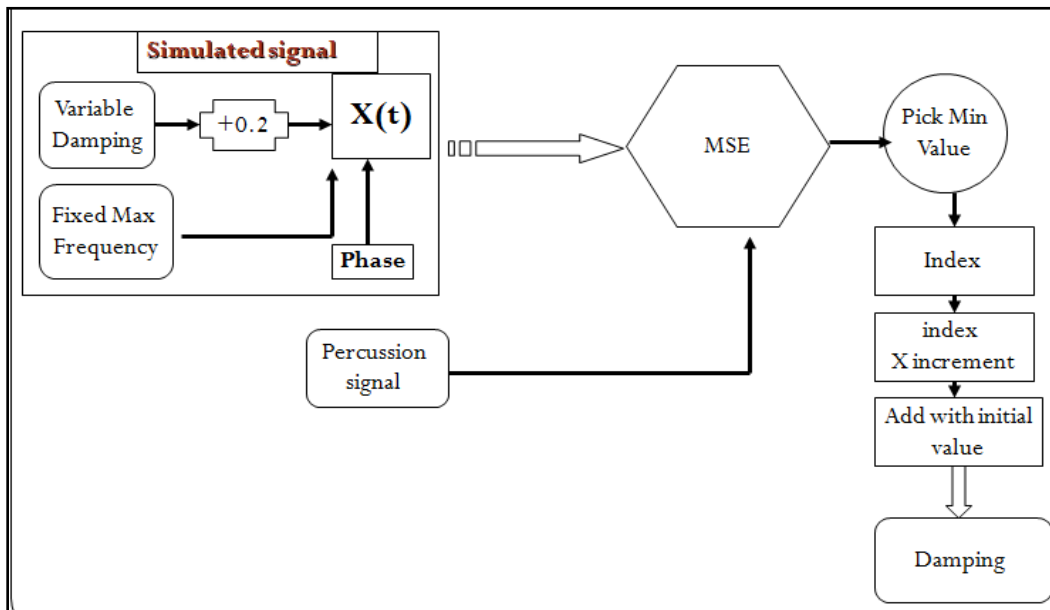


Figure 3.2 Algorithm for minimum correlated damping factor

Here we used the frequency value that we measured in the previous section and varied damping factor from five. We assumed that the damping value of the percussion signal will not be less than 5. We increased the damping value from 5 by 0.2 at all iterations until we hit the correlation value minimum. The MSE calculate the difference between the two signals and find the minimum value at which the signals are correlated. We documented the damping value as our target for the simulated signal that will be similar to our original percussion signal. Now we have all the four parameters for model based signal and the goal is to generate the model signal to compare with the original percussion signal. The generated percussion signal and the original percussion signal are placed together shown in figure 3.6. Before going to the reconstruction part, we like verify the accuracy of then frequency and damping value using most conventional method such as spectral analysis (frequency) and Hilbert transform (damping). This verification procedure shows the measured data accuracy.

### **3.1.3 Verification of damping and frequency value measured using cross-correlation procedure.**

The cross-correlation between model based EDS and original percussion are described in the previous sections. We have found the optimal frequency and minimum damping value for the arbitrary model signal. In this section, the frequency value will be verified using spectral method and the damping value will be verified using Hilbert transform described in the section 3.2. At first, the frequency value is verified for the percussion signals collected from the 30-healthy volunteers. The goal is measure the accuracy of cross-correlation data using another well-known method. Here we choose the Fourier based spectral method. We have done spectral analysis for the percussion signals collected from 30- individual volunteers' abdomen. The Figure 3.3 shows a sample spectrum of a percussion signal collected from the first volunteer's abdomen. This percussion signal is known as tympanic signal. We chose

tympanic signal as its nature like true EDS. We can observe from the figure 3.3 that the maximum frequency (peak) happens before the frequency 200 Hz. We found the maximum frequency (optimum) value is 160 Hz. This procedure followed for rest of the percussion signals. We have plotted the two frequency values collected from cross-correlation procedure and spectral analysis in figure 3.4.

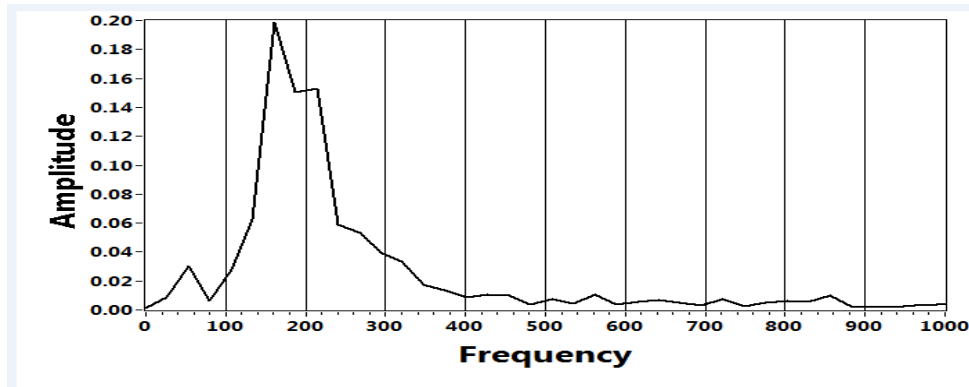


Figure 3.3 Tympanic signal spectrum

It can be observed from the figure 3.4 that there is a close similarity between the frequencies found from spectral analysis and the cross-correlated method.

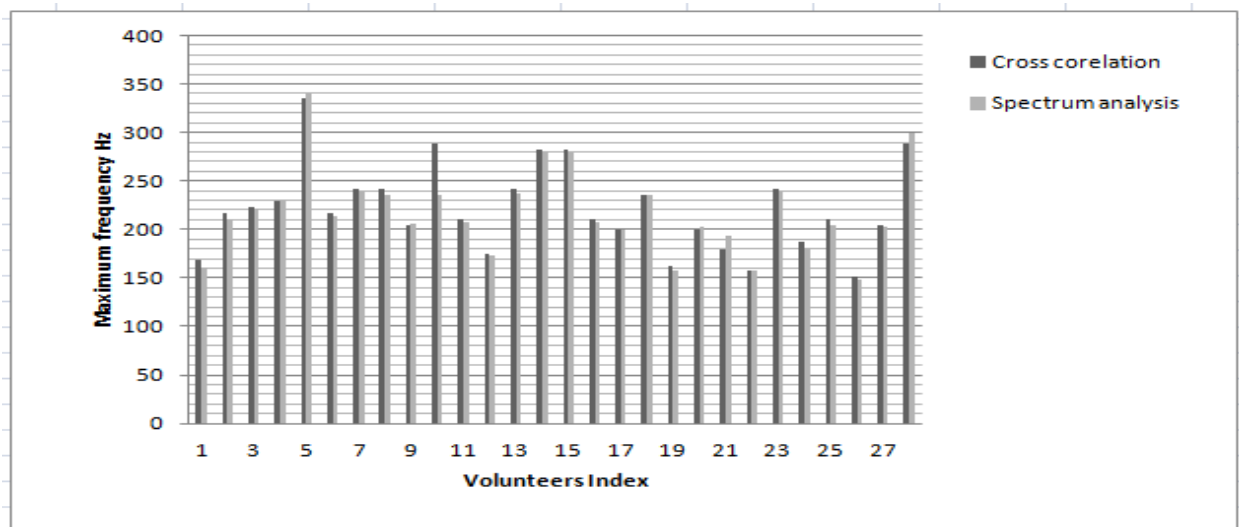


Figure 3.4 Optimal cross-correlated frequency and dominant frequency from the spectral analysis. The grey bar is for the frequency from spectrum analysis and dark bar for the cross-correlated analysis

The bar graph shows the frequency values ranged from 160 Hz to 350 Hz. We can assume from the figure that cross correlation values are justified. Now the second step is to verify the damping values that we got from the cross correlation procedure. The cross correlation procedures for searching damping values are described in the section 3.1.2. We have done the same procedure for the percussion signals of all 30 individual volunteers. Here it needs to be mentioned that the signals are collected from the abdomen named as tympanic. The damping values found in both methods for the signal of 30-individual volunteers are plotted in figure 3.5. The signals collected from the volunteer number 14 and 24 were corrupted. As such, the two damping values are different from others.

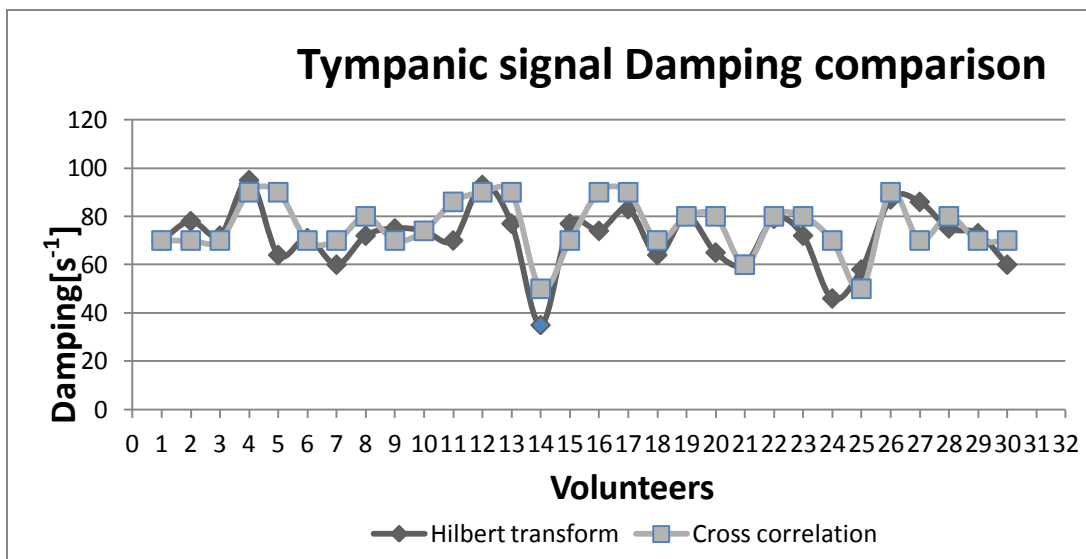


Figure 3.5 Tympanic signal damping values measured by cross correlation and Hilbert transform.

It can be noticed from figure 3.5 that the damping values found from cross-correlation procedure varies between 60 and 90. Now we like to see the accuracy of the damping values found from the cross-correlation procedure. We decided to use the well-known Hilbert transform to find out the damping value of the percussion signals. The procedure for

calculating damping values using Hilbert transform are described in the section 3.2. We can comment on the damping values accuracy found from cross-correlation procedure and Hilbert transform plotted in figure 3.5. The damping values found from two methods are pretty matched.

### 3.1.4 Tympanic signal reconstruction

We generate a tympanic signal based EDS model. According to our EDS model, four parameters are needed for generating a percussion signal. We have all the four parameters described in the above sections. We have described the ways of finding the optimal frequency and minimum damping value using cross-correlation method in the previous sections. The other two parameters (amplitude and initial phase) are assumed constant here. If we put these four parameters value in model equation, we will be able to get the tympanic signal. The generated tympanic signal is shown in figure 3.6 in white color.

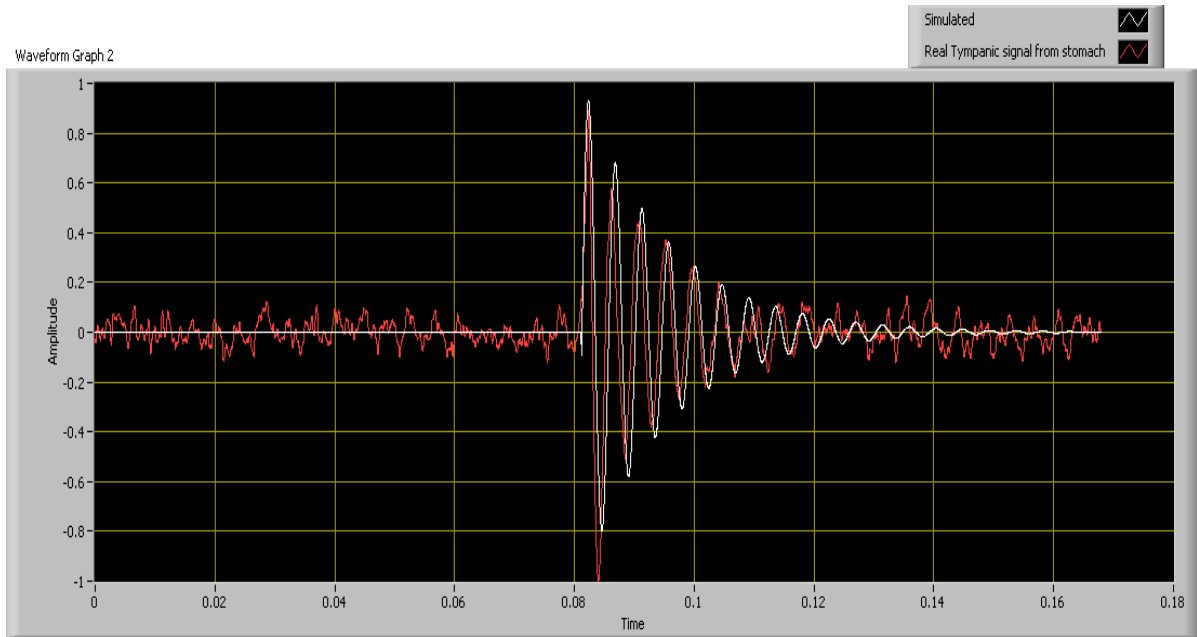


Figure 3.6 Reconstructed tympanic signal and original tympanic signal

We plotted the reconstructed signal and the original tympanic signal together in figure 3.6. The figure 3.6 shows that the two signals are visually well matched. We can comment from the above analysis that tympanic signal can be recognized based on cross-correlation procedure. However, it is very difficult to recognize the resonant signal as it doesn't hold clear damping characteristics. Now we like to describe the Hilbert transform that we chose for verification of cross-correlated damping values. The calculation of damping value based on Hilbert transform will be discussed in the next sections.

## **3.2 Hilbert transform**

The Hilbert Transform computes a time-domain signal that is 90° "out of phase" with the input signal [37]. In this study, the Hilbert transformation is used to investigate the damping factors of the percussion signals. Here we used the original tympanic signal. Tympanic signal contains a rapidly oscillating component. The amplitude of the oscillation varies slowly with time, and the shape of the slow time variation is called envelope. The envelope contains important information about the signal. The damping value of the percussion signal can be calculated from its envelope. In order to create an envelope of the percussion signal we need to create envelope of the signal. Envelope creation is based on the analytical signal. Next section analytical signal will be discussed before calculation the envelope.

### **3.2.1 Analytic signal**

Hilbert transform is used to create analytic signal, where the real part is the original signal and the imaginary part is the Hilbert transform of the original signal [37]. It is often useful to utilize the orthogonality relationship between the real signal and imaginary part of the complex signal. An analytic signal can be defined as

$$X_+(t) = x(t) + j\bar{x}(t) \quad (3.5)$$

Where  $x(t)$  is the input signal and its Hilbert transform is  $\overline{x(t)}$ . Therefore, the analytical signal  $X_+(t)$  will have the form shown by equation 3.5. The real and imaginary parts of the analytical signal can be expressed in polar coordinates form:

$$X_+(t) = A(t)e^{j\theta(t)} \quad (3.6)$$

Where

$$A(t) = \sqrt{x^2(t) + \overline{x^2(t)}} \quad (3.7)$$

$$\theta(t) = \arctan\left(\frac{\overline{x(t)}}{x(t)}\right) \quad (3.8)$$

Where,  $A(t)$  is the “envelope” or amplitude of the analytic signal and  $\theta(t)$  is the phase of the analytic signal.

### 3.2.2 Damping value calculation using signal envelope

The envelope is the overall shape of the amplitude maxima of an EDS signal [37]. If the signal is considered as a rotating vector, then the length of the vector is the envelope of the signal. The projections of the rotating vector on the X and Y-axes are its real and imaginary parts. However, we know the real and imaginary parts are 90 degree apart in geometry. The envelope of a signal is the outline of the signal [37]. We mentioned earlier that the Hilbert transform would be used to create envelope of the medical percussion signal. The block diagram (figure.3.7) is described the procedure to create an envelope of the percussion signals. Here analytic signal is used to create envelope.

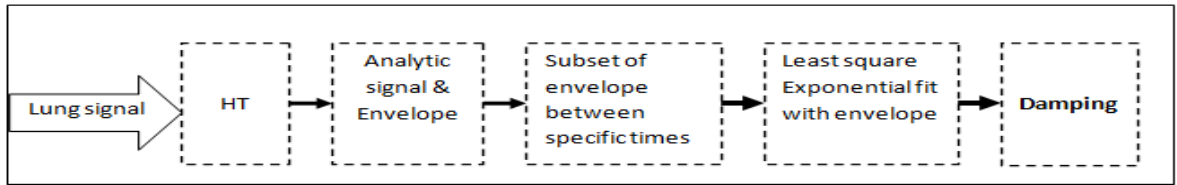


Figure 3.7 Block diagram of Hilbert transform envelope creation and damping calculation

The envelope of the signal can be found by taking the absolute value of the analytic signal. The above block diagram in figure-3.7 shows in details the envelope creation procedures using Hilbert transform. A sample envelope over the real tympanic signal is shown in figure 3.8. The red color waveform is the original signal and the black color line is the proposed envelope for the signal.

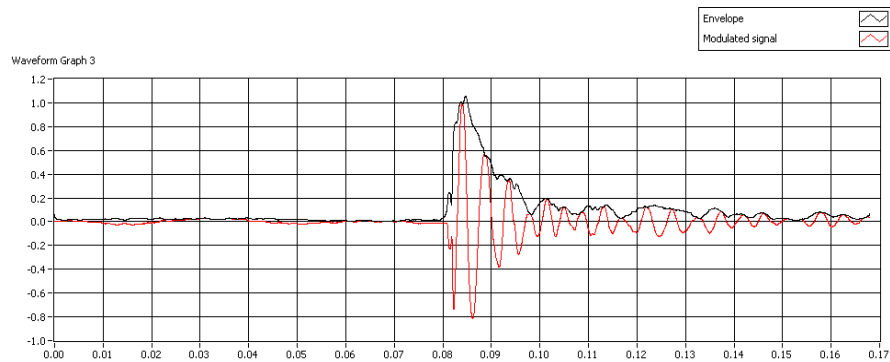


Figure 3.8 Envelope of a percussion signal (Tympanic)

The decay rate of the envelope is a dominant feature to calculate the damping of percussion signal. The envelope connects all the peaks of the percussion signal shown in figure 3.8 and show how the signal decays from its initial peak. After completing Hilbert transform of the percussion signal, the subsets of the envelope were calculated for a specific time. The start and end of the sample time were introduced for getting the exact waveform subset. We did assign the time stamp for specifying a specific time stamp to start and end. We considered the start point of the envelope is 0.085 s and the end is 0.12 sec. The portion of the signal is

our desired subset of the envelope. We have calculated the damping values of all percussion signals using Hilbert transform. We plotted these damping values in figure 3.9.

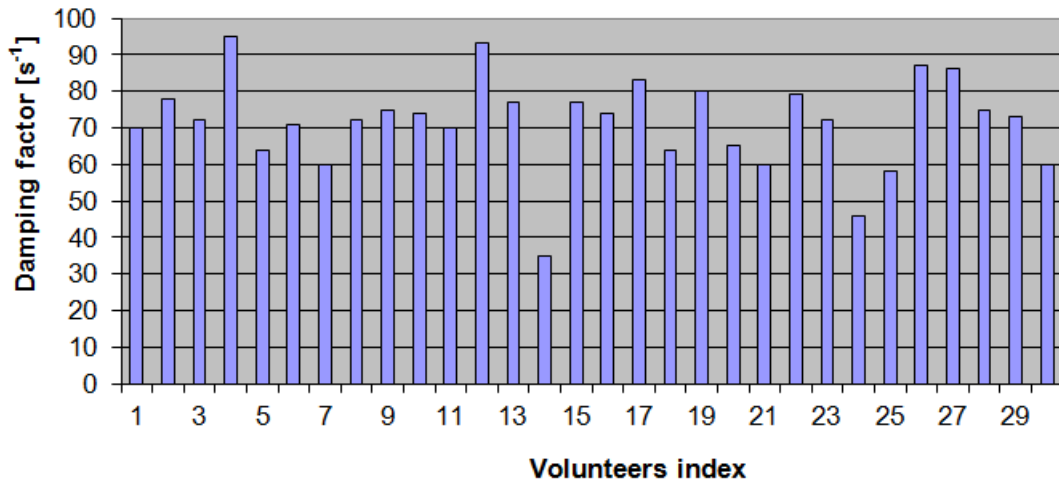


Figure 3.9 Tympanic signal damping values calculated based on Hilbert transform

Here, the envelope is isolated the decay portion used to find the best exponential curve fit described. The best-fit criterion is the minimization of least square differences between the curve and signal envelope, subject to the conditions that such a curve coincided with the envelope of the value at the maximum amplitude point [37].

### 3.3 Summary

This chapter describes the initial attempts to represent the medical percussion signals based EDS model. Here the attempts were taken based on the idea that the percussion signals contain a single EDS and attempts were taken to find out the corresponding parameters value of that EDS. The two parameters such as frequency and damping factor found based on the EDS model fitting to the real percussion signals. Initially, Cross correlation procedures were used. In this procedure, optimum frequency and minimum damping values were calculated for the EDS based model signal, where amplitude and phase were fixed. After

getting all the four parameters of the EDS model signal, a damped sinusoidal signal was generated based on those parameters. As expected, this procedure worked quite well for the simplest tympanic signals, and allowed to get the idea about the dominant frequency and damping factor of a tympanic signal. However, the task of fitting the EDS model to a resonant signal is much more complicated. Then we decided not to use the cross correlation technique for analyzing the percussion signals for the following reasons:

1. Cross correlation with an EDS provides a very coarse fit for most typical types of percussion signals. The algorithm was also very difficult to accommodate changes from signal to signal.
2. It was very difficult to get the frequency and damping for the resonant signal.
3. Amplitude and phase always assumed fixed here.
4. Real percussion signals consist of several EDS. However, here assumed a single EDS fitting procedure would not give the overall characteristic of the signals.

Considering all the above points, it is clear that this solution is not the perfect one for an efficient recognition of percussion signals. It could be an apparent solution of the actual solution only for the tympanic signal. As expected that the percussion signals contain several EDS, so the next research focus is to find out all the EDS from the percussion signals according to model of the percussion signal described in chapter 2. Based on this hypothesis, we decided to perform the decomposition of the percussion signals. We proposed EDS model for the percussion signals in the previous chapter. Therefore, model based signal decomposing would give all the parameters of constituent EDS to best fit the original signals. Before decrying the decomposition technique, the percussion signal noise cancellation procedure will be discussed in the next chapter.

# Chapter 4

## Analysis of noise in clinical percussion signals

---

### 4.1 Introduction

The term “noise” is commonly used to describe signal distortion. Signal noise is an unavoidable error source that reduces the quality of the measured signal significantly [38]. The main task of processing clinical percussion signals is to filter the signal of interest out of the noisy background and to extract from the pure signal a few representative parameters that could be used for subsequent signal classification and diagnostics of pathologies. Over the past two decades, the development in digital signal processing has resulted in a wide variety of noise removal techniques in a variety of practical applications. Unfortunately, there is no literature addressing the removal of noise from clinical percussion signals. Even the notable work by Murray and Neilson [1] did not focus on the elimination of noise from measured percussion signals. The level of noise in the measured data determines the reliability and the success of the analyses. The nature of the noise is rather complex, as the contributing factors are diverse and often not well understood. The noise can be completely random (white noise) or correlated (with itself or sometimes with the signal). In terms of frequency, it can be broadband (e.g. white noise) or concentrated in certain frequency bands (colored noise). A typical example of the latter is the 50Hz or 60Hz sinusoidal noise from the electrical mains [38]. In signal processing, white noise is a random signal with a flat (constant) power spectral density [38, 39]. White noise is evenly spread across all frequencies, whereas pink noise is noise with a flat spectrum within a certain frequency band [38]. An example of white noise often encountered by engineers is thermal noise [38]. All

electronic components, particularly resistors and semiconductors, generate electrical noise from the random motion of electrons, depending on the temperature [38]. Reducing the level of noise in clinical percussion signals could significantly improve the quality of the measured data, hence can increase the reliability of the signal analysis. This task is addressed by carefully designing the measurement equipment, using appropriate data collection procedures, as well as by applying analog and digital filtering techniques to the recorded signals. Multiple techniques are required as multiple sources of noise are present. The possible sources of noise in clinical percussion signals are discussed in the next section.

## 4.2 Noise in clinical percussion signals

Experimentally recorded audible percussion signals contain noise originating from the measurement equipment and the environment [39].

- **Ambient noise:** The ambient noise is a term for all extraneous sounds in the room, except the percussion sounds, that are picked up by the microphones and representing a sort of pollution in the receiver channel [39]. It typically includes a the rumble of the air conditioning or heating system turning on, hissing of the air blowing from the vents, the shuffling of the test participants in the room, medical personnel and patients walking in the corridor, traffic noise, alarms, and people talking [39]. The listed sources of ambient noise typically result in a constant, time-independent background noise, but can also create short, time-dependent bursts of noise with regular or random appearance. In the experiments described in this work, the ambient noise can be considered linear and additive. The mechanical noise from devices such as, refrigerators, air conditioning, power supplies and electrical motors.
- **Electronic noise:** For the percussion signals collected from healthy volunteers in hospital setting, the most significant sources of noise were the microphone/tripod

shaking due to vibration of the hospital building (moving elevators, etc.), pre-amplifier noise, ADC quantization noise, EM interference from computer components and other equipments in the room and the 60 Hz AC component from the computer power supply [39]. This type of noise is weak compare to the ambient noise.

In other words, the noise is independent of the amplitude of the (useful) percussion signal and is simply added to the percussion signal, received with the microphone. For all percussion signals recorded with the air microphone the described ambient and vibration noise was clearly dominant over the noise from electronic components, such as preamplifier noise, analog-to-digital conversion noise, etc. The 60 Hz noise from the AC power line was another strong contributor until we switched to battery-powered devices.

## **4.2.1 Noise spectrum of clinical percussion signal**

The signal collection procedures were discussed in section 2.1 and assumed the noise can be considered quasi-stationary, and therefore its spectral content should be approximately the same in different recording frames. Then it should be possible to judge about the noise in the signal by measuring the spectrum of the audio buffer contents captured prior to the percussion event and representing pure noise [22, 39, 44]. As the noise can also be considered additive, the spectrum of the original signal can be estimated by a spectral subtraction method [39, 44]. For this purpose, the equipment was set up to record a 62.5 ms-long (3000 samples) noise segment preceding the signal segment of the same length. For spectral comparison, both segments were windowed with a flat-top cosine window (using ratio of 0.05) to suppress the edge discontinuities due to cutting. The amplitude spectra of the chest signal and of the preceding noise segment are plotted in Fig. 4.1. The difference spectrum is shown as well. It can be seen that in the 50-600 Hz frequency range the noise power does not exceed 0.1% of the peak spectral power of the signal (3% of the peak

spectral amplitude). The raw and difference spectra are nearly identical, and hence all spectral peaks essential for our analysis are real features of the signal and not the noise-related artifacts.

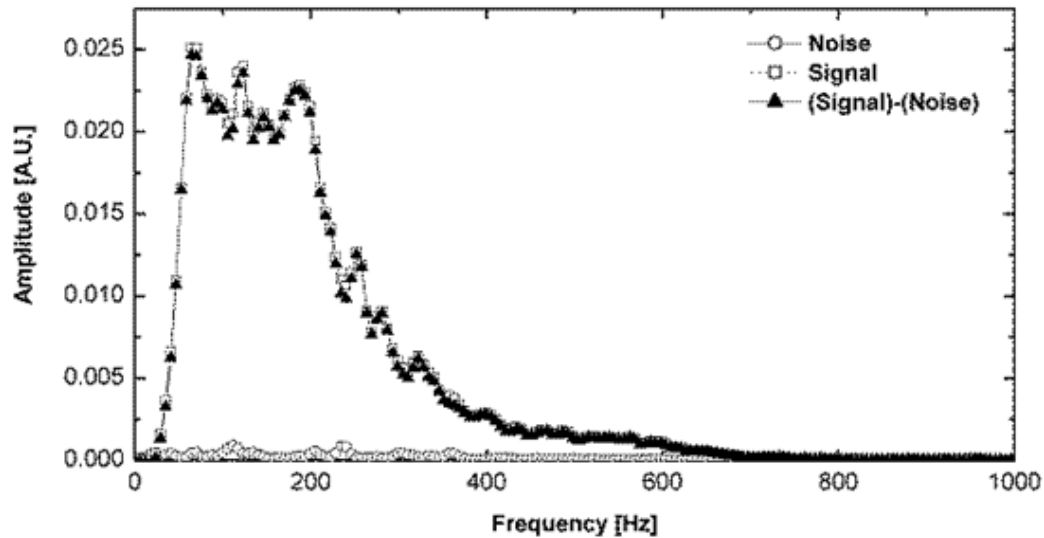


Figure 4.1 Amplitude spectrum of a resonant signal before and after subtracting the noise spectrum, which is shown as well.

Although the noise is not a big obstacle in the frequency domain, its time domain properties should be evaluated separately as they are critical for the MPM performance (see section 4.3 below). Hence, in order to separate the “real” EDS from those that MPM may artificially introduce in an attempt to fit the noise, we apply various empirical post-filtering approaches. For example, we discard the EDS lying outside the signal’s frequency band, as well as those with too low amplitudes or too high or negative damping. Although these procedures are helpful to some extent, the only radical way to cope with this problem is by improving the raw SNR, such as via signal averaging or detector optimization. The noise cancellation procedures will be discussed in the section 4.4. Before noise cancellation part, it necessary to

discuss the signal preparation as the percussion signal is not ready to plug to Matrix Pencil Method.

### **4.3 Signal preparation**

The medical percussion signals require preprocessing before they can be analyzed with the Matrix Pencil Method. The original medical percussion signals are shown in Figure 2.2. It can be seen that some portion at the beginning of the captured waveform and some portion at the end of it contain only noise. These portions are usually discarded from further analysis, since only the middle portion of the captured waveforms contains the actual percussion signal. To accurately identify and cut out this useful portion of the waveform one has to find the start and the end points of the signal among the noise. To find the signal start point we first estimate the noise level by examining a (usually discarded) section of the waveform preceding the signal. Based on the mean and standard deviation values of the noise in this section we establish an amplitude threshold  $\varepsilon$  and then look for the first point in the waveform exceeding that threshold. The flow diagram 4.2 shows the algorithm. Then we go back, sample by sample, until we find the first zero crossing with an appropriate sign of the slope (positive or negative). This point is declared the signal starting point. After examining all collected percussion signals, it was decided to discard first 3800 (at least) points from the beginning of the signals before searching for the onset point. These first 3800 points (at least) contain only noise, with maximum amplitude never exceeding 0.025 (the signals were normalized to 1), so we chose a searching threshold  $\varepsilon = 0.025$ . The total duration of recorded digital waveforms was  $\sim 170$  ms (8192 samples at 48 KHz).

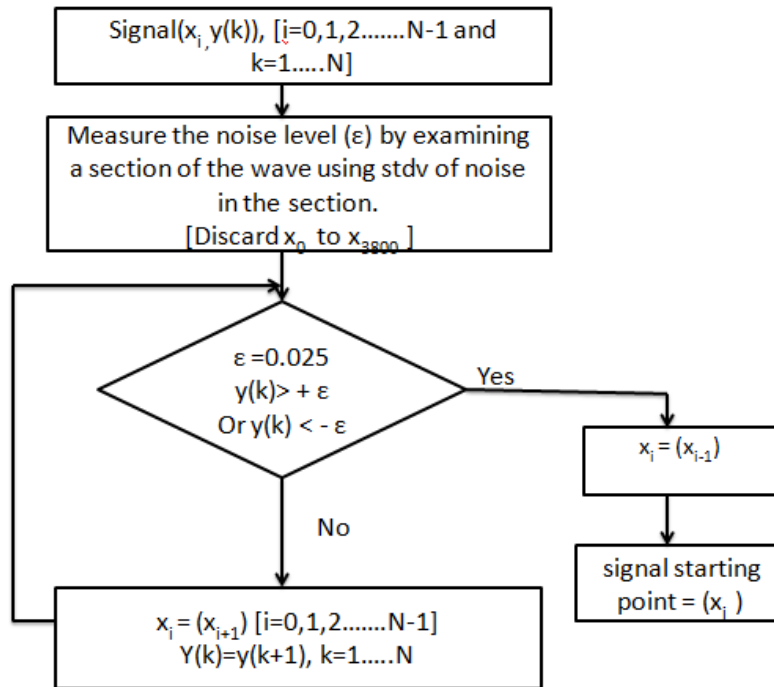


Figure 4.2 Signal preparation flow diagrams

However, due to damping, the actual duration of the signals is much less and changes from signal to signal (see Figures 2.2.a and 2.2.b). Determining the end point of the signal window is important for the success of subsequent MPM analysis. Indeed, the SNR of the clinical percussion signals is not constant but changes with time together with the signal's envelope. The signal amplitude is highest at its onset and then drops, as the signal fades out due to damping. For example, it is important to know the time interval after which the SNR drops below 20 dB to determine the end point of the signal window. It was found experimentally that for most signals in this work this condition is satisfied only within a 10-12 ms window (500-600 points), which is too short to capture the essential signal features. A 40 ms window is usually long enough to capture most percussion signals, but the SNR at its end often drops below 10 dB. In this work, we always keep 2048 points (~42 ms) out of 8192 samples, which is enough to accommodate the longest tympanic signal we have ever encountered in our

practice. With such a long window, the low SNR at the end begins to cause additional issues, which we have to deal with while designing the MPM procedure.

## **4.4 Noise cancellation procedures**

### **4.4.1 Signal conditioning**

As pointed out in [47], even though the MPM can filter out part of the noise by discarding the non-principal singular vectors of the data matrix, some effects of noise still exist in the principal singular vectors. Thus, noise reduction prior to applying the MPM is desirable. Below we describe several quite general signal-conditioning techniques applied to all percussion signals for their initial cleanup and standardization. For example, the 60 Hz ac component was removed by switching to battery operation. The spectral peak at 25–30 Hz caused by the building vibration was suppressed by applying a 50–1000 Hz Butterworth band-pass filter to the digitized signal. This filter provides no ripples in the pass-band and a zero roll-off response in the stop-band. Since the Butterworth filter is frequency-based, the effect of filtering can easily be understood and predicted. The high cutoff frequency and low cut off frequency of Butterworth filter were set 1000 Hz and 50 Hz respectively. Further pre-filtering would require extra care as the frequency band of the ambient noise often overlaps with that of the original signal.

A DC offset in the digitized percussion signals is undesirable mostly because it creates a strong zero-frequency peak in the Fourier power spectrum. Figure 4.3 shows the D.C offset removal and pre-filtering diagram applied to all signals as a part of their preconditioning. As the real signal and noise are naturally expected to have a zero mean value, the DC offset is computed as the mean amplitude of the waveform and then subtracted from each sample of

the percussion signal. After the DC offset removal, the percussion signal is sent to the Butterworth band pass filter, as shown in Figure 4.3.

$$\mu = \frac{1}{n} \sum_{i=0}^{n-1} x_i \quad (4.1)$$

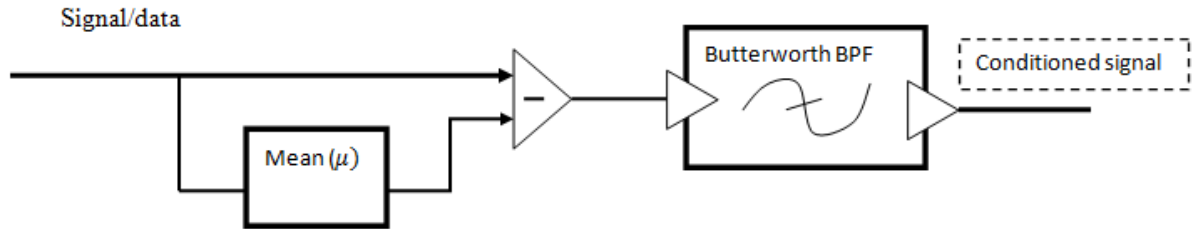


Figure 4.3 Percussion signals conditioning steps

Butterworth filters sacrifice roll off steepness for monotonicity in the pass and stop band. After conditioning the signal, the next step is to use Hankel-SVD filter to further reduce the amount of noise. However, before applying this filter we have to down sample the percussion signal, as the signal is still oversampled. At this stage, the total number of samples in the signal is 2048. In order to use Hankel-SVD filter, we have to reduce this number using appropriate decimation techniques discussed in the following section.

## 4.5. Configure decimation filter

The purpose of the decimation operation here is to prepare the signal for using the SVD filter and Matrix Pencil Method. The percussion signal is oversampled, as the sampling frequency is significantly higher than twice the bandwidth or the highest frequency of the signal being sampled. Though oversampling helps avoid aliasing, improves resolution and reduces noise, the large number of samples is prohibitive for the real-time MPM analysis. The figure 4.4 is the block diagram of down sampling of the percussion signals [45].



Figure 4.4 Multi-rate processing of percussion signals

The D-fold decimator takes an input  $x(n)$  and produces output  $y(n)$ .

$$y(n) = x(Dn) \quad (4.2)$$

Where, D is an integer. We can write output  $Y_D(e^{j\omega})$  in terms of  $X(e^{j\omega})$  as

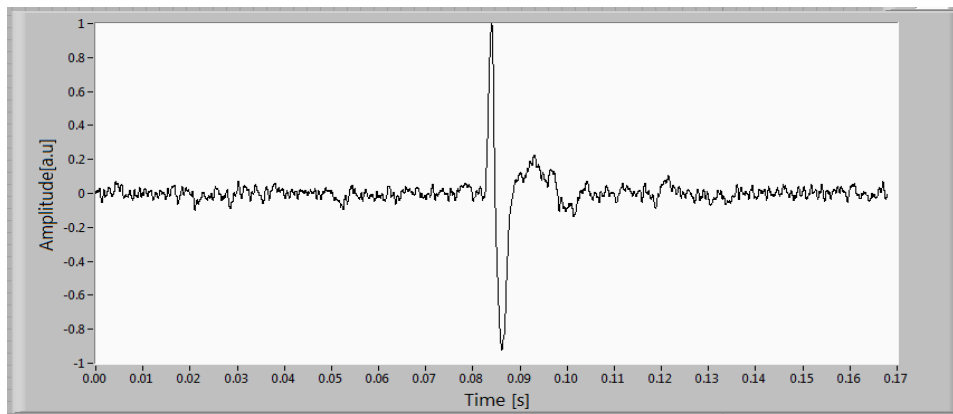
$$y(e^{j\omega}) = \frac{1}{D} \sum_{k=0}^{D-1} X(e^{j(\omega - 2\pi k)/D}) \quad (4.3)$$

This can be graphically interpreted as follows: (a) Stretch  $X(e^{j\omega})$  by a factor D to obtain  $(e^{j\omega/D})$ , (b) create D-1 copies of the stretched version by shifting it uniformly in successive amount of  $2\pi$  and (c) add all these shifted versions to the un-shifted stretched version  $X(e^{j\omega/D})$  and divide by D [38,39]. One of the most important issues in down sampling is to maintain the Shannon-Nyquist criteria in order to maintain the signal aliasing-free. If this sampling theorem does not satisfy then the resulting digital signal will have aliasing. The aliasing created by the decimation can be avoided, if  $x(n)$  passed through low pass filter before decimation and decimating signal is band limited to the region  $|\omega| < \pi/D$ . To satisfy the sampling theorem, a low-pass filter is used as an anti-aliasing filter to reduce the bandwidth of the signal before the signal to be down sampled (figure 4.4). The filter ensures that the signal being decimated is band limited. Table 4.1 shows the data that we used for decimation purpose.

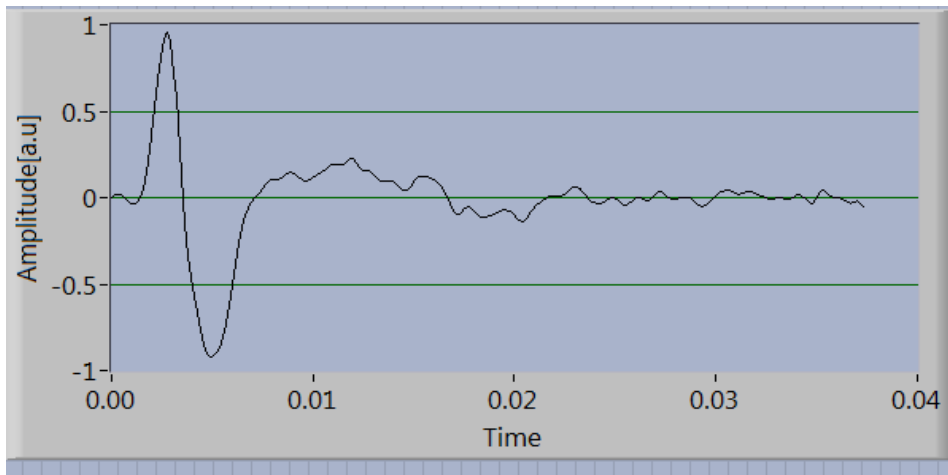
Table 4.1 Decimator filter [H (z)] design data

Filter	Equi- ripple FIR filter
Input sampling frequency	48.780 KHz
Decimation filter factor (D)	4
Output sampling frequency	12.195 KHz
Pass band edge frequency	1KHz
Stop band edge frequency	1.4 KHz
Pass band ripple	0.002 dB
Stop band attenuation	60 dB

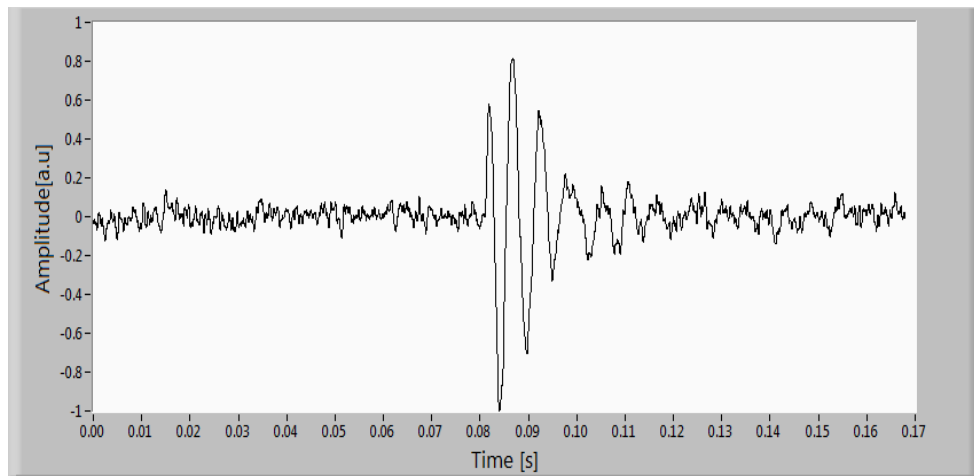
It is also noted that down sampling only changes the sample rate not the bandwidth of the signal. We used the LABview DFD MRate filtering Tool kits and Multi-rate FIR filter for decimation purpose [45]. After executing the Mrate signal processing operation, the sampling frequency is reduced to one fourth of the original rate in process called down-sampling. Now, the output sampling frequency is converted to 12.195 KHz, and the total number of samples comes down to 512 after decimation operation. The percussion signals before and after conditioning are shown in figure 4.5.



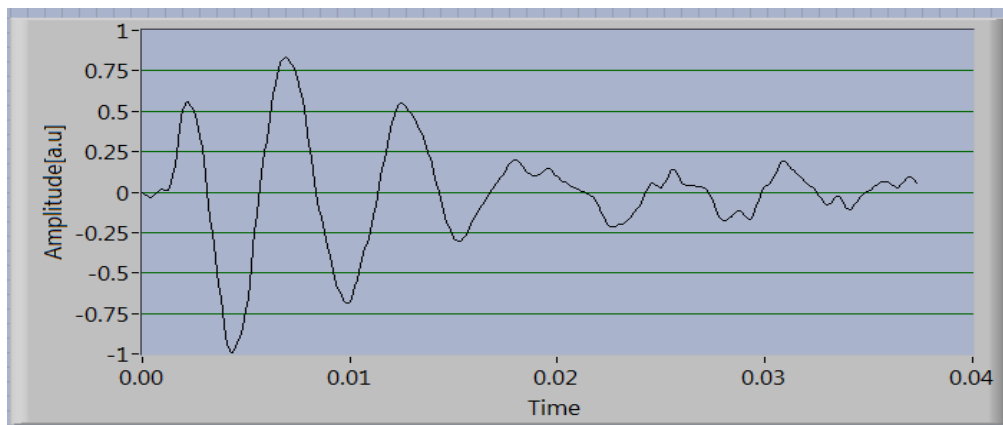
(a) Resonant Signal: Before conditioning



(b) Resonant Signal: After conditioning



(c) Tympanic Signal: Before conditioning



(d) Tympanic signal: after conditioning

Figure 4.5 Percussion signals before and after conditioning

The conditioned signals are clean and contain only the informative part of the signal fewer samples. After execution all of the above preprocessing operations, the percussion signals are ready for the SVD analysis as well as for the MPM decomposition. The next section discusses the noise cancellation mechanism of the Matrix Pencil Method using SVD method.

## **4.6 Percussion signal noise cancellation technique using Singular Value Decomposition (SVD).**

### **4.6.1 Introduction**

The noise effect is very challenging in medical percussion signals. Practical considerations such as additive noise presence and computational inaccuracies results in a need to estimate the number of significant EDS. It is usually not enough to just filter the signal because:

1. In practical measurements, the received percussion signals contain noise, which complicates the recognition task and makes the classification unreliable.
2. The band pass filtering (BPF) method reduces the level of noise by considering some prior assumptions. For example, when using BPF, it is assumed that the noise limited to the specific frequency band, which does not overlap the signal's frequency band.

The band pass filter used for conditioning of the percussion signals only helps better emphasize their physical frequency range (50-1kHz). It is inherently assumed here that the spectral contents of both percussion signals and the noise fall within this frequency band. Hence, the same filter is applied to all captured signals. Nonetheless, noise suppression would likely be more effective if the filter stop band could be selected adaptively according to the local noise characteristics of the individual signals. By considering the above-mentioned reasons, we decided to choose the eigen

vector-based Matrix Pencil Method that uses SVD for reducing inherent noise in the signals.

## 4.6.2 SVD background

Singular Value Decomposition (SVD) is a way of factoring matrices into a series of linear approximations that expose the underlying structure of the matrix [42]. It decomposes a matrix into a product of three simpler matrices [40, 41]. The singular value decomposition is used to reduce the dataset containing a large number of values to a dataset containing significantly fewer values, but which still contains a large fraction of the variability present in the original data [42,43]. Since SVD was developed to extract useful information from noisy signals, it has been widely used in speech, image, mobile communication, and electric power applications [42, 43]. SVD based algorithm is a nonlinear filtering method by which a noisy matrix derived from the data is decomposed to get the “signal” part and the “noise” part [42]. The basic idea behind this approach is to approximate the matrix derived from the noisy data, with another matrix of lower rank from which the reconstructed signal is derived [43]. The number of nonzero singular values from its SVD can directly determine the rank of a matrix [40, 42,43]. The Hankel Matrix is formed from the noisy data and reduced its rank by SVD [42]. The high-energy components are supposed to contain only signal, whereas the low energy components are supposed to contain only noise [40,42]. We used the singular value decomposition (SVD) algorithm to express percussion signals in terms of a few basic functions. In this section, we discuss the SVD approach to observe the noise in data. First we look at the distribution of singular values of the percussion signals, one-step before the calculation of complex exponentials in MPM. These singular values, although remotely related with complex exponentials, carries as much information about the model as complex exponentials.

### **4.6.3 Square Hankel matrix issue**

For a given data with a sample number of  $N$ , a square or a nearly square Hankel matrix can be constructed. A square Hankel Matrix is symmetric. However, it is neither necessary nor desirable to construct a square or nearly square Hankel matrix for practical applications of the method [42]. Instead, a rectangular matrix with appropriate selection of the smaller dimension can be used effectively [42]. Provided that the smaller dimension, i.e., the maximum possible rank, is large enough to represent the system behavior including the effect of noise [46]. The reason for this is that nearly square Hankel matrix may require unnecessary computations while inadequate setting of the maximum possible rank of the system may cause loss of performance [42]. It is seen that if the number of columns is less than the rank of the system, the Hankel matrix will not be capable of representing the system [41,46]. Hence, it will not be possible to identify the noise threshold. On the other hand, appropriate settings of the matrix dimensions lead to an asymptote that in turn leads to the identification of the noise threshold [46]. It is obvious that a square or nearly square Hankel matrix is preferred if the computation cost is not an issue.

### **4.6.4 Reduced rank approximation**

The rank of a matrix is the dimension of the space spanned by its columns. It is also the number of non-zero singular values. It happens often that a most of the non-zero singular values of a large matrix are very small compared to the largest ones. Setting the small singular values to zero results in a matrix not much different from but with much smaller rank [46]. Furthermore, that procedure produces the optimal low rank approximation of the matrix in the least squares sense [41]. This is one of the most important uses of the SVD in practice. The main step in reduced rank noise reduction algorithm is to approximate a matrix by another one with lower rank [41,46]. Full rank SVD recreates the underlying matrix

exactly, whereas lower-order SVD provides the best (in the least square error sense) approximation of a matrix by orthogonal row and column factors [42]. The key idea is to form a Hankel matrix from the noisy data, then implement SVD on the proposed Hankel matrix, and discard the smaller singular values those are known a noise. These lower-order approximations to the larger matrix may uncover interesting relationships among the rows and/or columns of the underlying matrix [42]. It is also worth mentioning that the rank of the Hankel matrix is related to the number of modes affecting the measured data, i.e., number of modes within the frequency range of interest plus the number of residual modes [46].

### 4.6.5 SVD Theory

We consider the noisy signal  $Y = [x(0), x(1) \dots \dots \dots x(N - 1)]^T$  contains N samples.

$$Y[kT_s] = X[kT_s] + n[kT_s] \quad (4.4)$$

Let us consider the Y Hankel matrix which is directly obtained from  $x(kT_s)$ , and each column of Y is a windowed part of the original data vector  $\{x(0)x(1)x(2) \dots \dots \dots x(N - 1)$ . Where  $T_s$  is normalized here. An  $N \times N$  Hankel matrix which is determined by its last row and first column, total of  $2N-1$  entries, in contrast with  $(N^2 + N)/2$  entries for general symmetric matrix. Due to the special structure of the Hankel matrix, its matrix-vector multiplication can be performed in  $O(n \log n)$  flops using the fast Discrete-Fourier Transform (DFT) [46]. We can construct the Henkel matrix of rows  $(N - L - 1)$  and column L illustrated as follows

$$Y = \begin{bmatrix} x(0) & x(1) \dots & x(L) \\ x(1) & x(2) \dots & x(L + 1) \\ \vdots & \vdots & \vdots \\ x(N - L - 1) & x(N - L) & x(N - 1) \end{bmatrix}_{(N-L) \times (L+1)} \quad (4.5)$$

According to SVD theorem, if  $Y \in R^{L \times M}$  with  $L \geq M$ , then there exist matrix  $U \in R^{L \times M}$  and  $V^T \in M^{M \times M}$  with orthogonal columns such that



subspace would be  $Y_S = U_S \Sigma_S V_S^H$  and the noise sub-space  $Y_N = U_N \Sigma_N V_N^H$  respectively. By subtracting  $Y_N$  from  $Y$ , we can get the estimated data matrix suppressed noise. These  $r - M$  smallest singular values of  $Y$  are not important for the signals [51]. The lower singular values can be removed, selecting a lower rank matrix  $Y$ . Here, SVD distinguish between significantly small and insignificantly large singular values (SV's). Furthermore, it is significantly very important to know how the selection of singular values affects the performance of de-noising techniques.

$$[U]^H [Y] [V] = [\Sigma] \quad (4.10)$$

Next, we will describe the threshold technique to select the signal part in the signal and separate the noisy part.

#### 4.6.6 Threshold value

As we mentioned before, the selecting the values of the parameters  $L$  and  $M$  is very important in order to obtain the correct number of EDS. Here,  $L$  is called the pencil parameter and  $M$  is the number of Exponential Damped Sinusoids (EDS). We use the thresholding technique to identify the signal part and the noise part in the noise-contaminated signals [47]. This step is very important as the lower value of  $M$  results in the information loss, while a greater value of  $M$  leads to a matrix, which is not absolutely noise free. Generally, the noise causes all the singular values of the Hankel matrix to be non-zero. Threshold technique is for distinguishing between significant and non-significant singular values. The criterion for selecting the significant modes is given by equation 4.11 [39,47,51,64,71,74]. It refers to the ratio of dividing all singular values by the highest singular value. It is noted that the first singular value is the maximum by default. Here we define the ratio as follows:

$$\frac{\sigma_c}{\sigma_{max}} = 10^{-p} \quad (4.11)$$

The parameter  $p$  is typically chosen in respect to the desired accuracy. If the data is accurate up to 3 significant digits, then the singular values for which the ratio is above  $10^{-3}$  are of interest. The value lower than  $10^{-3}$  is typically considered as noise. The filtered matrix  $[V']^T$  only contains  $M$  dominant right singular vectors of  $[V]$ . The noise filtering mechanism is shown in the figure 4.6. We can get the noise part as well as signal part by using the algorithm shown.

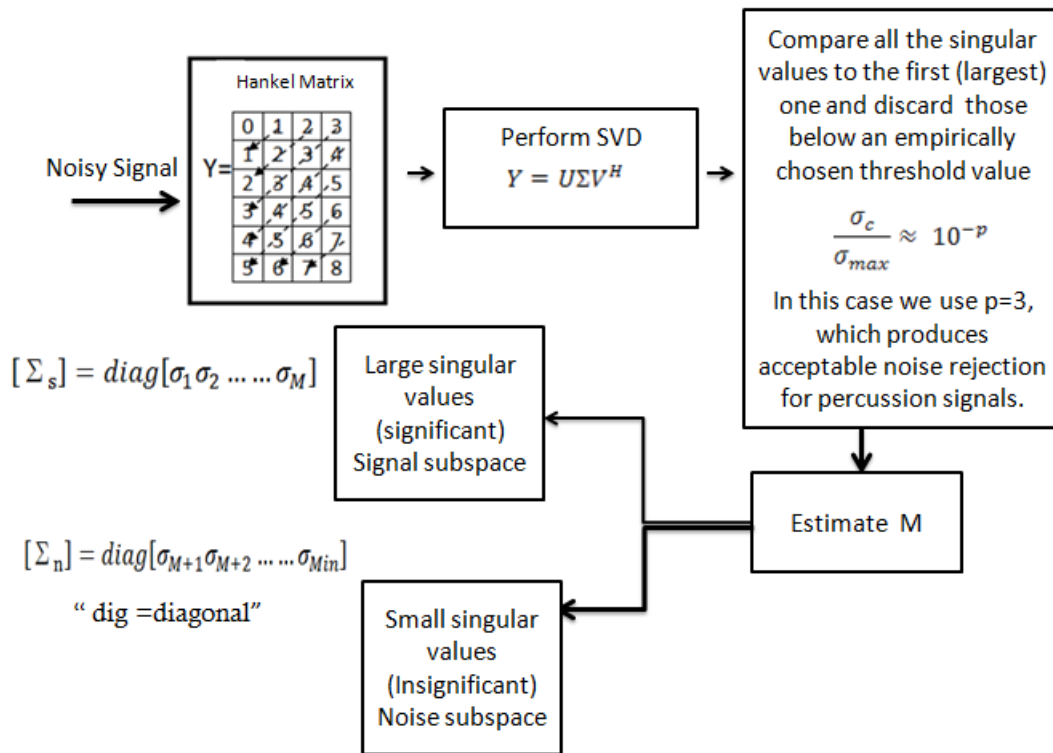


Figure 4.6 Flow diagram of SVD based threshold technique to separate noise space and the signal space.

## 4.6.7 Experimental analysis of threshold value

### 4.6.7.1 Synthetic signal

In this section, we demonstrate an experimental analysis for verifying the threshold criteria on a known synthetic signal. Four EDS were added together to form a multi-component signal with total 16 known independent parameters listed in Table 4.2. The signal is shown in figure 4.7. The aim of this analysis is to verify the performance of the thresholding technique before applying it to the real data. In the real data, the number of EDS is not known in advance, as well as the values of their parameters. As such, the idea is to get the results for known signal results first to see whether the threshold technique is a valid concept or not.

$$y(kT_s) = x(kT_s) + n(kT_s) = \sum_{i=1}^M R_i Z_i^k + n(kT_s) \quad (4.12)$$

Where  $k=0 \dots N-1$ ,  $i=1 \dots M$ ,  $T_s$  is the sampling period  $R_i = A_i e^{-j\theta_i}$  are complex amplitudes, and  $z_i = e^{(j2\pi f_i - d_i)T_s}$  are signal poles.

Table 4.2 EDS simulated signal parameters

Frequency [Hz]	100	110	180	220
Amplitudes [a.u.]	0.4	1	0.89	1
Damping $d_i$ [ $s^{-1}$ ]	70	50	90	80
Initial phase [deg]	$\frac{\pi}{6}$	$\frac{\pi}{6}$	$\frac{\pi}{6}$	$\frac{\pi}{6}$

The signal contained 1000 points sampled at 10 kHz. We added additive white Gaussian noise with 50 dB SNR. The SVD output results are listed in Table 4.3. The results are organized in three columns.

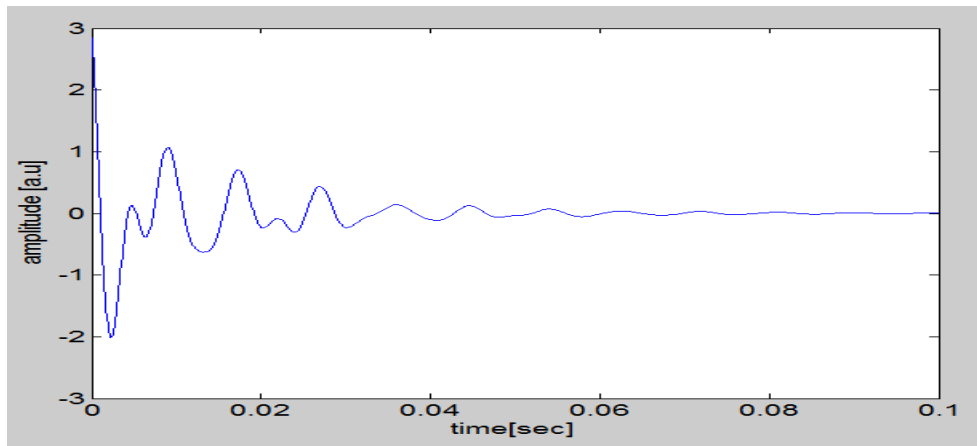


Figure 4.7 Synthesis signal

The first and the second columns are for the original and noisy signals respectively. The threshold values are placed in the 3<sup>rd</sup> column. It can be observed that the singular values in the first and second columns are similar up to a certain index (here it is equal to 8). These singular values represent the signal part. Now, we can fix the threshold point  $M$ . The rest of the values in column 2 are related to the noise.

Table 4.3 Simulated signal SVD values and identifying threshold criteria.

<i>Index</i>	<i>Signal</i>	<i>Signal+noise</i>	$\frac{\sigma_c}{\sigma_{max}}$
1	58.9914	58.9932	1.0000
2	51.8753	51.8752	0.8794
3	30.4874	30.4952	0.5169
4	30.2602	30.2661	0.5131
5	15.6555	15.6518	0.2655
6	15.3978	15.3926	0.2611
7	2.4864	2.4971	0.0425
8	2.3663	2.3769	0.0404
9	0.0000	0.0680	0.0010
10	0.0000	0.0679	0.0010
	↓ All Zeros	↓ More nonzero Values	↓ More nonzero Values

It can be seen that choosing the threshold value of 0.001 will result in discarding of the last singular values starting from below the index eight and keeping only those eight values (EDS) that were originally present in the signal. The above-mentioned analysis SNR was 50dB. It can be expected that with the increasing level of added noise the value of the threshold will also increase. Figure 4.8 shows the threshold value variation for different SNR. It can be seen that the threshold values are indeed closely related to the SNR of the signal.

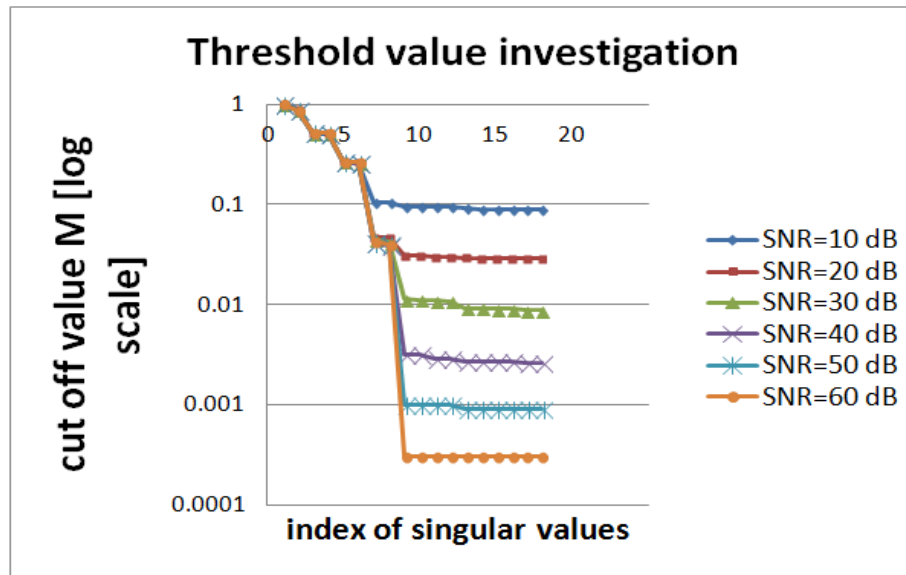


Figure 4.8 Threshold value plot after SVD operation on simulated noisy signal

For example, if we still want to keep the original eight EDS when a -30dB noise is added to the signal, we will have to discard singular values using the threshold value of 0.01 in this example. In this work use the threshold value of 0.001 to discard the noise below -50dB and not accidentally harm any original EDS. This is a very conservative threshold, because the real noise level in the raw percussion signals before any conditioning is almost always higher than -30dB. The singular values corresponding to the signal contain more energy than noisy one. We can show the percentage of energy corresponding to the individual singular values (figure 4.9).

The following information can be derived from figure 4.9 :

(1) The percentage of energy of the individual singular values;

(2) The first couple of singular values contains major portion of the signal's energy. As such, these singular values are dominant in the signal.

We observed that the first four (may vary for other cases) singular value contain the ~90% of the signal energy. These singular values have much stronger contribution to the signal than the remaining singular values.

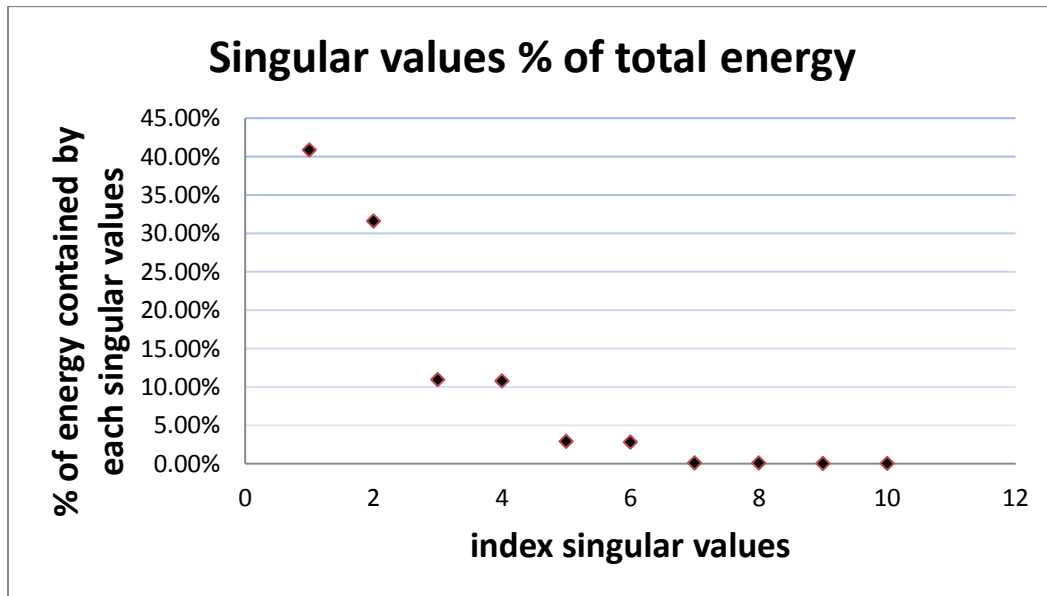


Figure 4.9 Energy calculation of different singular values

When reconstructing the signal from the EDS, we usually want to remove as much noise as possible. However, we do not want to lose much energy from signal. The idea is to identify the signal subspace by means of energy considerations and then project the observation onto the signal subspace and thereby eliminate the dimensions, which only contribute to the noise. The high-energy components are assumed to be dominating in the signal whereas the low energy components are supposed to contain only noise. The energy of the original signal will be preserved if one retains only the first couple of singular values.

### 4.6.7.2 SVD operation on medical percussion signals

The hybrid mechanism of noise reduction that we mentioned earlier will be implemented on noisy percussion signals in this section. This section analysis is based only on the SVD technique, as we have done all the conditioning of the percussion signals before. The waveform of the percussion signal after conditioning is shown in figure 4.5. In this section, we will observe the noise cancellation based on the thresholding technique.

The basic idea of the SVD based noise reduction is to de-correlate the signal by projecting signal onto orthogonal axes. Once we discover the basis functions of the independent axes in the signal and separate them out by projecting the data onto these axes, we can then use this technique to filter out the noise. We arranged the percussion signal data in a Hankel matrix form. We assumed the value of  $L$  is  $2N/3$ . We applied SVD onto the percussion signals. The eigenvalues associated with the first few eigenvectors are much larger than the eigenvalues associated with subsequent eigenvectors. We plotted the singular values in figure 4.10.

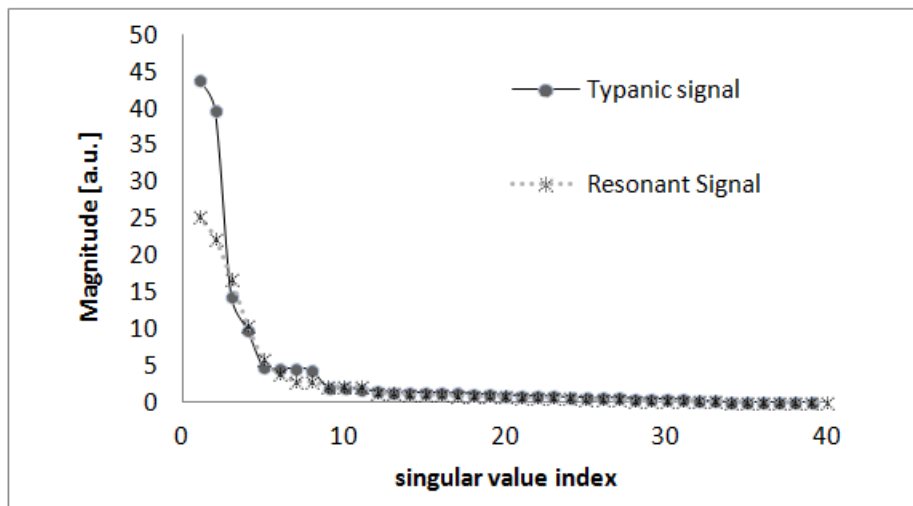


Figure 4.10 Percussion signal singular value plot

Figure 4.10 shows that the singular values drop in magnitude as their index increases. The slope of the decreasing curve is very sharp for the first couple of singular values; then the

curve becomes nearly horizontal (reaches saturation). It is also observed from the figure 4.10 that the curve for tympanic signal decreases more rapidly than for the resonant signal. According to SVD theory, we mentioned earlier that first few eigenvalues account for most of the variation present in the original data. The first few eigenvectors will point in directions where the data jointly exhibits large variation. The remaining eigenvectors will point to directions where the data jointly exhibits less variation. For this reason, it is often possible to capture most of the variation by considering only the first few eigenvectors. The remaining eigenvectors, along with their corresponding principal components, are truncated. The ability of SVD to eliminate a large proportion of the data is a primary reason for its use. We mentioned earlier that the threshold value 0.001 will be the key point for drawing the line between the signal part and noise part. An arrow in figure 4.11 shows the threshold value for the percussion signal. We can measure the number of singular values needed for the noise free signal from the figure 4.11.

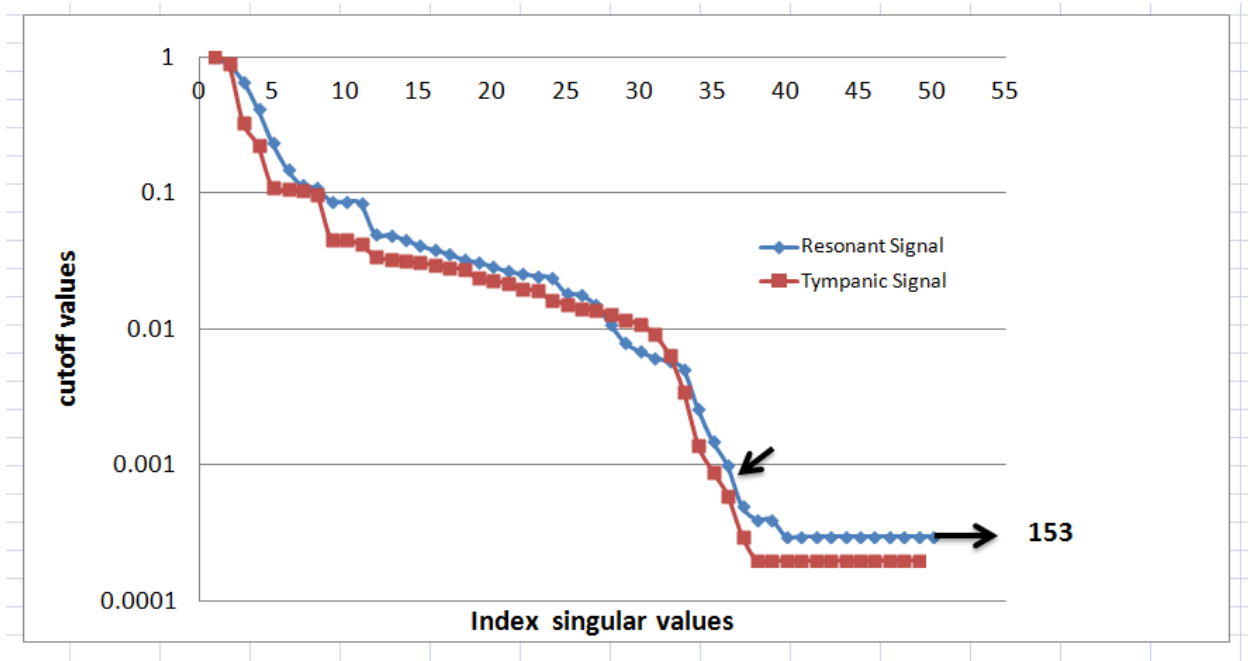


Figure 4.11 threshold value indications after SVD for medical percussion signal

According to the threshold point, the resonant signal takes around 40 singular values whereas tympanic signal takes only 38 singular values in the case of noise free signal. Here, without knowing anything of the signal, we can separate the signal part and noise after SVD calculation. This threshold value gives the opportunity to get the right number of EDS from the unknown percussion signals. The rest of the singular values consider as noise and we can discard those singular values. The total number of noise related singular values is  $(153-40) = 113$  for resonant signal and  $(153-38) = 115$  for the tympanic signal. We observe that tympanic signals need less number of singular values to catch the point 0.001 compared to the resonant signal. This scenario changes from signal to signal and it is not fixed for all signals. Based on this analysis, we can calculate the SNR of the percussion signals.

#### 4.6.8. Percussion signal SNR measurement

The signal-to-noise ratio (SNR) provides a comparison of the amount of signal with the amount of background noise in a particular signal, such that a higher SNR indicates the background noise is less noticeable. Signal-to-noise is defined as the ratio of signal power to the noise power of the noisy contaminated signal. A high SNR guarantees clear acquisitions with low distortions and artifacts caused by noise. In addition, signal-to-noise ratio is inversely proportional to the relative standard deviation of the signal amplitude. The better the SNR, the better the signal quality is. We can measure the SNR of the percussion signals as follows:

$$SNR = 10 \log \left[ \frac{\sigma_{sig}^2}{\sigma_n^2} \right] \quad (4.14)$$

**Tympanic signal SNR:**

$$SNR = 10 \log \left[ \frac{\sum_{i=1}^{37} \sigma_{sig}^2}{\sum_{i=38}^{152} \sigma_n^2} \right] \text{ or } SNR = 10 \log \left[ \frac{3946.443}{0.003811} \right] = 60.151 \text{ dB}$$

### Resonant signal SNR:

$$\text{SNR} = 10 \log \left[ \frac{\sum_{i=1}^{40} \sigma_{sig}^2}{\sum_{i=41}^{152} \sigma_n^2} \right] \text{ or } \text{SNR} = 10 \log \left[ \frac{1630.152}{0.00301} \right] = 57.33 \text{ dB.}$$

The above calculation is for a particular percussion signal. However, we can see the overall scenario for the fifteen percussion signals collected from different healthy volunteers. We can observe from the figure 4.12 that the SNR of the percussion signals are above 50dB. The high SNR of the percussion signal is due to the optimized conditioning and implementation of hybrid noise filtering mechanism.

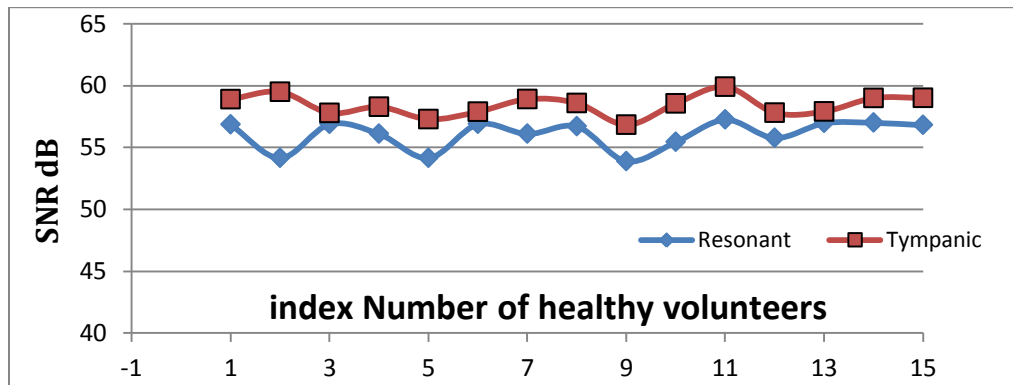


Figure 4.12 Medical Percussion signals SNR

### 4.6.9 Singular values energy distribution

The distribution of the signal energy among singular values is shown in figure 4.13. The energy carried by the first singular value can be expressed as follows:

$$E_1 = \frac{\sigma_1^2}{\sum_{i=1}^M \sigma_i^2} \quad (4.15)$$

When the signal contains noise this becomes

$$E_1 = \frac{\sigma_1^2 - \sigma_{noise}^2}{\sum_{i=1}^M (\sigma_i^2 - \sigma_{noise}^2)} \quad (4.16)$$

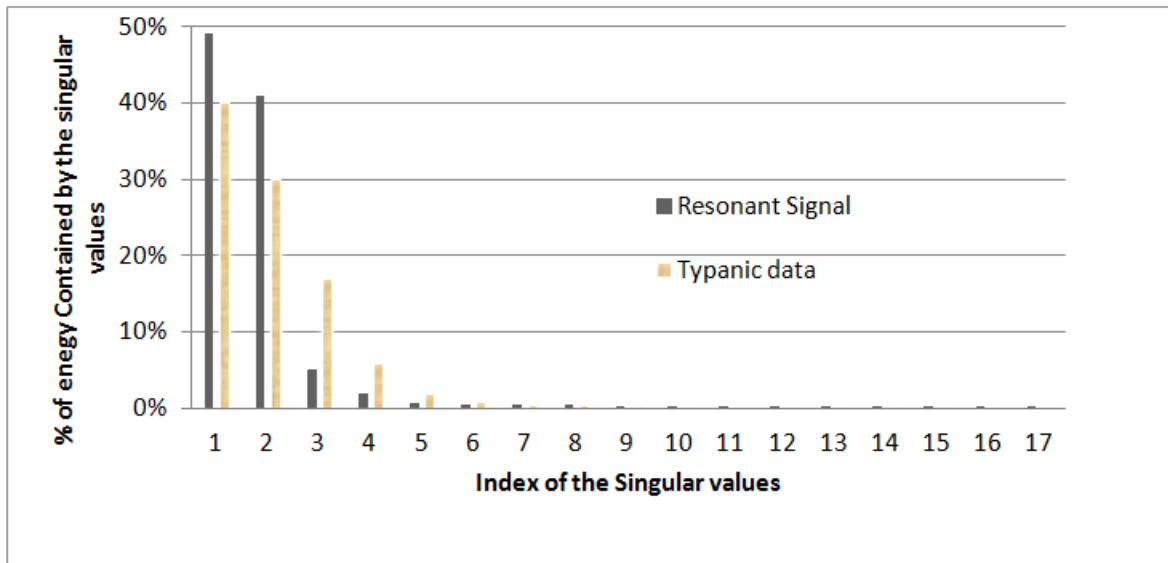


Figure 4.13 Energy distributions between different singular values in clinical percussion signals

By comparing the energy, contributions of singular values for the resonant signal and tympanic signal (figure 4.13), it can be observed that the first five singular values contain the major portion of the signal’s energy. The energy distributions of the tympanic and resonant signals are not identical. In particular, they are different in the respective shapes of the energy distributions.

### 4.7 Summary

In this chapter, we have discussed various aspects of noise in medical percussion signals. At first, we have discussed the signal preparation procedure, where it was shown how to select the informative part of the signal from the raw signal. Then we have focused on conditioning of the percussion signal. We have mentioned a noise filtering mechanism called the hybrid noise filtering technique, which combines the Band Pass Filtering (BPF) and Hankel-SVD filtering. We have briefly described the SVD process and discussed the thresholding

technique for identifying the signal part and the noise part in the percussion signal. Finally, we applied the thresholding technique to a synthetic signal and to real percussion signals. After applying all mentioned conditioning and denoising techniques we can consider the percussion signal essentially noise-free and ready for subsequent analysis with the Matrix Pencil Method, which is discussed in the next chapter.

# Chapter 5

## Matrix Pencil Method

---

### 5.1 Introduction

The Exponentially Damped Sinusoidal (EDS) model was proposed for the medical percussion signals in chapter 2. In this chapter, we will discuss the Matrix Pencil Method for decomposing the medical percussion signals. The proposed EDS modeling effort consists of finding the basis functions of the percussion signals and to show how relatively simple way can represent the percussion signals in time domain. To simplify the percussion signal modeling effort, we assume that the percussion signal consist of several damped sinusoidal signals. Thus, each EDS signal consists of four parameters such as amplitude, frequency, damping and initial phase. In order to fit the model, the next research focus is to find the best estimates of  $R_i$  and  $z_i$  from the signal (Equation 2.5). We already talked about the parameter  $M$ , which is the number of EDS in the signal. Though finding the parameters of EDS is a non-linear problem, sometimes solving the linear problem, in many cases, equivalent to the solving of nonlinear problem [47]. The benefits of using Matrix Pencil Method are described in brief in the following section.

There are two linear methods for estimation of the parameters, the “polynomial” method ( Prony, Kumaresan-Tufts, Root-MUSIC, ESPRIT etc.) and the “Matrix Pencil” method [47, 61]. The Polynomial method is a two-step process of finding poles where Matrix pencil method is one-step process of finding poles. In Matrix Pencil Method, the poles are found as

the solution of generalized Eigenvalue problem [62]. There is no practical limitation of the number of poles in MPM, where only 50 poles can be achieved from polynomial method [47]. These two methods are the two special cases of matrix prediction approach, but MPM is more efficient in computation and less sensitive to noise [39, 51, 55, and 70].

MP method also called super-resolution estimation technique, widely used to estimate complex exponentials in a signal [59]. There are other high-resolution methods which are also used to estimate the parameters of damped sinusoidal signals such as Kumaresan-Tufts Method, root-MUSIC (Multiple Signal Classifications), ESPRIT (Estimation of Signal Parameters via Rotational Invariance Technique) [70-73]. In case of these methods, covariance matrix is required to calculate before calculating the poles of a signal. However, there is no need to calculate covariance matrix for MPM. For this reason, MPM is called one-step method.

ESPRIT is a stochastic spectrum estimation technique [74]. It uses the auto and cross covariance matrices to determine the poles [62]. The MP algorithm is a non-stochastic estimating technique that uses a snapshot of data to calculate its parameters [73, 74]. The MP method is also preferable for real-time systems, since there is no need to collect multiple data to form the covariance matrix [47, 72]. The pencil parameter considering as free moving window is a great feature in MP method. It is proved that a proper choice of the pencil parameter results in significant improvement in noise sensitivity compare to other methods [47, 54] as discussed above. In addition, MP method reconstructs the signal without calculating the reconstruction error in the signal [64-66].

Finally we can compare with DFT. MP method has a superior ability of finding closely spaced frequency [48, 49, 58, 67, and 72]. This method can determine the frequencies to be placed exactly at the locations, where DFT placed the frequencies on prearranged bin [48, 58]. It is

possible to find the damping parameter using MPM [47-58]. However, there is no direct way to calculate damping parameter in DFT.

## 5.2 Matrix Pencil Method (MPM) theory

Gantmacher is the pioneer who first introduced the term “pencil” in 1960 [47]. Similar to Gantmacher definition, the matrix pencil arises, when two functions defined on a common interval with a scalar parameter. If we consider two function such as  $g(t)$  and  $h(t)$ , and a scalar parameter  $\lambda$ , then,

$$f(t, \lambda) = g(t) + \lambda h(t) \quad (5.1)$$

Here,  $f(t, \lambda)$  is called a pencil of function  $g(t)$  and  $h(t)$  [47,56]. On the other hand, If we consider two square matrix A and B, then A and B can be relate as [67, 74]

$$A\bar{x} = \lambda B\bar{x} \quad (5.2)$$

$$\text{Or } (A - \lambda B)\bar{x} = 0 \quad (5.3)$$

The equation 5.3 is called a generalized Eigen-value problem. The Eigen-value set  $\lambda(A, B)$ , are said to be the pencil parameter values or the roots of A relative to B. Here  $\lambda \in \mathbb{C}$  where C is defined as complex numbers and  $\bar{x}$  is an Eigen vector provided  $\bar{x}$  is not zero [58, 71]. For getting the pencil parameter, the following solution must need to be exists [56, 67].

1.  $\bar{x} \neq 0$ , that solve the equation  $(A - \lambda B)\bar{x} = 0$
2. The  $\det(A - \lambda B) = 0$  for all value of  $\lambda$
3. The rank of the matrix is depend on the number of non zero values of  $\lambda$
4. If the matrix is not square then  $(A - \lambda B)$  is multiplied either  $A^H$  or  $B^H$ . Where, H stands for hermitian (conjugate transpose)..

Matrix Pencil Method (MPM) is a suitable method that can decompose the damped sinusoidal signals in order to get all the parameters of individual EDS described as a model signal [47-71]. First, Hankel matrix [Y] is constructed by using the samples data from  $x(kT_s)$  and each part of the [Y] is a windowed part of the original data vector  $\{x(0), x(1), x(2) \dots \dots x(N - 1)\}$ .

$$[Y] = \begin{bmatrix} x(0) & x(1) & \dots & x(L) \\ x(1) & x(2) & \dots & x(L+1) \\ \vdots & \vdots & \vdots & \vdots \\ x(N-L-1) & x(N-L) & \dots & x(N-1) \end{bmatrix} (N-L)x(L+1) \quad (5.4)$$

Here  $L$  is the pencil parameter and its range is  $M < L < N - M$ , and  $M$  is the total number of EDS in the signal. According to the Cramer-Rao Lower Bound (CRLB),  $L$  is chosen between  $N/3$  and  $N/2$  for effective noise filtering [58]. The variance of the estimated values of  $R_i$  and  $z_i$  will be minimal if the values of  $L$  chosen in this range [47, 58, 68, 69]. Here  $N$  is the total number of sample of a signal. For noise free data, equation (2.5) can be written in Matrix Form

$$Y = ZR \quad (5.5)$$

Where the residue parameters of percussion signal is represented by

$$R = \begin{bmatrix} R_1 \\ R_2 \\ R_3 \\ R_4 \\ \vdots \\ R_M \end{bmatrix} \quad (5.6)$$

And the pole parameters represent by

$$Z = \begin{bmatrix} 1 & 1 & \dots & 1 \\ z_1 & z_2 & \dots & z_M \\ \vdots & \vdots & \vdots & \vdots \\ z_1^{N-1} & z_2^{N-1} & \dots & z_M^{N-1} \end{bmatrix} (N \times M) \quad (5.7)$$

The equation (5.4) can also be written in the matrix form,

$$[Y] = \begin{bmatrix} \sum_{i=1}^M R_i & \sum_{i=1}^M R_i z_i & \cdots & \sum_{i=1}^M R_i z_i^L \\ \sum_{i=1}^M R_i z_i & \sum_{i=1}^M R_i z_i^2 & \cdots & \sum_{i=1}^M R_i z_i^{L+1} \\ \vdots & \vdots & \ddots & \vdots \\ \sum_{i=1}^M R_i z_i^{N-L-1} & \sum_{i=1}^M R_i z_i^{N-L} & \cdots & \sum_{i=1}^M R_i z_i^{N-1} \end{bmatrix} (N-L) \times (L+1) \quad (5.8)$$

Recall the Matrix Pencil method in the following form

$$Y_2 = zY_1 \quad (5.9)$$

Here,  $z$  is the set of eigen values, in which for the MP method are the poles.

Where  $[Y]$  we can define two sub matrices

$$[Y_1] = \begin{bmatrix} x(0) & \cdots & x(L-1) \\ \vdots & \ddots & \vdots \\ x(N-L-1) & \cdots & x(N-2) \end{bmatrix} (N-L) \times L \quad (5.10)$$

$$[Y_2] = \begin{bmatrix} x(1) & \cdots & x(L) \\ \vdots & \ddots & \vdots \\ x(N-L) & \cdots & x(N-1) \end{bmatrix} (N-L) \times L \quad (5.11)$$

The above two matrices  $[Y_1]$  and  $[Y_2]$  are constructed from  $[Y]$  by deleting its last and first columns respectively where they are related by the delay of one sample and can be expressed in terms of the poles and residues of the signal (equation 5.9) as follows:

$$[Y_1] = [Z_1][R][Z_2] \text{ and } [Y_2] = [Z_1][R][Z_0][Z_2], \quad (5.12)$$

Where,

$$Z_1 = \begin{bmatrix} 1 & 1 & \cdots & 1 \\ z_1 & z_2 & \cdots & z_M \\ \vdots & \vdots & \ddots & \vdots \\ z_1^{N-L-1} & z_2^{N-L-1} & \cdots & z_M^{N-L-1} \end{bmatrix} (N-L) \times M \quad (5.13)$$

$$Z_2 = \begin{bmatrix} 1 & z_1 & \cdots & z_1^{L-1} \\ 1 & z_2 & \cdots & z_2^{L-1} \\ \vdots & \vdots & \vdots & \vdots \\ 1 & z_M & \cdots & z_M^{L-1} \end{bmatrix} \quad (M \times L) \quad (5.14)$$

$$Z_0 = \text{diag}(z_1, z_2 \cdots z_M) \text{ and } R_0 = \text{diag}(R_1, R_2 \cdots R_M) \quad (5.15)$$

To show this relationship, a 3x3 matrix example will help clarify deviation [67].

$$[Y_1] = \begin{bmatrix} 1 & 1 & 1 \\ z_1 & z_2 & z_3 \\ z_1^2 & z_2^2 & z_3^2 \end{bmatrix} \begin{bmatrix} R_1 & 0 & 0 \\ 0 & R_2 & 0 \\ 0 & 0 & R_3 \end{bmatrix} \begin{bmatrix} 1 & z_1 & z_1^2 \\ 1 & z_2 & z_2^2 \\ 1 & z_3 & z_3^2 \end{bmatrix} \quad (5.16)$$

$$[Y_1] = \begin{bmatrix} R_1 + R_2 + R_3 & R_1 z_1 + R_2 z_2 + R_3 z_3 & R_1 z_1^2 + R_2 z_2^2 + R_3 z_3^2 \\ R_1 z_1 + R_2 z_2 + R_3 z_3 & R_1 z_1^2 + R_2 z_2^2 + R_3 z_3^2 & R_1 z_1^3 + R_2 z_2^3 + R_3 z_3^3 \\ R_1 z_1^2 + R_2 z_2^2 + R_3 z_3^2 & R_1 z_1^3 + R_2 z_2^3 + R_3 z_3^3 & R_1 z_1^4 + R_2 z_2^4 + R_3 z_3^4 \end{bmatrix} =$$

$$\begin{bmatrix} X(0) & X(1) & X(2) \\ X(1) & X(2) & X(3) \\ X(2) & X(3) & X(4) \end{bmatrix} \quad (5.17)$$

$$[Y_2] = \begin{bmatrix} 1 & 1 & 1 \\ z_1 & z_2 & z_3 \\ z_1^2 & z_2^2 & z_3^2 \end{bmatrix} \begin{bmatrix} R_1 & 0 & 0 \\ 0 & R_2 & 0 \\ 0 & 0 & R_3 \end{bmatrix} \begin{bmatrix} z_1 & 0 & 0 \\ 0 & z_2 & 0 \\ 0 & 0 & z_3 \end{bmatrix} \begin{bmatrix} 1 & z_1 & z_1^2 \\ 1 & z_2 & z_2^2 \\ 1 & z_3 & z_3^2 \end{bmatrix}$$

$$= \begin{bmatrix} X(1) & X(2) & X(3) \\ X(2) & X(3) & X(4) \\ X(3) & X(4) & X(5) \end{bmatrix} \quad (5.18)$$

$$[Y_2] = \begin{bmatrix} R_1 z_1 + R_2 z_2 + R_3 z_3 & R_1 z_1^2 + R_2 z_2^2 + R_3 z_3^2 & R_1 z_1^3 + R_2 z_2^3 + R_3 z_3^3 \\ R_1 z_1^2 + R_2 z_2^2 + R_3 z_3^2 & R_1 z_1^3 + R_2 z_2^3 + R_3 z_3^3 & R_1 z_1^4 + R_2 z_2^4 + R_3 z_3^4 \\ R_1 z_1^3 + R_2 z_2^3 + R_3 z_3^3 & R_1 z_1^4 + R_2 z_2^4 + R_3 z_3^4 & R_1 z_1^5 + R_2 z_2^5 + R_3 z_3^5 \end{bmatrix} =$$

$$= \begin{bmatrix} X(1) & X(2) & X(3) \\ X(2) & X(3) & X(4) \\ X(3) & X(4) & X(5) \end{bmatrix} \quad (5.19)$$

M was 3 for the above mentioned matrix. Let us now write the matrix pencil again

$$Y_2 - \lambda Y_1 = Z_1 R (Z_0 - \lambda I) Z_2 = 0 \quad (5.20)$$

Where,  $[I]$  is the  $M \times M$  identity matrix and  $\lambda$  is a scalar parameter. One can demonstrate that, in general, if  $M \leq L \leq (N - M)$ , the rank of the eq. (5.20) will be  $M$  [47-71]. However, if  $z = \lambda = z_i, i = 1, 2, \dots, M$ , the  $i^{th}$  row of  $\{[Z_0] - \lambda[I]\}$  is zero, and the rank of the Matrix is  $M - 1$ [47]. Therefore  $z_i$  may be found as the generalized eigen values of Matrix pair  $\{[Y_2][Y_1]\}$ . To solve the generalized eigenvalues in eq. (5.20), the Moore-Penrose Pseudo inverse (MPP) is used. The MPP is defined as  $Y^+ = [Y^H Y]^{-1} Y^H$ , Where  $H$  denotes the conjugate transpose.

Therefore, solution of equation 5.20 is

$$zI = Y_1^+ Y_2 \text{ and } zI = [Y_1^H Y_1]^{-1} Y_1^H Y_2 \quad (5.21)$$

Here, the poles  $z_i$  of a signal in equation 2.5 are solved. Now the residue parameter can be solved from the pole parameters. We can use the equation 5.5 to solve the residue parameters  $R$ .

$$R = Z^+ Y \quad (5.22)$$

In case noise contaminated we need to filter the real time data for better results. The choice of the number of  $M$  is the key factor to separate the signal part and noise part in the noise-contaminated signal. The Total Least Square Matrix Pencil Method (TLSMP) would be an alternative [47]. Practical consideration such as additive noise presence and computational inaccuracies results in a need to estimate the number of poles ( $M$ ).

Generally, singular value decomposition (SVD) of the matrix  $[Y]$  is carried out for noise cancellation. We have discussed in details the SVD based noise cancellation in chapter 4. However, we proposed Hybrid noise cancellation mechanism for the better results. After using the hybrid operation, the percussion signal becomes two parts such as noise apart and signal part. The percussion can demonstrate as follows [47,65,67]:

$$[Y] = [U_s][\Sigma_s] [V_s]^H + [U_n][\Sigma_n] [V_n]^H \quad (5.23)$$

The signal subspace has the dimension (the number of signals) that corresponds the principle Eigen values of matrix $[\Sigma]$ . The noise subspace is related to the rest of eigenvalues, so we can write the two sub-spaces as Table 5.1.

Table 5.1: Signal and noise subspaces

Signal Subspace	Noise subspace
$[U_s] = [u_1 u_2 \dots \dots \dots u_M]$	$[U_n] = [u_{M+1} u_{M+2} \dots \dots \dots u_{Min}]$
$[\Sigma_s] = \text{diag}[\sigma_1 \sigma_2 \dots \dots \sigma_M]$	$[\Sigma_n] = \text{diag}[\sigma_{M+1} \sigma_{M+2} \dots \dots \sigma_{Min}]$
$[v_s] = [v_1 v_2 \dots \dots v_M]$	$[v_n] = [v_{M+1} v_{M+2} \dots \dots v_{min}]$

Now consider the signal part only for applying matrix pencil method. We can discard the noise part of the signal. Matrices  $U$  and  $V$  represent the signal space of the segmented frame of data. Therefore, if we take first  $M$  eigenvectors of either  $U$  or  $V$  (for this case we will use  $U$ ) and perform the MP algorithm, the  $M$  most dominant pole will be calculated [47, 74].

$$[Y_s] = [U_s][\Sigma_s] [V_s]^H \quad (5.24)$$

One can write matrix pencil as follows

$$[U_{2s}] - \lambda[U_{1s}] = 0 \quad (5.25)$$

$[U_{1s}]$ :  $[U_s]$  with last row deleted

$[U_{2s}]$ :  $[U_s]$  with the first row deleted

So the rank reducing numbers of the matrix  $[U_{2s}] - \lambda[U_{1s}]$  will be the poles, which is the generalized eigenvalues of  $\{[U_{1s}], [U_{2s}]\}$ . It can be solved as before as the eigenvalues of  $[U_{1s}]^+[U_{2s}]$  is the poles.

Therefore,

$$zI = \{[U_{1s}^H U_{1s}]^{-1} U_{1s}^H U_{2s}\}. \quad (5.26)$$

The variable  $z$  represents the individual eigenvalues, which are the poles of the signal. Once the pole is calculated, the residue part can be calculated as before. Using  $M$  and  $z_i$ , the residues  $R_i$  can be found from the following least square problem [47]:

$$\begin{bmatrix} y_0 \\ y_1 \\ \vdots \\ y_{N-1} \end{bmatrix} = \begin{bmatrix} 1 & 1 & \cdots & 1 \\ z_1 & z_2 & \cdots & z_M \\ \vdots & \vdots & \ddots & \vdots \\ z_1^{N-1} & z_2^{N-1} & \cdots & z_M^{N-1} \end{bmatrix} \begin{bmatrix} R_1 \\ R_2 \\ \vdots \\ R_M \end{bmatrix} \quad (5.27)$$

The EDS frequencies and damping factors are then derived as  $f_i = \arg(\lambda_i) / (2\pi T_s)$  and  $d_i = -\text{Re}(\lambda_i) / T_s$ . This allows the signal to be represented by the amplitude, initial phase, and poles (frequency and decay).

### 5.3 Summary

Matrix pencil method is a model based parameter estimation method for damped sinusoidal signals. The method has presented in details in this chapter. We have presented all the mathematical equations and procedures of the method. It is proved from the previous research (references described in this chapter) that the matrix pencil is capable of finding all the parameters of exponentially damped sinusoidal signal. In our case, we proposed to use this method for finding the parameters of the percussion signals. The analysis of the percussion signals would be presented in the subsequent chapters.

## Chapter 6

# Estimating the parameters of clinical percussion signals

---

### 6.1 Introduction

In the previous chapter, we explored the Matrix pencil method. This method will be used for estimating the parameters of the medical percussion signals. The key idea behind this approach is to decompose an arbitrary audible clinical percussion signal into a sum of exponentially damped sinusoids (EDS) signals. Judging by the apparent damped oscillatory character of most abdominal (“tympanic”) signals, EDS should provide a natural basis for their decomposition of medical percussion signals. In this approach, clinical percussion signals from normal volunteers are decomposed into a sum of exponentially damped sinusoids (EDS) whose parameters are determined using the Matrix Pencil Method. Chest percussion signals also result from the more or less damped oscillations of various anatomical subsystems excited by the percussion event, and therefore EDS decomposition could help identify and fully characterize these individual oscillation modes. In the previous work by our group, this hypothesis was validated by approximating various percussion signals with 1 to 3 damped harmonics via nonlinear spectral fitting procedures [34]. However, these procedures are difficult to automate due to their complexity and semi-empirical choice of fitting parameters.

Being able to automatically decompose the recorded percussion signal into its damped harmonic constituents would have answered several key questions. Namely, if  $M$  EDS

representing the signal with the required tolerance were recovered, then one would have  $4M$  parameters completely representing the original signal (because each EDS is fully described by its four parameters: amplitude, phase, frequency, and damping). With the help of these parameters, the signals were classified into distinct groups for diagnostic purposes. In addition, one would obtain a powerful tool for monitoring signal changes in time (e.g. during the inhale/exhale cycle), as well as comparing signals between different points on the same patient and between different patients.

## **6.2 Clinical Percussion signals decomposition using Matrix Pencil Method**

Among many available methods approximating a function by a sum of complex exponentials the Matrix Pencil Method (MPM) was chosen since it is robust to noise and computationally efficient. MPM models the signal as a linear combination of damped complex exponentials and provides estimation of their frequencies, damping factors, amplitudes, and phases. The Singular Value Decomposition (SVD) is applied to noisy percussion signals to reduce the amount of noise by eliminating the smallest singular values. This noise cancellation procedure was discussed in chapter 4. The majority of preceding work attempting the objective classification of percussion sounds is based on Fourier analysis [1]. Decomposition of medical percussion signals has not yet been under study. In an attempt to find a natural basis for the percussion signals, we have noticed that the damped oscillatory character of most abdominal (“tympanic”) signals. We further hypothesized that other signal types are also composed of more or less damped oscillations produced by one or more organs excited by the percussion event. Two examples of typical percussion signals are shown in Figure 6.1 (a,b).

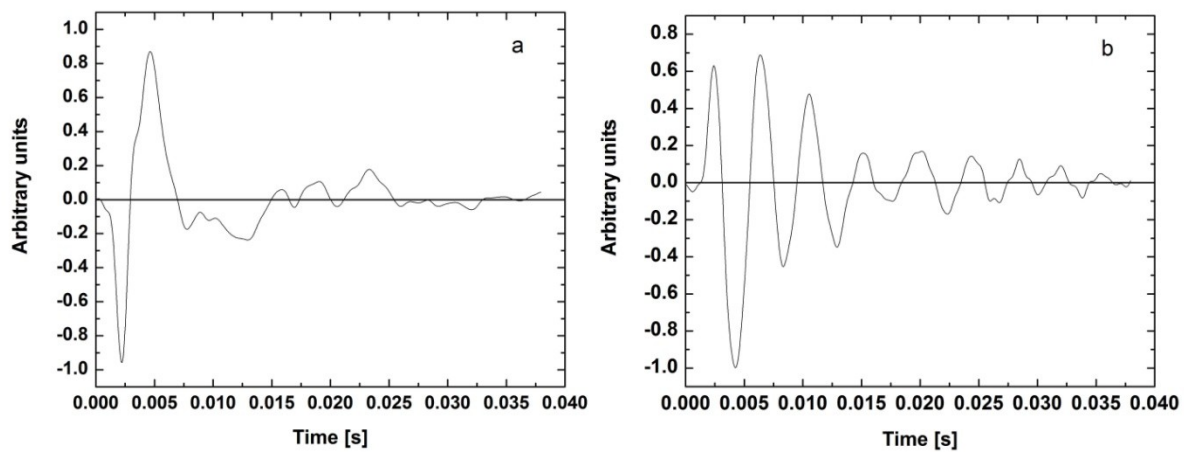


Figure 6.1: Two examples of audible percussion signals collected from healthy volunteers: **(a)** – signal collected over the left subclavicular area (“resonant” character); **(b)** – signal collected over the left abdominal area (“tympanic” character).

The signal 6.1 (b) was collected over the abdomen, and due to the hollow sound produced by an oscillating abdominal wall in the presence of intestinal gas pockets is historically known as “tympanic” [1]. This signal, albeit noisy, exhibits a slowly decaying oscillation and allows for a direct fit with a single exponentially damped sinusoid (EDS), which can be fully characterized by only four parameters: amplitude, phase, frequency, and damping. Other “tympanic” signals typically recorded over the abdomen may contain several (2–3) EDS components, as more than one air pocket could have been involved.

The resonant signal in Figure 6.1.a was acquired over the subclavicular area. The chest percussion signal has a more complex shape, not readily associated with damped harmonic oscillations. However, using a nonlinear spectral fitting procedure [34], it is possible to represent an arbitrary “resonant” signal as a superposition of a relatively few EDS. If these EDS correspond to actual physical processes, such as normal oscillation modes of different parts of the body [34], they could provide a natural basis for efficient decomposition and

parameterization of percussion signals. Their proper identification could also help single out percussion responses of individual organs. Both signals represent transient responses of the human body to the percussion impact. Their amplitude is highest at the onset and then rapidly fades out below the noise level, so that the respective duration of the signals in Figures 6.1.a and 6.1.b is approximately 40 ms.

### 6.3 Decomposition results and analysis

In this section, we describe the application of the MPM algorithm to the decomposition of a clinical percussion signal into a sum of damped oscillatory components. We used the Labview implementation of the Matrix Pencil Method described in [47]. We have done all the preprocess that is discussed in chapter 4. The results of the MPM decomposition of typical resonant and tympanic signals (figure 6.1 (a) and (b)) are presented in Tables-6.1 and 6.2 respectively. The resonant signal from Figure 6.1.a appears to be composed of 11 EDS whereas the tympanic signal from Figure 6.1.b contains 8 EDS. Some of these damped sinusoids can be treated as the original simple tones capturing the real features of the signal, while others are there to fit the noise remaining after the SVD filtering.

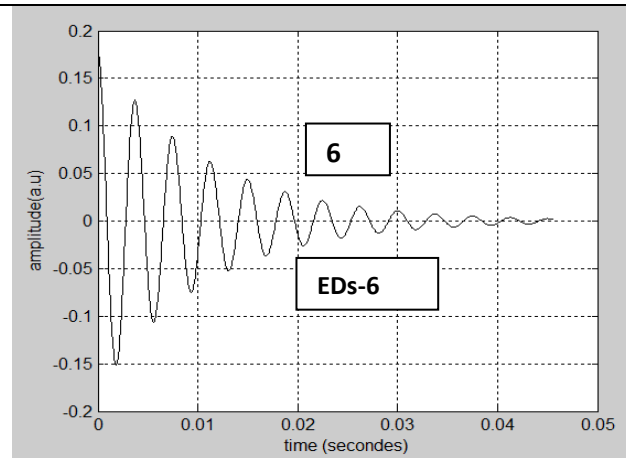
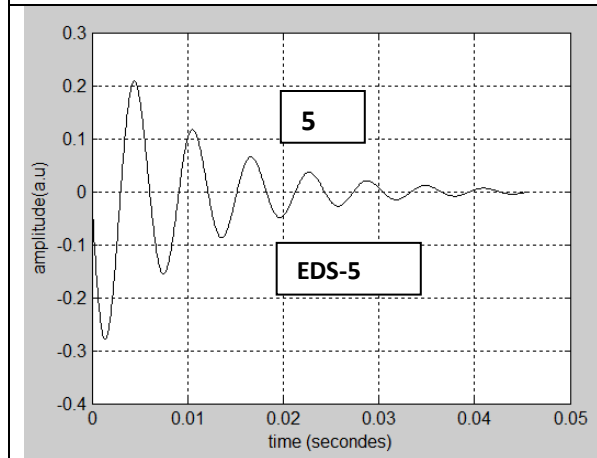
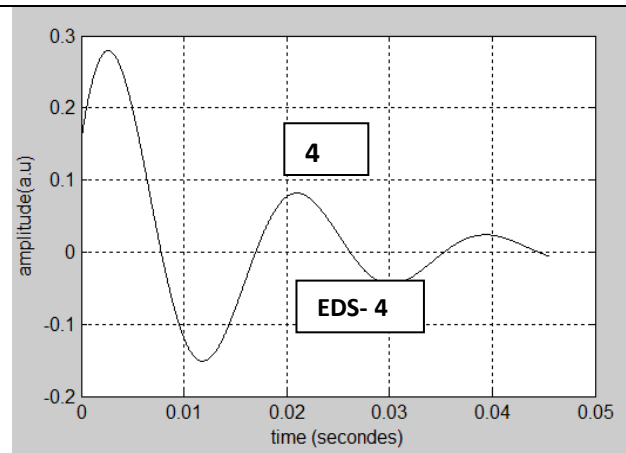
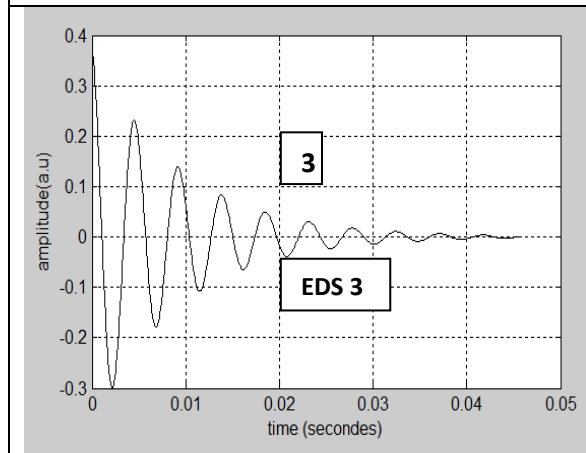
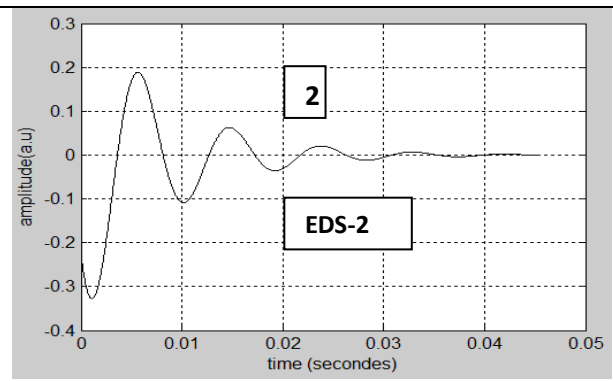
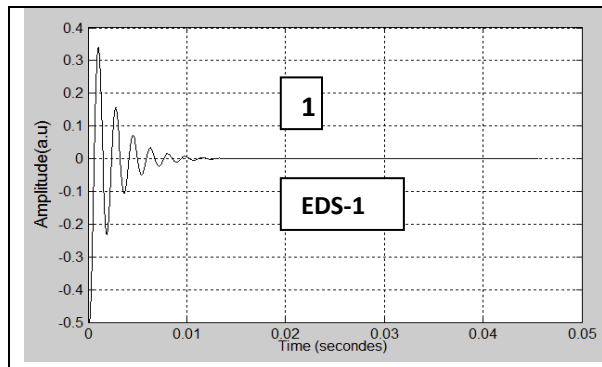
Table-6.1 MPM decomposition results for the resonant signal from Figure 6.1.a

EDS	Frequency (f) [Hz]	Damping (d) [s <sup>-1</sup> ]	Amplitude [a.u]	Phase( $\varphi$ ) [rad]
1	568.4136	439.7309	0.54	0.785278
2	110.2193	121.512	0.38	0.702722
3	214.5606	109.451	0.38	0.044167
4	54.48771	66.89012	0.34	-0.35056
5	164.1704	95.30471	0.32	0.515389
6	266.1824	93.89007	0.18	0.016278
7	798.962	377.5481	0.18	-0.44683
8	338.8896	44.42675	0.04	-0.29767
9	410.9627	57.9877	0.02	-0.8075
10	695.767	47.45113	0.02	0.107944
11	951.327	252.2069	0.02	-0.36089

Table-6.2 MPM decomposition results for the tympanic signal from Figure 1.b

EDS	Frequency, f [Hz]	Damping, d [s <sup>-1</sup> ]	Amplitude [a.u]	Phase (deg.)
1	225.7679	101.2071	1.02	-127.31
2	291.3409	276.7678	0.94	60.88
3	100.1096	116.4388	0.3	42.52
4	501.5601	234.0484	0.14	-68.93
5	645.7305	64.4511	0.04	160.23
6	61.04875	43.21943	0.02	178.06
7	813.0717	120.9754	0.02	102.05
8	970.815	61.93891	0.02	37.43

We plot the individual EDS components of the percussion signals in figure 6.2 for resonance and figure 6.3 for tympanic signal. It can be observed from the EDS that they are different from each other. These are the basis functions of the original signal. Therefore, the MPM decomposition shows more informative than the approaches we started earlier described in chapter 3. Here we can observe that the MPM decompose an original percussion signal into its primitive or fundamental constituents [73]. It is possible to perform simple operations separately on each component, thereby, accomplishment of sophisticated operations by a combination of individually simple operations also possible. It is also possible to identify the most dominant EDS in the signal. Some of these damped sinusoids can be treated as the original simple tones capturing the real features of the signal. The practice of breaking signals into smooth damped oscillating would a perfect way to recognize the percussion signals will be discussed in the next chapters .



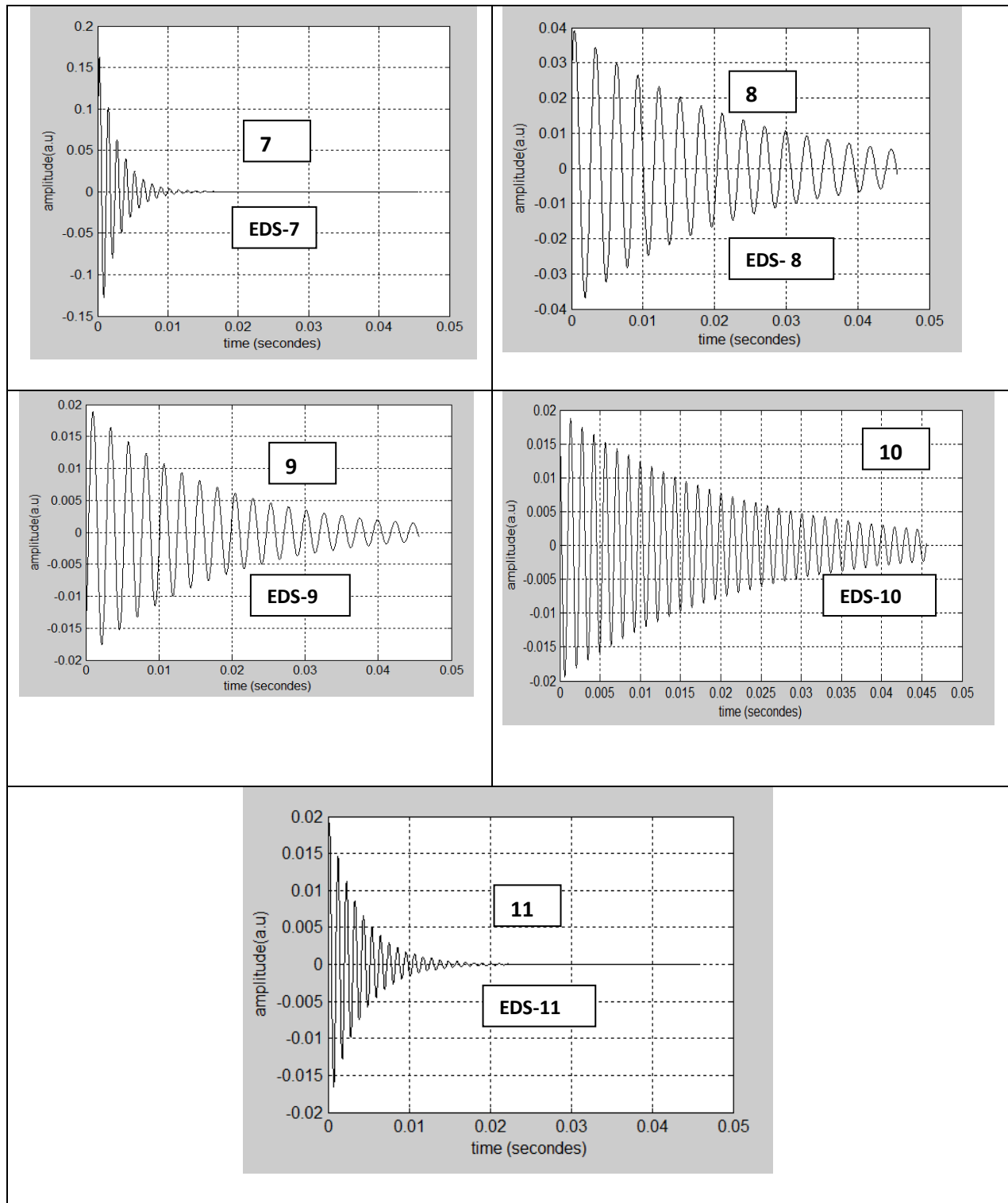


Figure 6.2 Resonant Signal EDSs

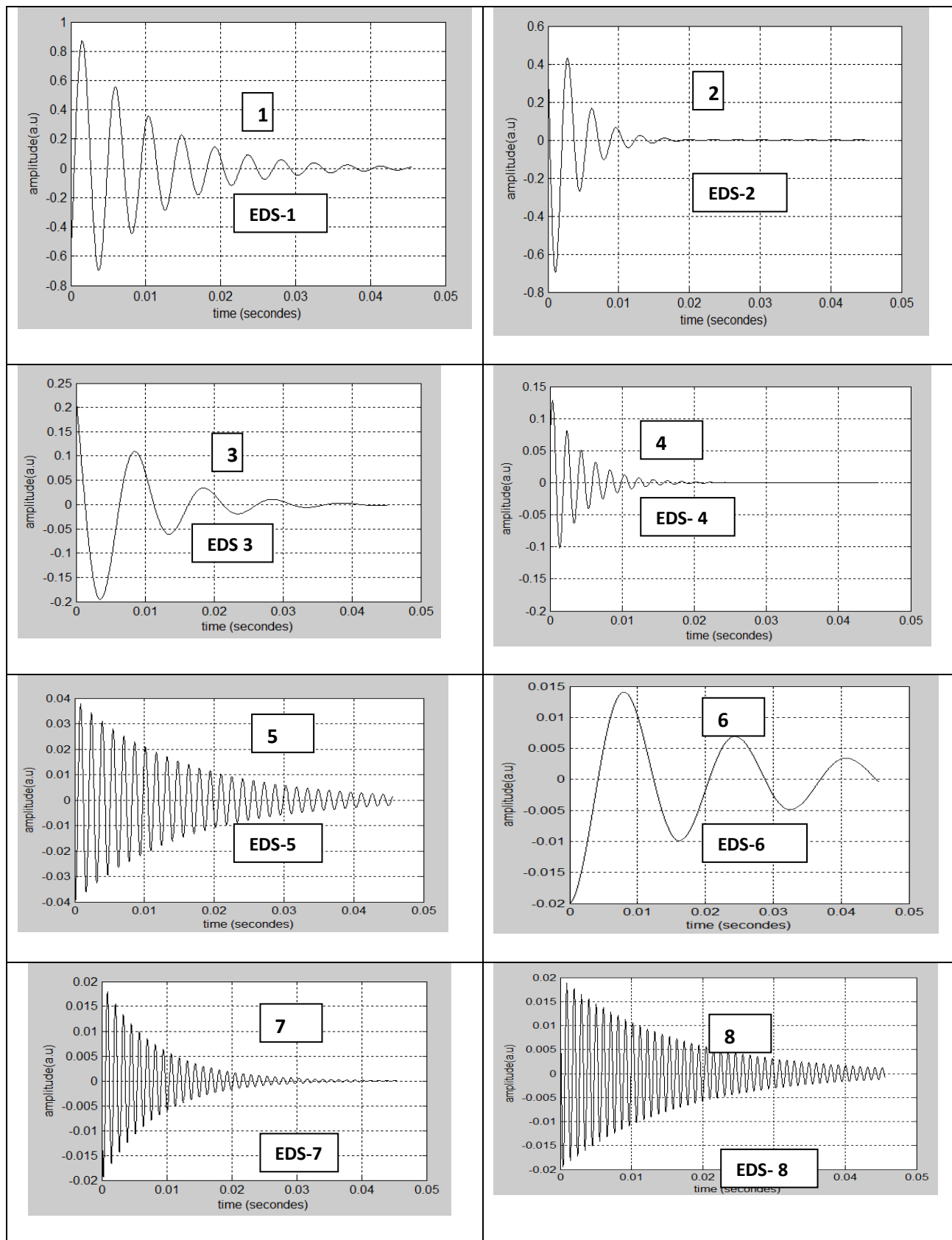
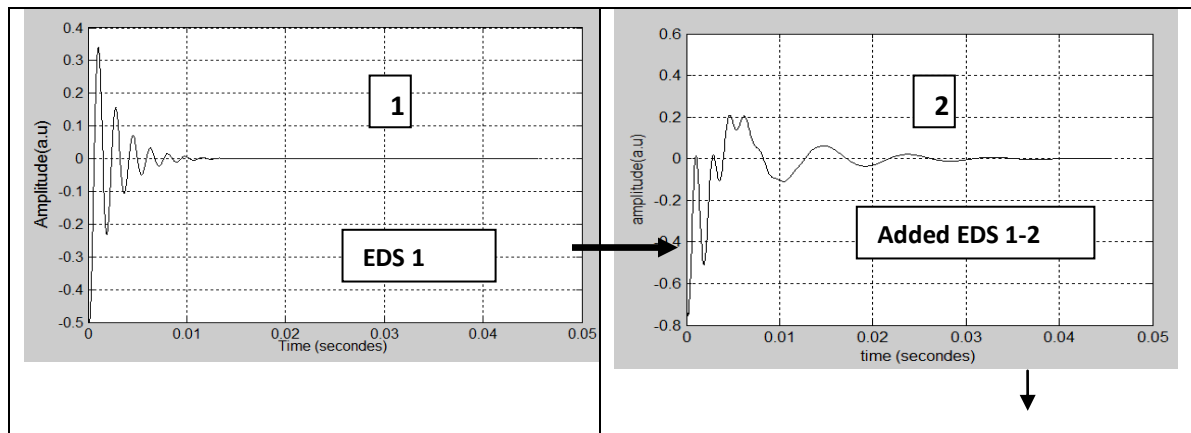
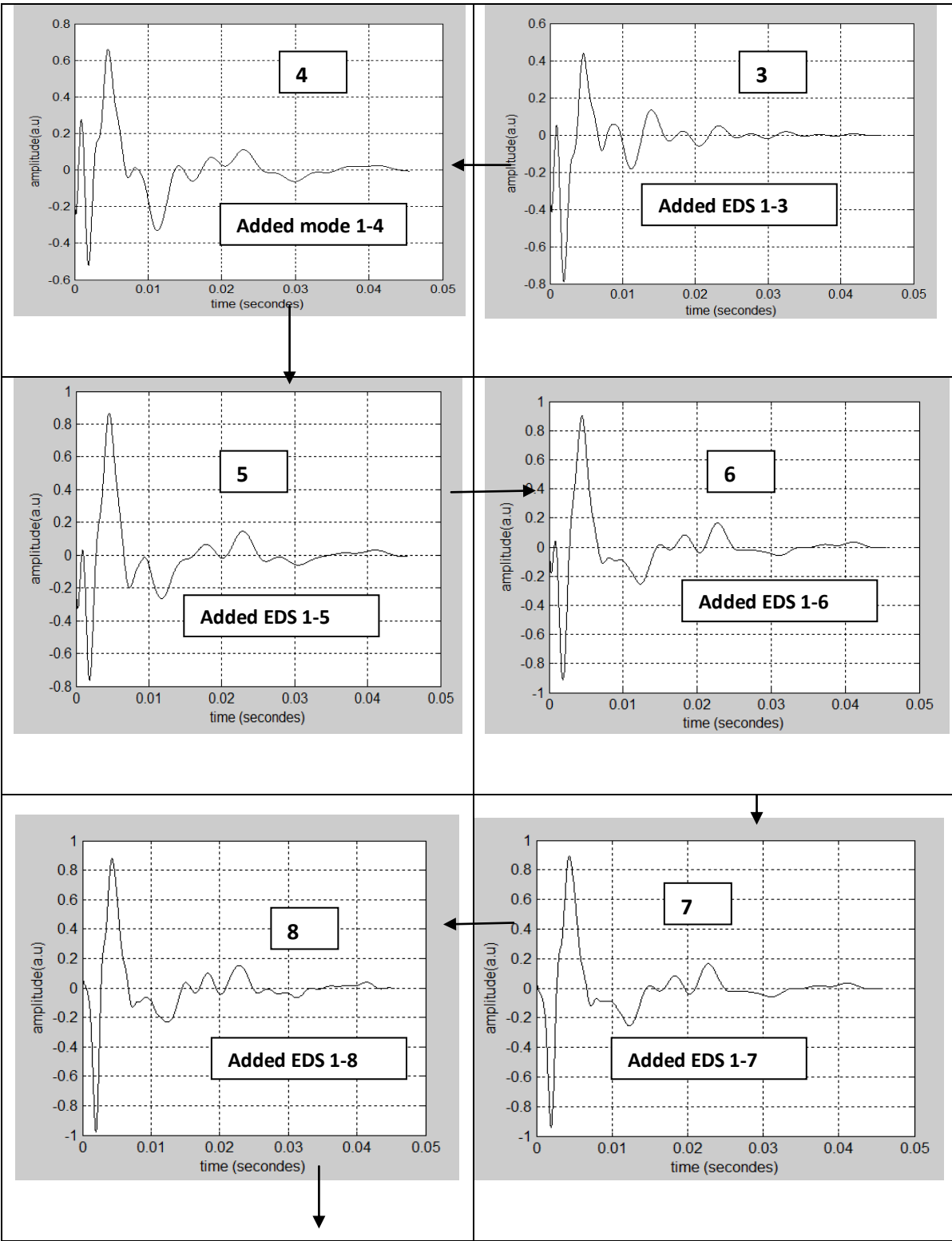
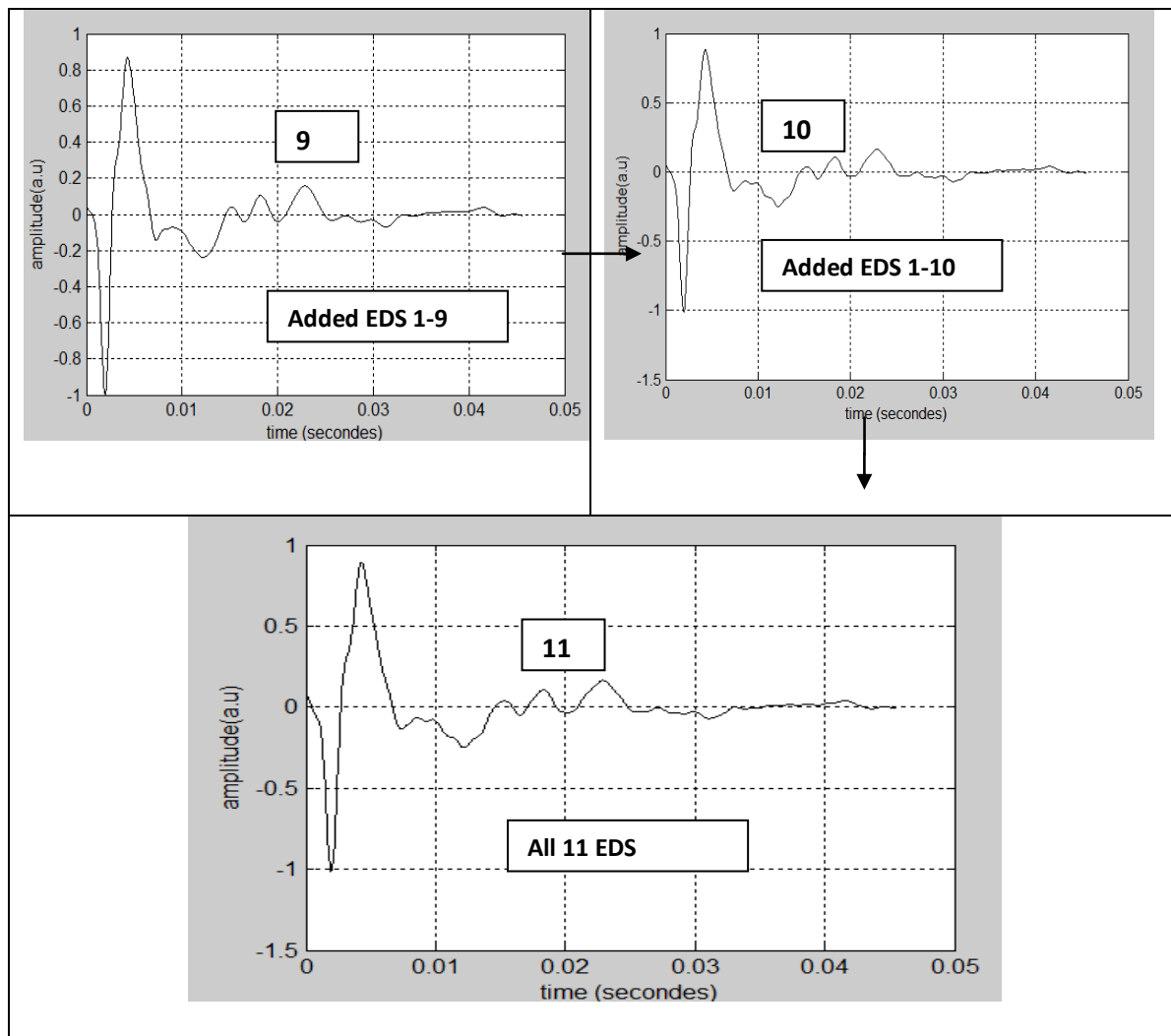


Figure 6.3 Tympanic signal EDSs

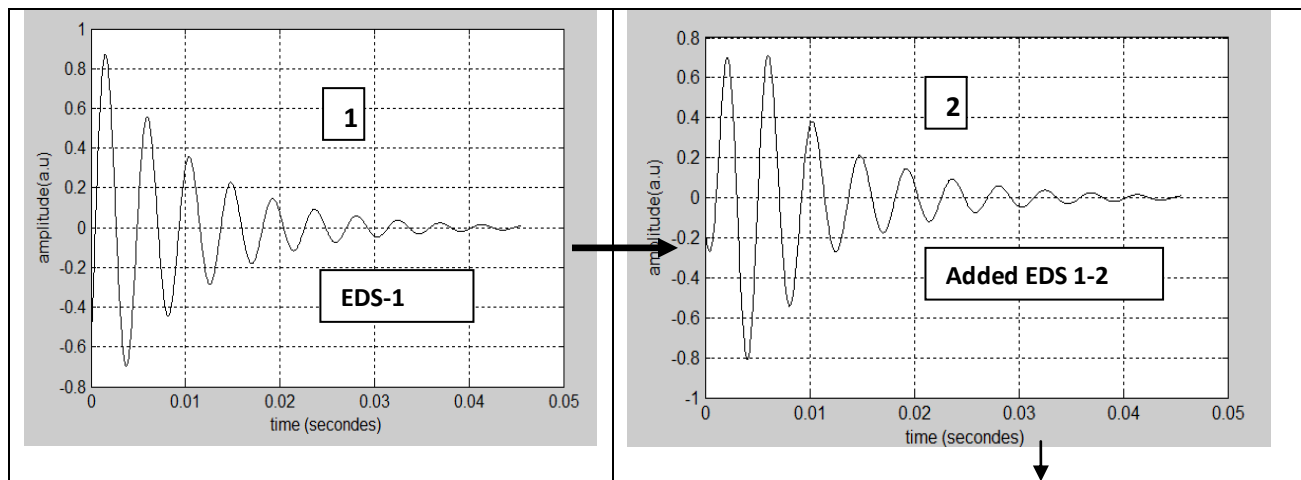
We can also observe from figure 6.3 that the EDS frequencies are different. They are not similar. Some of them are high frequency and some of them are not. As we have all the constituent parts of the percussion signals, it is very simple way to consider reconstruction the percussion signal and verify whether these EDS can give back the original signal. In addition, it would be meaningful if we reconstruct the percussion signals based on these EDSs. Normally all the EDSs combination should give the original signal back. We started reconstruction process of the original signal from the most dominant EDS as the EDS contribute more in the signal. In the second step, we added the second most dominant EDS with first one. The dominant EDS selection was based on the highest amplitude EDS. This process continued until the addition process completed of all the EDSs. The waveform shapes of added signals are shown in the figure 6.4 (a,b). This is a flow of signal reconstruction. We will be able to observe how the percussion signals reconstruction process changes the shapes of the waveform from one addition to another.

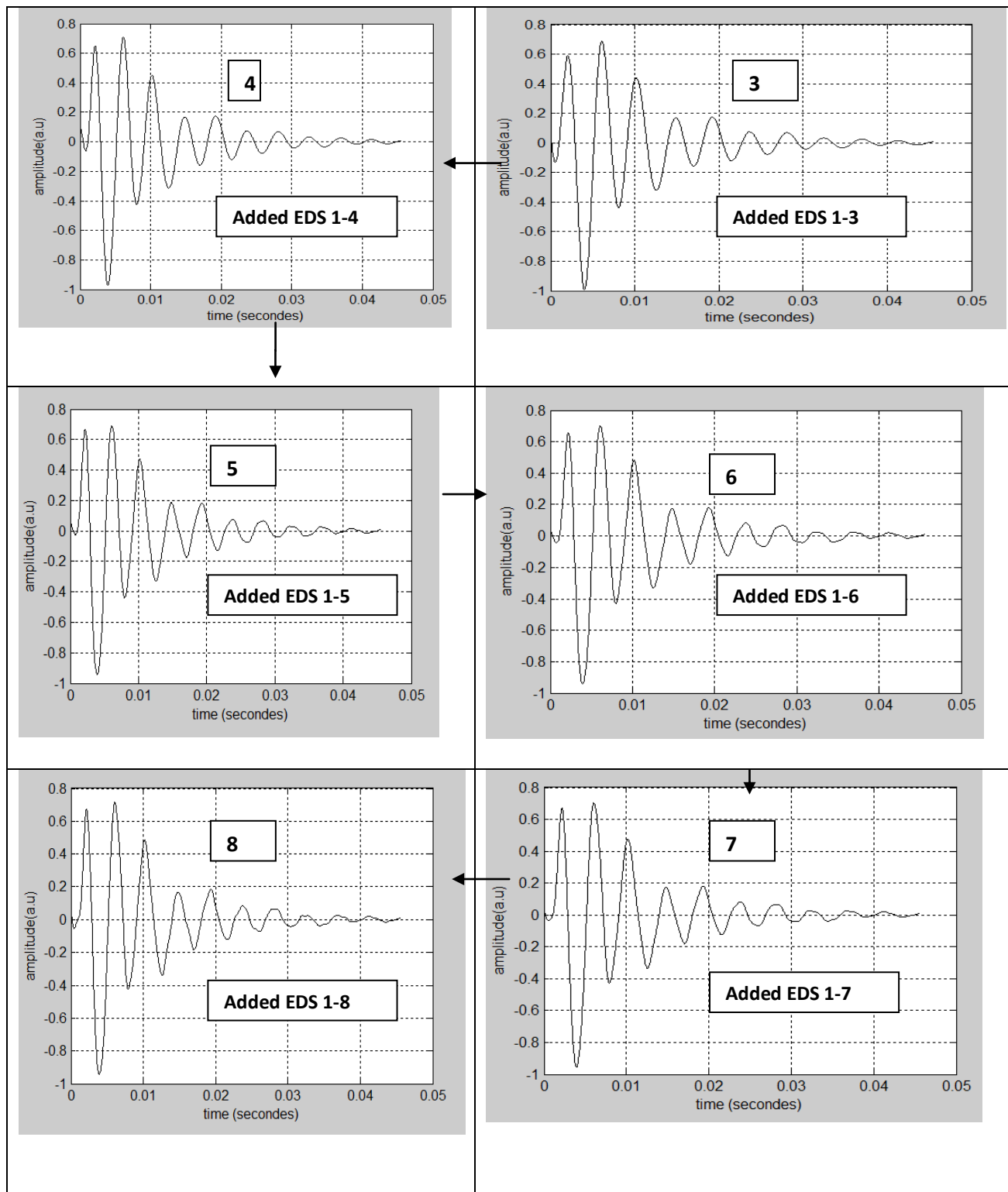






(a) Resonant signal reconstruction flow





(b) Tympanic signal reconstruction flow

Figure 6.4 Reconstruction of the medical Percussion signals (a) resonant signal and (b) Tympanic signal.

This procedure shows the simple way to predict the percussion signals. It is noticeable from the figure 6.4 that the shape of the original resonant signal does not show up until seven or eight EDS are added together. At this point further addition of EDS does not noticeably change the waveform. However, the situation is different for the tympanic signal. Tympanic signal gets the shape after the two or three EDS addition. The reconstructed signal is the estimated signal of the original signal. Therefore, it is very desirable to measure the reconstruction error of the reconstructed signal comparing with the original signal. We will discuss the reconstruction error analysis in the next section.

## 6.4 Reconstruction analysis

MPM directly estimates the parameters value for  $M$  real EDS components of the original signal. After comparing relative amplitudes of different EDS in each of the Tables 6.1 and 6.2, it can be noticed that some of them have significantly lower values than the others. In addition, the frequencies of these low-amplitude EDS are sometimes higher than the frequency limit of percussion signals. It is expected that these low-amplitude or too high-frequency components are not critically important for the purposes of signal classification (the MPM generates them to fit the noise) and can be neglected for computational efficiency and for data compression purposes. We will discuss in details the percussion signal recognition and classification based on this idea in chapter 9. In order to verify this hypothesis as well as to check the validity of the MPM decomposition we reconstructed the original signal from varying numbers of EDS sorted by the amplitude in the descending order. In this process, individual EDS were numerically synthesized from their 4 parameters and then added together. The results are shown in Figures 6. 5.a and 6. 5.b.

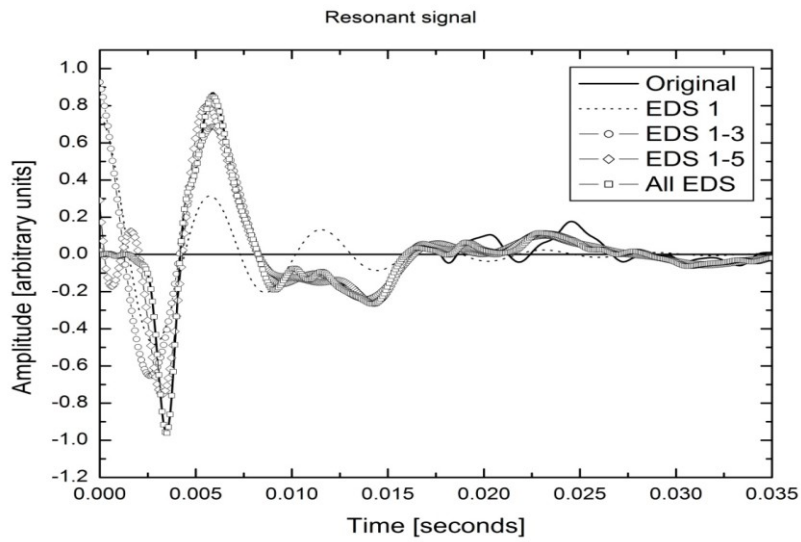


Figure 6.5 (a) Reconstruction of the original resonant signal from the increasing number of EDS components sorted by the amplitude

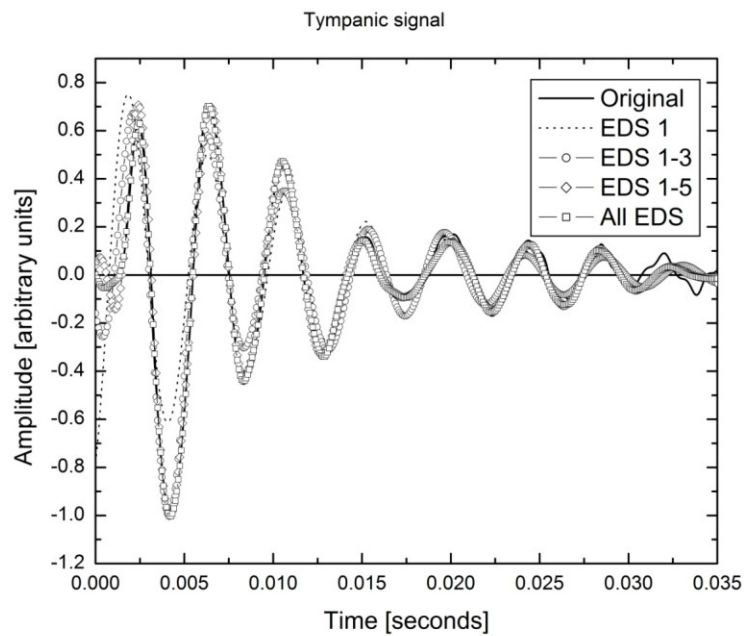


Figure 6. 5 (b) Reconstruction of the original tympanic signal from the increasing number of EDS components sorted by the amplitude

The hypothesis of reconstruction percussion signals using lesser number of EDS has some benefits. This would also help increase computational efficiency and further compress the signal by storing only  $4n$  coefficients where  $n$  is the number of significant modes. The procedure of selecting the most significant EDS modes can be automated. The ability to automatically identify the most significant EDS has several practical applications. First, these  $m$  EDS adequately represent the signal, which now can be stored as  $4m$  floating point coefficients ( $16m$  bytes). Since typically  $K \leq 10$ , and the original signal length is  $456 \times 2 = 912$  bytes, the compression rate is better than 6 (or better than 100 if compared to the original 8192-point buffer). Hence, the percussion signals can be efficiently compressed for storage or transmission over the network. Second, knowing the most significant EDS greatly simplifies other signal processing tasks, such as spectral analysis and diagnostic classification.

## **6.4.1 Reconstruction error analysis**

### **6.4.1.1 Theory**

The reconstructed signals illustrated in figure 6.4 and figure 6.5 can be achieved by adding less number of EDS. This is obvious that addition less number of EDS would not give the original signal back. Therefore, reconstruction errors generates in the estimated signals. This error depends on the different factor of the signal such as energy of the signal and the numbers of parameters those were used to reconstruct the signals [67]. We have discussed the SVD procedure in chapter 4. Here we will analyze the reconstruction error based on singular values; those are placed diagonally in the diagonal matrix  $[\Sigma]$  matrix in the SVD operation [67]. The threshold criterion was discussed in chapter 4 to determine the number

of singular values those are belongs to signal part and those are belongs to the noise part.

Based on this criterion we will illustrate the reconstruction error analysis.

Let the reconstructed signal is represent by the  $\hat{Y}$  as

$$\hat{Y} = U\hat{\Sigma}V^H \quad (6.1)$$

Where

$$\hat{\Sigma} = \begin{bmatrix} \sigma_1 & 0 & 0 & 0 & 0 & 0 \\ 0 & \sigma_2 & 0 & 0 & 0 & 0 \\ 0 & 0 & \sigma_M & 0 & 0 & 0 \\ 0 & 0 & 0 & 0 & 0 & 0 \\ 0 & 0 & 0 & 0 & 0 & 0 \\ 0 & 0 & 0 & 0 & 0 & 0 \end{bmatrix}_{(N-L) \times L} \quad (6.2)$$

Here (N-L) is total parameters needed for the original signal and M number parameters needed for the reconstructed signal. Therefore, the error signal would be

$$\text{Reconst\_error} = U \begin{bmatrix} \sigma_1 & 0 & 0 & 0 & 0 & 0 \\ 0 & \sigma_2 & 0 & 0 & 0 & 0 \\ 0 & 0 & \sigma_M & 0 & 0 & 0 \\ 0 & 0 & 0 & \sigma_{M+1} & 0 & 0 \\ 0 & 0 & 0 & 0 & \ddots & 0 \\ 0 & 0 & 0 & 0 & 0 & \sigma_r \end{bmatrix} V^H - U \begin{bmatrix} \sigma_1 & 0 & 0 & 0 & 0 & 0 \\ 0 & \sigma_2 & 0 & 0 & 0 & 0 \\ 0 & 0 & \sigma_M & 0 & 0 & 0 \\ 0 & 0 & 0 & 0 & 0 & 0 \\ 0 & 0 & 0 & 0 & 0 & 0 \\ 0 & 0 & 0 & 0 & 0 & 0 \end{bmatrix} V^H \quad (6.3)$$

$$= U \left\{ \begin{bmatrix} \sigma_1 & 0 & 0 & 0 & 0 & 0 \\ 0 & \sigma_2 & 0 & 0 & 0 & 0 \\ 0 & 0 & \sigma_M & 0 & 0 & 0 \\ 0 & 0 & 0 & \sigma_{M+1} & 0 & 0 \\ 0 & 0 & 0 & 0 & \ddots & 0 \\ 0 & 0 & 0 & 0 & 0 & \sigma_r \end{bmatrix} - \begin{bmatrix} \sigma_1 & 0 & 0 & 0 & 0 & 0 \\ 0 & \sigma_2 & 0 & 0 & 0 & 0 \\ 0 & 0 & \sigma_M & 0 & 0 & 0 \\ 0 & 0 & 0 & 0 & 0 & 0 \\ 0 & 0 & 0 & 0 & 0 & 0 \\ 0 & 0 & 0 & 0 & 0 & 0 \end{bmatrix} \right\} V^H \quad (6.4)$$

$$= U \begin{bmatrix} 0 & 0 & 0 & 0 & 0 & 0 \\ 0 & 0 & 0 & 0 & 0 & 0 \\ 0 & 0 & 0 & 0 & 0 & 0 \\ 0 & 0 & 0 & \sigma_{M+1} & 0 & 0 \\ 0 & 0 & 0 & 0 & \ddots & 0 \\ 0 & 0 & 0 & 0 & 0 & \sigma_r \end{bmatrix} V^H \quad (6.5)$$

$$= U\widehat{\Sigma_{\Theta-M}}V^H$$

$$\text{Reconst\_error}^* \text{Reconst\_error}^H = U \widehat{\Sigma_{\Theta-M}} V^H * \{ U \widehat{\Sigma_{\Theta-M}} V^H \}^H \quad (6.6)$$

$$= U \widehat{\Sigma_{\Theta-M}} \widehat{\Sigma_{\Theta-M}} U^H \quad (6.7)$$

$$E[\text{Reconst\_error}^* \text{Reconst\_error}^H] = E[\widehat{\Sigma_{\Theta-M}} U^H U \widehat{\Sigma_{\Theta-M}}] \quad (6.8)$$

$$E[\text{Reconst\_error}^* \text{Reconst\_error}^H] = E[\sum_{i=M+1}^{\Theta} \sum_{j=M+1}^{\Theta} \sigma_i \sigma_j u_i^H u_j] \quad (6.9)$$

The symbols  $\sigma$  are the individual eigenvalues.

$$E[\text{Reconst\_error}^* \text{Reconst\_error}^H] = \sum_{i=M+1}^{\Theta} \sum_{j=M+1}^{\Theta} E[\sigma_i \sigma_j u_i^H u_j]. \quad (6.10)$$

Since the eigenvector  $u_i^H$  and  $u_j$  are orthogonal, where

$$u_i^H * u_j = 1 \text{ when } i=j$$

And

$$u_i^H u_j = 0, \text{ when } i \neq j \text{ and } u_i^H u_j = 1$$

$$E[\text{Reconst\_error}^* \text{Reconst\_error}^H] = \sum_{i=M+1}^{\Theta} \sigma_i^2 \quad (6.11)$$

$$\text{Similarly, Reconstructed signal} = \sum_{i=1}^M \sigma_i^2 \quad (6.12)$$

### 6.4.1.2 Reconstruction performance analysis

The error can be calculated by summing up the square of unused singular values. This procedure shows how we can calculate the percussion signal reconstruction error prior to reconstruct the signal. The SVD operation on the Hankel matrix is the key tools here to find the error in the signals. First, we estimate the error related to discarding the smallest singular values ( $M+1$  to  $N-L$ ) in the matrix  $\Sigma$ , as they are considered noise. Where

$$\Sigma = \sigma_1 \cdots \sigma_M \cdots \sigma_{N-L} \quad (6.13)$$

Here only the  $M$  numbers of singular values would be used to reconstruct the percussion signal. The noise part and signal part will be used to calculate the percentage of reconstruction accuracy of the signal.

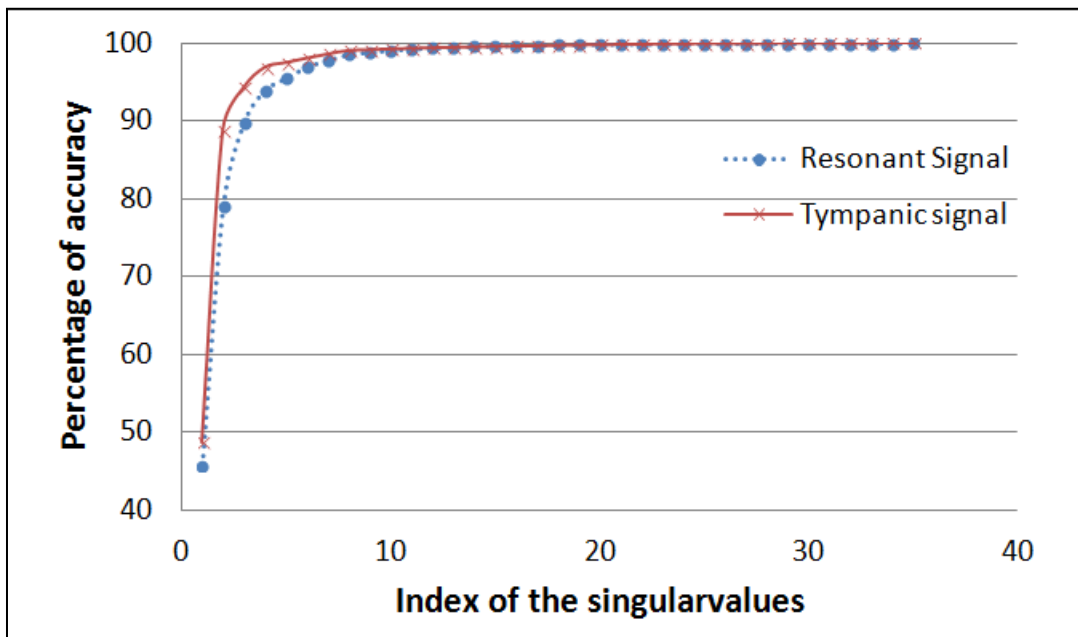


Figure 6.6 Reconstruction performance analyses for resonant and tympanic signals

$$\text{Reconstruction accuracy percentage} = \left\{ \frac{\sigma_1^2}{\sum_{i=1}^{N-L} \sigma_i^2}, \frac{\sum_{i=1}^2 \sigma_i^2}{\sum_{i=1}^{N-L} \sigma_i^2}, \frac{\sum_{i=1}^3 \sigma_i^2}{\sum_{i=1}^{N-L} \sigma_i^2}, \dots, \frac{\sum_{i=1}^M \sigma_i^2}{\sum_{i=1}^{N-L} \sigma_i^2} \right\} \times 100\% \quad (6.14)$$

We divide the squared of the first singular value by the total number of singular values squared as shown in the equation 6.14. Next, we add the second singular values squared with the first one and divide by the all-singular values squared. We continue this process until the  $M$  number of singular values is used. We have plotted the results in figure 6.6 to show the reconstruction accuracy efficiency. We can observe from the figure 6.6 that the performance of the algorithm at the beginning is not that great. As an example, the first singular value gives less than 50% accurate signal compared to the original one. The performance gets better for adding increasing number of singular values. We notice from the figure that the 12 singular values can give the optimal reconstruction accuracy, which is 99.87%. Here this only

12 singular values are used out of 153. This is huge saving in terms of storage and computation. It shows that we can get the same performance with the help of fewer parameters. As such, we can discard the rest of the singular values. It is also possible to measure the signal truncation error in terms of this discarded portion as:

$$SVD\_trunc\_error_{dB} = 10 \log_{10} \left[ \frac{\sigma_{M+1}^2 + \dots + \sigma_{N-L}^2}{\sigma_1^2 + \dots + \sigma_M^2} \right] \quad (6.15)$$

The level of the of the discarded portion of raw percussion signals collected during the normal volunteer pilot study was consistently in the range of -50 to -60 dB (-56.0+/- 1.2 dB for the resonant and -58.0+/- 0.8 dB for the tympanic signals), which is magnitude-compatible with the selected threshold  $\epsilon = 10^{-3}$  on singular value amplitudes.

## 6.5 Summary

In this chapter, we have successfully decomposed typical clinical percussion signals using Matrix Pencil Method and presented the analysis of resulting parameters. The EDSs of tympanic and resonant signals illustrated in this chapter. To check the validity of the method, the damped harmonics were added together in order to reconstruct the original signal. It was verified that the reconstructed signal is a good approximation of the original signal. It was also observed that only a subset of EDS components produced by the MPM algorithm is often enough to reconstruct the original signal with acceptable accuracy. We have plotted the reconstruction accuracy curve for better understanding. The high frequency and low-amplitude components can be discarded yielding computationally efficient reconstruction from a relatively small number of EDS. We have also demonstrated a possibility of efficient compression of percussion signals using only a few coefficients, which could be helpful when storing large amounts of percussion data or wirelessly transmitting data from the embedded

controller to the remote host. The damped harmonic decomposition can potentially be used to identify the main oscillating anatomical subsystems activated by the percussion event. It can also be used for the signal classification purposes because it provides natural parameterization of the data and its mapping onto a 4M dimensional space where the signals can be automatically clustered for further diagnostics. As a consequence, the entire analysis and classification process can be fully automated (and hence made objective), unlike the nonlinear fitting procedure described in [31].

# Chapter 7

## Super-resolution modal analysis of medical percussion signals

---

### 7.1 Introduction

In this chapter, we will introduce super-resolution modal analysis of medical percussion signals based on Matrix pencil method. Although clinical percussion is one of the most widespread noninvasive methods for diagnosing pulmonary disease, the available analysis of physical characteristics of the percussion sound using modern signal processing techniques is still quite limited. Most previously reported attempts to objectively characterize percussion sound signals are based on Fourier spectral analysis [1, 26, 31,39]. However, Fourier analysis, which represents the signal as a sum of infinite periodic harmonics, is not naturally suited for decomposition of short, aperiodic, and damped percussion signals. As suggested in [34], the spectral peaks referred to as “modes” could represent individual oscillating subsystems excited by the percussion event. These individual modes can be extracted and studied using an appropriate analysis algorithm. This modal analysis may also be of significant interest for further understanding of the physical origin of the chest percussion signals, for example, in conjunction with the acoustic resonance circuit model of the respiratory system and the chest wall suggested in [22,39]. Percussion is usually performed over a rib or between the ribs. In either case, at least two or three ribs (if not all) are excited by the percussion and the rib cage oscillates as a strongly damped oscillator, the damping being provided by the spongy alveolar tissue of the lung. It would be of interest to study the dependence of the modal character of the percussion signals on the location of the

administration point. The main issue with using the Fourier analysis for this purpose is broadening of the spectral peaks due to inherent damping of the vibrations induced by the percussion event, which causes peak overlapping and masking of the lower amplitude peaks. Being able to automatically identify the damped harmonic modes in the signal would immediately address the aforementioned issue. In this study, an attempt is made to automatically decompose percussion signals into a sum of exponentially damped harmonics, which in this case form a more natural basis than Fourier harmonics and thus allow for a more robust representation of the signal in the parametric space. The Matrix Pencil Method is a super resolution spectrum estimation technique that estimates the complex frequencies from the percussion signals.

## **7.2 Drawbacks of Fourier spectral analysis**

Spectral analysis based on the DFT is widespread and computationally efficient. However, these benefits often come together with serious drawbacks, such as limited frequency resolution, spectral leakage, picket-fence effect, and scalloping loss [39,48, 77-82]. Finite frequency resolution (the ability to separate closely spaced frequency components) is one of the most common limitations of the discrete Discrete-Fourier Transform [39,78, 82]. In fact, the conventional discrete Discrete-Fourier Transform cannot resolve frequencies separated by less than or equal to  $1 / NT$  Hz, where  $N$  is the number of samples in the digitized signal and  $T$  is the sampling interval. It is possible to reduce the bin size by zero-padding the signal, which leads to the frequency-domain interpolation and helps better delineate the shapes of the spectral peaks by preventing attenuation of frequencies between the adjacent bins. As any interpolation, however, zero padding does not add new information and therefore does not increase the actual frequency resolution [39]. The latter is defined as the ability to resolve two closely spaced frequency components in the original signal and can only be

improved by extending its time base. The length of the clinical percussion signals is limited by their nature, and therefore, their DFT resolution cannot be improved. On the other hand, each spectral peak has fixed natural width (the width of a Lorentzian curve obtained by continuous Discrete-Fourier Transform of the corresponding EDS) due to physical damping [39]. If the peaks are closely spaced, they can partially or fully overlap, hiding the smaller ones in between. In such cases, the MPM is expected to outperform DFT in terms of resolution.

Spectral leakage occurs when the time domain waveform is truncated to a fraction of a period. In these cases, the energy of the signal will be distributed between several adjacent spectral lines, “leaking” into the side lobes and distorting the overall spectral response [39,81-82]. Proper windowing can reduce the side lobe leakage, but always at the expense of resolution [82]. Also, when applying DFT to the sampled signal, the harmonic spectrum cannot be properly expressed if the harmonic frequency is not an integer multiple of the frequency resolution [39, 81]. This problem leads to the actual harmonic components appearing on the closest scale of the harmonic frequency, which is known as the picket-fence effect [39, 79]. In addition, there is a reduction in coherent gain of a particular frequency component that falls in between the multiples of the frequency resolution, which is termed scalloping loss. The correct application of the DFT relies upon the assumption that each frequency in the signal is an integer multiple of the fundamental frequency. On the other hand, the correct truncation of the signal requires a prior knowledge of the fundamental period of the signal. This means that the correct application of the DFT can only be achieved if one knows in advance the sinusoidal frequencies contained in the analyzed signal, but in the real world it is not possible to know the fundamental frequency in advance. All mentioned DFT-related issues can be mitigated to some extent by choosing proper

apodization, averaging, zero-padding, increasing the sampling rate, and other well-known methods [39]. However, the main motivation behind this work was our observation that Fourier spectral methods are not optimally suitable for the analysis of percussion signals. Indeed, the percussion signals are usually very short and aperiodic, so that their representation as a sum of infinite-duration, periodic sine waves would be somewhat artificial and require unnecessarily many terms.

### 7.3 Super resolution spectral analysis

In the context of the spectrum analysis, super-resolution technique for percussion signal presents interesting alternative to classical Discrete-Fourier Transform (DFT) [48]. Unlike nonparametric methods, parametric high-resolution methods assume that the observed signal has a special underlying structure and rely heavily on the resulting properties [48]. Most of these methods depend on signal model. MPM is one of the methods that belong to that category. Therefore, the MP method is used and its results are compared with the Discrete-Fourier Transform technique in this chapter. One of most important advantages of MPM is that it can determine the exact locations of the dominant frequencies and has the potential of distinguishing closely spaced frequency components, which could be helpful when attempting to detect subtle differences between percussion signals [39,48].

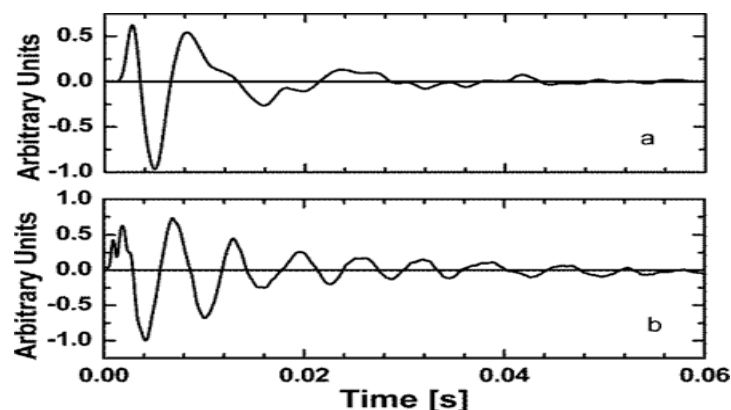


Figure 7.1 Examples of clinical percussion signals from (a) chest and (b) abdomen.

Another advantage of the MPM over the DFT is that its variance comes closer to that of the Cramer-Rao bound [58]. The major advantage of the MPM is that the frequencies are estimated directly from the temporal data series on a snapshot-by-snapshot basis. Employing this efficient algorithm decomposing the percussion signal into a sum of damped complex exponentials would constitute a considerable improvement over the laborious nonlinear fitting technique [34].

An example percussion signal shown in Fig. 7.1(b) was collected over the abdomen, and due to the hollow sound produced by an oscillating abdominal wall in the presence of intestinal gas pockets is historically known as “tympanic” [1]. In summary, the MPM is a super-resolution, adaptive damped harmonic decomposition method whose applicability to the percussion signal analysis is evaluated in the subsequent sections.

## **7.4 Results and analysis**

### **7.4.1 Comparison of the spectral and MPM analysis using a simulated signal**

The plan to use simulated signal is that the parameters of the signal are known before analysis the signal using MPM and DFT. Therefore, the accuracy of the modal analysis using both methods could be easily testified. As such, any inaccurate results would be identified before applying the methods on a real signal as the components of the real signal are always unknown. An idealized noise-free signal (figure 7.2) was constructed as a sum of six EDS with the following parameters shown in Table 7.1.

TABLE 7.1: Parameters of six EDS in the simulated signal

Frequency $f_i$ [Hz]	50	105	110	120	150	180
Amplitude $A_i$ [a. u.]	0.4	0.5	0.1	0.3	0.4	0.2
Damping $d_i$ [ $s^{-1}$ ]	21	10	18	16	12	10
Initial phase $\varphi_i$ [deg]	30	30	30	30	30	30

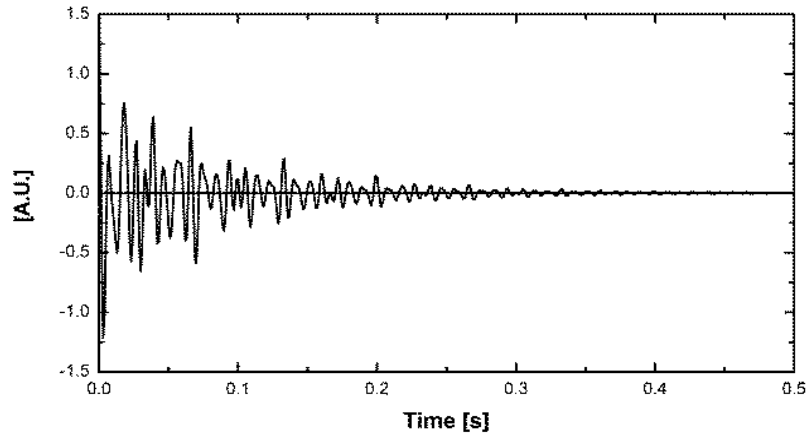


Fig. 7.2 Simulated signal waveform (no noise case)

The goal of this test was to find out whether the MPM is able to resolve frequency differences undetectable with the traditional Discrete-Fourier Transform, namely,  $\Delta f \leq \frac{1}{N\Delta t}$ . The results for MPM and DFT are placed together in the figure 7.3. The vertical lines in Fig. 7.3 indicate the frequencies of individual EDS components detected by the MPM in this signal. It should be noted that this theoretical frequency resolution applies to the ability of the DFT algorithm to resolve closely spaced undamped harmonics. If damping is present (as in our case), each Fourier peak has its own natural minimum width (the width of a Lorentzian curve obtained by continuous Discrete-Fourier Transform) and cannot be made any narrower for physical reasons.

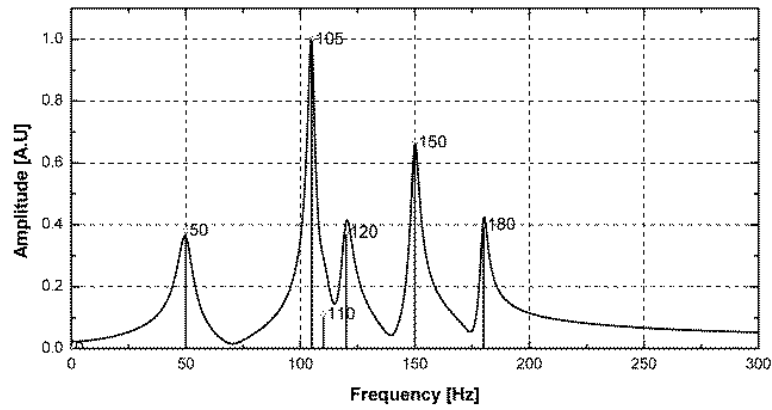


Fig. 7.3 DFT and Matrix Pencil Method spectra of the simulated signal shown in Fig. 7.2  
(rescaled)

Therefore, closely spaced peaks will continue masking each other, and the resolution will not improve with further increase of  $(N\Delta t)$ . It can be observed from Figure 7.3 that the 105 Hz and 110 Hz frequencies cannot be distinguished in the DFT spectrum. Therefore, the weaker EDS at 110 Hz does not show up as a separate peak in the DFT spectrum even though its separation from the higher amplitude EDS at 105 Hz is 10 times larger than the frequency resolution. Although the DFT also contains the information about the 110 Hz peak, extracting this information would require sophisticated fitting methods, which are prone to error even in this simplest noise-free case and get even less reliable when there are more than two closely spaced components. The MPM, on the other hand, accurately identifies and quantifies all the components up to its resolution limit. Notably, for the noise-free signal the MPM has produced exactly the same EDS parameters as the original ones listed in Table 7.1. The MPM approach, on the other hand, has correctly identified all six original frequency components. It can further be observed (Figure 7.3) that the positions of the Fourier peaks corresponding to individual EDS are shifted from the actual EDS frequencies. Notably, the MPM finds the original, undamped EDS frequencies  $f_i$ , while the locations of the spectral maxima

correspond to damped frequencies  $F_i = \sqrt{f_i^2 - (2\pi d_i)^2}$ . Although the difference between  $f_i$  and  $F_i$  is usually small and can be neglected, it becomes noticeable in the highly damped and low frequency resonant percussion signals. In general, the heights of the spectral peaks are different from the EDS amplitudes. Analytically, the power spectrum of the  $i$ -th EDS is given by:  $|\tilde{x}_i(f)|^2 = \frac{A_i^2}{d_i^2 + 4\pi^2(f - F_i)^2}$ , so that the height of the  $i$ -th spectral peak is equal to  $A_i/d_i$ . After dividing the amplitudes  $A_i$  of individual EDS by the corresponding damping factors  $d_i$  and normalizing the resulting values by the height of the dominant spectral peak, the MPM and DFT results can be conveniently compared on the same plot (Fig. 7.3).

The above example illustrates that MPM can be more robust than DFT in resolving closely spaced frequencies in short, strongly damped signals, such as the ones occurring in clinical percussion. Hence, the MPM provides a more accurate value for the modal frequency, which is closer to the undamped value than that provided by the DFT. So, it can be concluded that the Matrix Pencil Method is more appropriate for calculating closely spaced frequencies, especially for the systems with damping, than the DFT, and that is why it is also called a super-resolution spectral analysis [58,59].

## **7.4.2 Comparison of the MPM and DFT analysis of clinical percussion signals.**

The local anatomy of each human body is unique, and in this sense each percussion signal is unique as well. None of the existing theoretical models can accurately predict the frequencies and the number of the fundamental oscillation modes that will be excited by the particular percussion event. Fig. 7.4.a shows the amplitude spectrum of the resonant percussion signal

from Fig. 7.1.a. Several peaks are visible, such as the highest one below 100 Hz, the second one below 150 Hz, and the third one around 200 Hz, but they are not clearly resolved.

TABLE 7.2: Frequency and  $A/d$  values for 10 strongest EDS found in percussion signals shown in Fig. 1(a, b)

(a) Resonant signal			(b) Tympanic signal	
	f [Hz]	A/d [a.u.]	f [Hz]	A/d [a.u.]
1	66.7	1	163.3	1
2	194.9	0.6	207.8	0.23
3	130.7	0.41	98.7	0.195
4	46.4	0.39	286.4	0.185
5	254.9	0.2	42.1	0.097
6	130.8	0.18	258.2	0.092
7	278.3	0.08	137.6	0.077
8	346.3	0.07	360.7	0.069
9	578.1	0.06	472.4	0.043
10	575.4	0.03	341.8	0.027

Similarly, in the case of a tympanic signal (Fig. 7.4 b), one clearly dominant spectral peak is surrounded with several overlapping satellite peaks. Alongside with the Fourier spectra, Figs. 7.4 a and 7.4 b show the frequency and amplitude values of the individual EDS derived by the MPM. The amplitude values  $A_i$  were divided by the damping factors  $d_i$  and then normalized. Only the EDS with frequencies below 1 KHz are of interest, as determined by the band-pass filter in the recording software and by the natural bandwidth of the percussion signals. Applying the empirical rule of thumb to the case of 48 kHz sampling rate,  $N=3000$ ;  $L=N/3=1000$ , the maximum resolvable beat period would be 10000-20000 samples, or 0.2-

0.4s. So, the MPM should be able to resolve 2.5-5 Hz beat frequencies in the percussion signals.

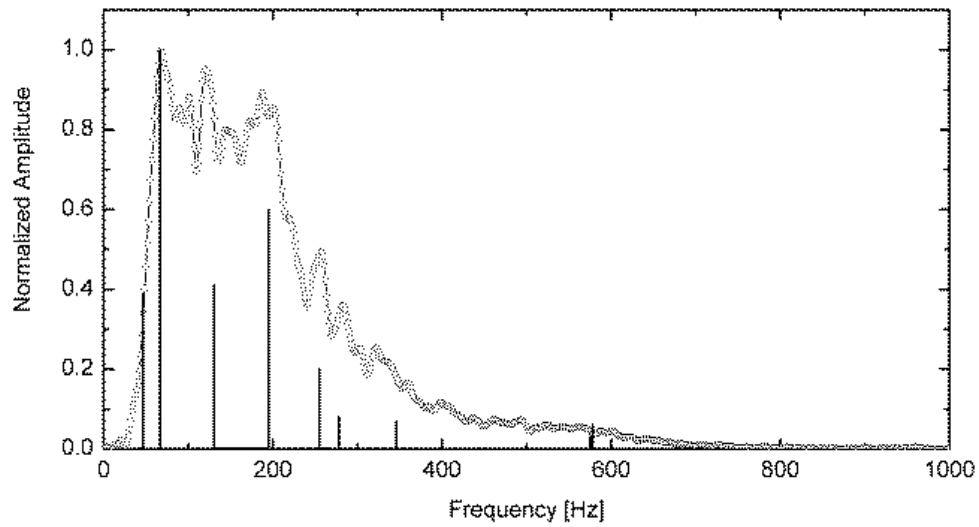


Fig.7.4a Spectrum of the resonant percussion signal shown in Fig.7. 1.a. Normalized EDS are shown as well to illustrate matching

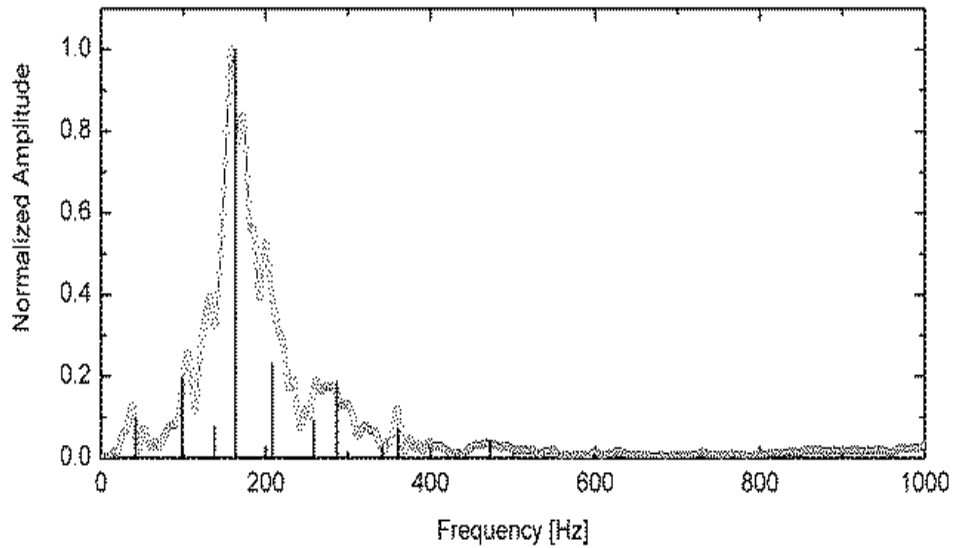


Fig.7.4 b Spectrum of the tympanic percussion signal shown in Fig. 7.1.b. Normalized EDS are shown as well to illustrate matching.

Table 7.2 provides the values of  $f_i$  and  $(A_i/d_i)$  for 10 dominant EDS for both tympanic and resonant signals. The frequencies of the highest magnitude EDS in the resonant and tympanic signals are 66.7 Hz and 163.3 Hz respectively. From Fig. 7.4a, one can also see that three frequencies (66.7 Hz, 194 Hz, and 130.7 Hz) represent the most significant EDS components of the resonant signal. In the case of tympanic signal (Fig. 7.4b), only one EDS is clearly dominant. Comparing the MPM and spectral analysis results (Fig. 7.4a, b) one can notice that the EDS frequencies detected by the MPM are correlated with locations of the maxima of the spectral peaks detected by the DFT. In fact, each EDS corresponds to a peak in the Fourier spectrum. When the peak is relatively isolated, its spectral amplitude is approximately equal to the  $A/d$  value of the corresponding EDS. When the peaks overlap, the resulting spectral amplitudes are in general higher than those of individual peaks, and hence the  $A/d$  values appear below the spectral line. It can also be noticed that some minor spectral peaks do not have corresponding EDS components. Although major components of the percussion signal can be assumed exponentially damped oscillations, the real signal always deviates from the EDS model due to presence of noise and possibly different damping mechanisms. Therefore, mentioned mismatch can be explained as a fitting artifact. Most of these minor peaks are correctly reproduced in the spectrum of the signal reconstructed from the EDS components. The imperfections in the reconstruction can be explained by the SVD truncation error.

### **7.4.3 Analysis of the fine structure of the spectral peaks**

A closer inspection of the structure of the main broad peak in the frequency spectra of the chest signals often reveals two or three separate peaks (such as those present in Figure 7.4.a). These peaks consistently appear in the spectra of the signals obtained over the same body point (left sub-clavicular), on the same subject, but at different times. The relative

amplitudes of these peaks may change, which can be attributed to small round-to-round variations in the location of the percussion point, changes in the intensity and direction of percussion or/and variations in the position of the diaphragm due to the inhale-exhale cycle. From the physical standpoint, these distinct fine peaks comprising the main spectral peak of a typical (resonant) chest signal could be attributed to percussion excitation of several anatomical subsystems including the rib cage, the bronchial tree, and even the air-filled stomach [22].

We considered of interest to compare the distribution of the location of the three peaks for a group of 30 volunteers obtained with the Matrix Pencil and spectral approaches. Fig. 7.5 a and 7.5 b show the peak frequency histograms obtained with the two methods. Both distributions show similar grouping of the peaks into several frequency bands, such as 50-100, 100-150, 150-170 and 190-220 Hz etc. It took several days to extract the Lorentzian modes from all signals by nonlinear fitting in order to produce data for Fig. 7.5 a. As a clear advantage, the MPM procedure was easy to automate, and it took several minutes to process the same amount of data and to generate Fig. 7.5.b. Also, unlike the Fourier analysis, which readily provides only the amplitudes and peak frequencies of the dominant peaks, the MPM fully characterizes each mode in terms of its four parameters.

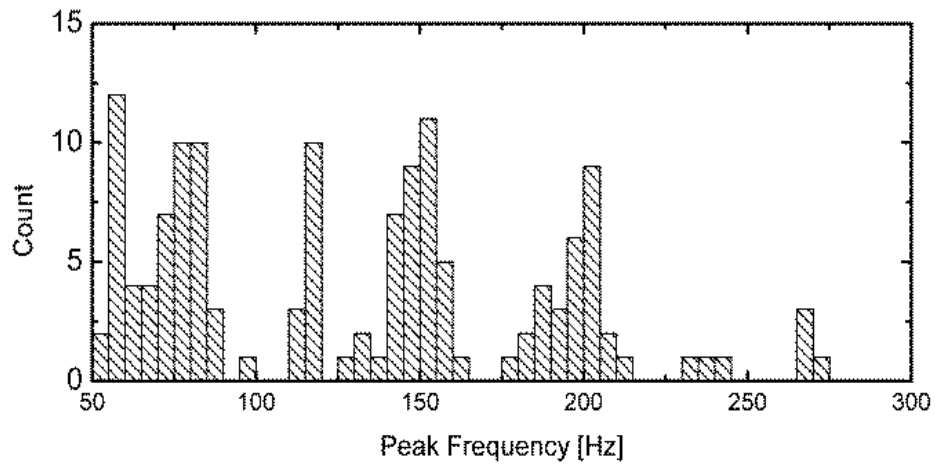


Fig.7.5.a. Frequency histogram of the spectral peaks of the upper chest signals from 30 volunteers using the DFT method (the frequency bin was set to 5 Hz).

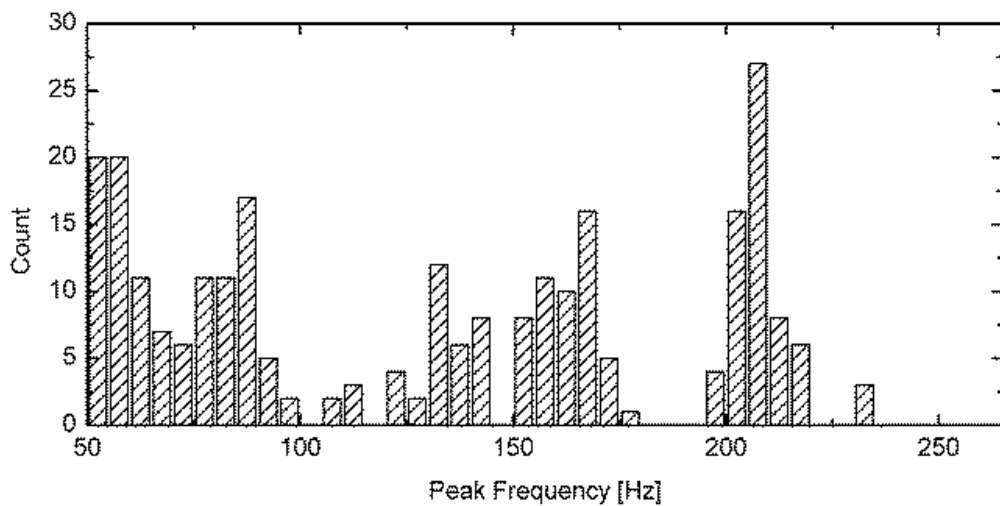


Fig.7.5.b. Frequency histogram of the main EDS for the upper chest signals from 30 volunteers decomposed by the MPM [the frequency bin was set to 5 Hz]

Understanding the physical nature of the observed frequency bands could lead to a more efficient interpretation of the complex character of chest percussion signals and eventually to better diagnostics of pulmonary diseases. The percussed chest wall behaves as a strongly damped oscillator, the damping being provided by the muscles and the lung parenchyma.

Finding the parameters of this oscillation (i.e. identifying and characterizing a particular spectral peak) is critical for our ability to detect physical abnormalities, such as pneumo- and hemothorax. Despite the existence of many complex physical models of the thorax oscillation in the literature, none of them has been able to successfully identify these various peaks. One possible explanation of the multi-band structure of the chest percussion spectra, first expressed in [34], is the indirect excitation of abdominal gas cavities. When the percussion impact on the chest wall is strong enough, the diaphragm could vibrate as a membrane damped by the abdominal content. If a significant amount of gas is present under the diaphragm (the size, location and number of gas pockets in the intestines and stomach usually change during the day and may depend on the time passed since the last meal), the damping decreases, producing a strong tympanic component. To systematically analyze this effect, a histogram of frequencies of several dominant EDS found in the chest and abdominal percussion signals from 30 volunteers was plotted in Fig. 7.6. Five highest-amplitude EDS were taken from each chest signal and one from each tympanic signal. It can be noticed that the frequency band of abdominal signals (150-350 Hz) overlaps with the bands of the three higher frequency EDS of the chest signals. The lowest chest band (50-130 Hz) is very distinct and sustainable across all volunteers. The observed in Fig. 7.6 correlation between the frequencies of chest and abdominal responses to percussion prompts a hypothesis that these signals may have common physical origin.

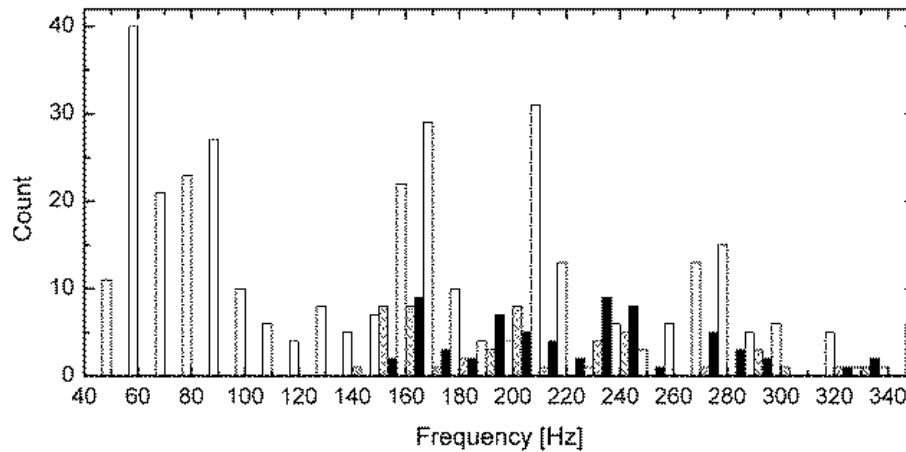


Fig.7.6 EDS frequencies of chest (white), right abdominal (black) and stomach (hatched) percussion signals from 30 volunteers (for some volunteers the data were taken more than once)

To verify this hypothesis, the following experiment was conducted. One of the volunteers was withdrawn from food for 15 hours, and his stomach was empty. As a consequence, the percussion response of the stomach was dull, while the response of the right abdomen was weakly tympanic, showing 2-3 cycles in the time domain and the frequency peak at ~250Hz. The chest signal was typical resonant, with a smooth broad single spectral peak (Fig. 7.7). Once this volunteer consumed a carbonated drink, the stomach response remained dull, while the right abdominal response became strongly tympanic, showing 5-6 cycles in the time domain and a narrow frequency peak at ~170 Hz (Fig. 7.8). The chest signal also exhibited notable changes in the form of additional oscillations in the time domain and splitting of the main spectral peak in the frequency domain. The analysis of this split shows that the rightmost peak at ~70Hz remained almost the same, while the ~170 MHz peak became more pronounced, resulting in a gap between the two peaks (Fig. 7.8). This experiment is a direct demonstration of how adding gas to the abdomen directly affects the chest percussion signal. Notably, the changes in the chest signal spectrum appear to correlate

with the frequency of the abdominal oscillation. In the no-gas experiment (Fig.7.7), the abdominal bubble was very small and located deeply in the intestines, far from the diaphragm, so it did not affect its damping. Consumption of the carbonated drink introduced a larger pocket located directly under the diaphragm, noticeably reducing its damping.

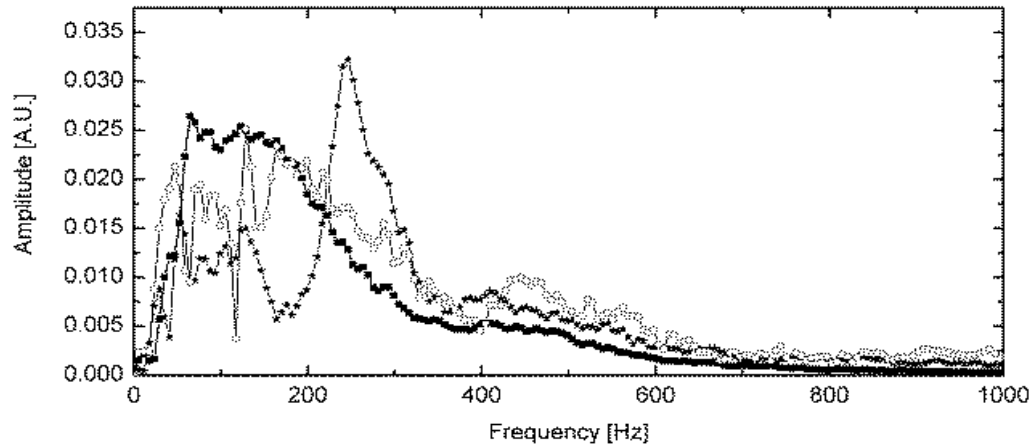


Fig.7.7. Frequency spectrum of the percussion signals for the subject with no gas in the abdominal cavity. (Black squares – chest, open circles – stomach, black triangles – abdomen)

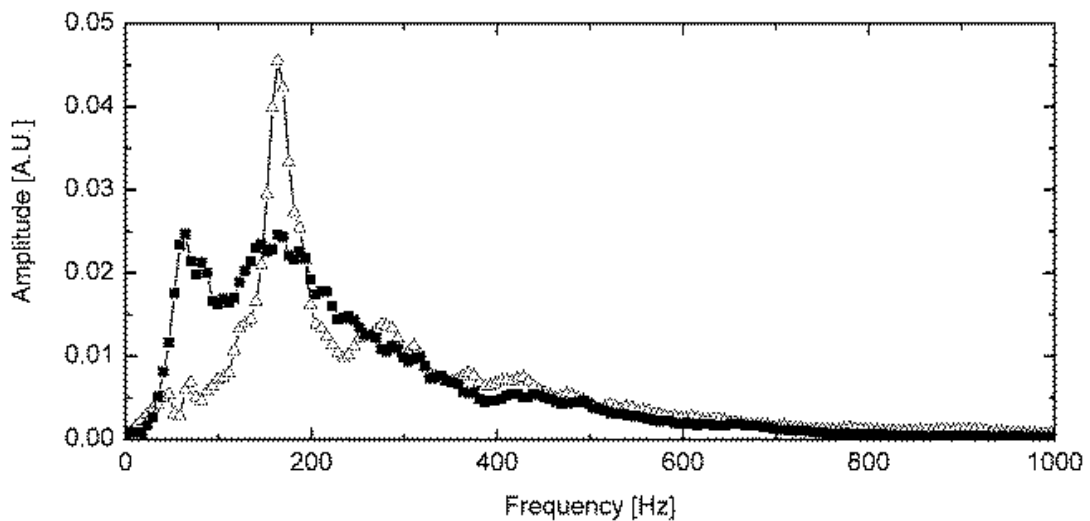


Fig.7.8. Frequency spectrum of the percussion signals from the subject with gas in the abdominal cavity. (black squares – chest, open triangles – abdomen).

Also notably, after introducing gas in the abdomen the width of the second peak was reduced (lower damping) leading to better exposure of the first peak (Fig. 7.8). More information can be revealed by comparing five most significant EDS produced by the MPM for the chest signals acquired before and after consuming the carbonated drink (Table 7.3). It can be seen that the amplitudes and damping factors of most EDS did not change significantly after introducing gas into the abdomen. The exception is the EDS at 120-135 Hz, which shows a significant decrease in damping (from 180 to 112), while the others exhibit much weaker changes. This mode is invisible in the DFT spectrum, but is detected with the MPM. After reconstructing the original signal from its EDS components we analyzed the effect of changing their parameters on the overall shape of the Fourier spectrum. By varying the EDS amplitudes alone it was impossible to transform the “no-gas” chest spectrum (black squares, Fig. 7.7) into the “gas” chest spectrum (black squares, Fig. 7.8). By varying damping of the first 4-5 modes, such transformation became possible. The main effect (creation of the gap between two sub-peaks in Fig. 7.8) was achieved after changing the damping of the middle mode at 120-135 Hz.

TABLE 7.3: Five most significant EDS produced by the MPM for the chest signals acquired before and after carbonated drink consumption

No gas				Gas		
A/d	f	d		A/d	f	d
0.45	44.7	63.6		0.62	51.5	63.4
1.0	65.6	91.5		1.0	70.3	101.6
0.79	164.0	192.4		0.96	172.8	198.4
0.75	134.3	180.4		0.42	122.8	111.9
0.28	236.2	274.5		0.18	244.6	235.5

Based on the above experimental evidence a hypothesis is put forward that the first, lowest frequency peak represents the pure chest response to percussion while the higher frequency peaks are caused by the indirect excitation of the diaphragm damped by the abdominal content. The goal then is to eliminate the effect of the diaphragm and extract the pure chest response for further analysis and diagnostics of pneumothorax. One way to tackle this problem is to use nonlinear spectral fitting with Lorentzians, as described in [34] and above and retain only the mode representing the first dominant peak. However, this procedure is labor-intensive, prone to error, and difficult to automate. MPM offers an easy solution as only the EDS in the frequency range 50-100 Hz can be kept, and the chest response can be reconstructed from them.

Comparing the results of the MPM and traditional DFT analysis one can notice that the positions of the EDS detected by the MPM are correlated with locations of the maxima of the spectral peaks detected by the DFT. In addition to this, MPM is cable of finding the close frequencies into the signal specially EDS signal.

## **7.5 Summary**

The conventional spectral analysis of the chest and abdominal signals reveals a few general observations regarding their spectral characteristics. For the chest signals, the positions of the modes for a given subject are not affected by variations in the percussion strength, direction or exact location of the percussion point. Different rounds of measurements tend to provide consistent values for the positions of the modes in the frequency space. The relative amplitudes however may change from round to round, and so the overall shape of the frequency spectrum will change. The positions of the modes have variations from patient to

patient but they seem to fall in three distinct ranges (at least for the three strongest modes studied) with very little overlapping. For abdominal signals, the characteristic frequencies of the signals are, on average, higher than those of the resonant signals. The main spectral peak is much narrower than for the chest signals. A significant number of signals have single mode character (single narrow peak). The positions of the spectral peaks are not well defined, as in resonant signals, but change randomly from subject to subject.

It has been demonstrated that a super-resolution spectral analysis method, such as Matrix Pencil Method, is extremely appropriate for the task of estimating the dominant oscillation modes present in the clinical percussion signals. The main advantage of the MPM (and of damped harmonic decomposition in general) over the Fourier-based methods is reduction of the number of components (compared to Fourier harmonics) accurately representing the observed signal. As a consequence, the amount of information necessary to fully describe and then classify the percussion signal reduces dramatically. In addition, the MPM decomposition allows bringing more insight into the physical nature of percussion signals by identifying and fully characterizing individual oscillating subsystems excited by the percussion event. Based on these advantages, it is recommended that the MP method should be employed instead of the popular DFT in application to diagnostic classification of clinical percussion signals.

# Chapter 8

## Time-frequency analysis of medical percussion signals

---

### 8.1 Introduction

Time-frequency analysis is important to identify the localized information of a non-stationary signal in the time and frequency domains simultaneously [83, 85]. This signal representation technique transform a 1-D signal into a 2-D time-frequency map, which describes how the spectral content of the data evolves with time, thus providing an ideal tool to dissect, analyze and interpret non-stationary signals. Conventional analysis methods which work well for stationary signals (e.g. spectral analysis) do not provide information about the evolution of the spectral content over time, which is essential in many applications [84-88]. Therefore time-frequency analysis of such signals is necessary to adequately represent the signal in both time and frequency domains [89]. In addition, based on the energy distribution in the time-frequency space, one can isolate and evaluate the behavior of different signal components independently [90], as they show up on the plot as localized areas of increased brightness [84,87]. Also, time-frequency analysis combines the advantages of the pure time-domain and spectral methods, and brings important additional benefits, such as the ability to trace the evolution of the spectral content with time [83,84,87,90]. This work describes an attempt to construct a TF representation specifically tailored to clinical percussion signals to achieve better resolution of individual components corresponding to

physical oscillation modes. In this approach, percussion signals are represented as linear combinations of exponentially damped sinusoids (EDS), which fit this type of signals more efficiently than Fourier harmonics. Matrix Pencil Method (MPM) is used to decompose the signal into a set of EDS, which are then plotted in the time-frequency plane. Such representation provides better visualization of the signal structure than commonly used frequency-amplitude plots and facilitates tracking subtle changes in the signal for diagnostic purposes. The performance of our approach is compared with several conventional TFD for both ideal and real percussion signals. The results can be interpreted in favor of the EDS-based model. The MPM-based time-frequency analysis is shown to be a better choice for clinical percussion signals than conventional TFDs, while its ability to visualize damping has immediate practical applications.

## **8.2 Motivation for time-frequency analysis of medical percussion signal**

### **8.2.1 Inherent causes**

Percussion response from the chest would change due to impedance mismatch at the air cavity boundary [4]. As a result, the percussion signal elongates the duration of acoustical energy transfer, and the slower amplitude drops [4]. The core hypothesis is that the imposed air cavity would be a leading cause of time-varying frequency in case of chest percussion response [3, 10,15,17,20]. On the other hand, the normal lung fills the pleural space and absorbs the sound energy rapidly [4, 21]. The goal of this work is to come up with a way to visualize this effect of changed damping of certain signal components in the time-frequency plane. In performing time-frequency of the medical percussion signals, we target the

percussion signals comprised of components whose energy is in some sense would be localized in the time-frequency (TF) Plane. This approach identifies how many components are there, describes the nature of their energy structure, and probabilistically associates time-frequency locations with the components.

## **8.2.2 Methodological causes**

Medical percussion signal is a non-stationary and multi-component signal [92, 83]. The first term means that the spectral contents of the signal may change over time, while the second term means presence of more than one frequency component. A clinical percussion signal represents free transient response of the human body to a brief mechanical impact. Due to damping, the amplitude of these signals changes with time, and hence they can be considered non-stationary in the broad sense of this definition [84,92-95,]. Since the impact usually excites oscillations of more than one anatomical subsystem, percussion signals usually represent more than one independent oscillation mode with different frequencies, and hence can be considered multi-component, again, in the broad sense of this term [75, 76, 91-97]. Various properties and statistics of these signals may vary temporally or spatially [99], and their energy may be concentrated in several localized time-frequency regions. Representing such signals in the time-frequency domain is not always easy due to their short duration and possible coexistence of multiple frequency components with very different amplitudes[83,95].

Most traditional time-frequency distributions (TFD) perform well on the mono-component, non-stationary signals [85,89,90,92,95,96,100]. The analysis of short, highly damped percussion signals using conventional Time-Frequency Distributions (TFD) meets certain difficulties, such as poor time-frequency localization, cross terms, and masking of the lower

energy features by the higher energy ones [85,89,90,92,96]. Such drawbacks severely distort the time-frequency portrait of percussion signals, limiting practical applications. The above shortcomings lead to inaccurate and ambiguous representation of the signal behavior in the time-frequency plane.

### **8.3 Review of existing TFDs**

The most extensively exploited linear time-frequency analysis methods are the Short Time Discrete-Fourier Transform (STFT) and Wavelet Transforms [83,85,87,90,101]. Although STFT is immune to cross-terms, its biggest limitation is the tradeoff between the time and frequency resolution due to the Heisenberg uncertainty principle [83,85,86]. In case of the wavelet transform, the frequency resolution decreases with increasing frequency [87,101]. If more than one frequency component exists in the signal, satisfactory resolution for all modes cannot be obtained. This is an inherent characteristic of the wavelet analysis [101]. On the other hand, the quadratic (Cohen's class) time-frequency distributions are based on estimation of instantaneous energy using bilinear operation on the signal [88, 97]. Among the most commonly used time-frequency distributions from the Cohen class are Wigner-Ville Distribution (WVD), Choi-Williams Distribution (CWD), and Zhao-Atlas Marks (ZAM) distribution [83,84,86,87,90]. WVD has excellent time-frequency resolution due to the absence of averaging over any finite time interval [92, 97, 87,102]. While performing well on the single-component signals, the WVD's performance degrades dramatically as the number of components increases, because of the spurious peaks arising from the cross terms and confusing the visual interpretation of its time frequency spectrum [89,92,93]. CWD is an improvement of the WVD intended to suppress the 'cross terms' by multiplying it with a kernel function [84, 87]. Unfortunately, increased suppression of the cross-terms invariably leads to smearing or loss of resolution of the auto terms in the time-frequency plane.

Similarly, CWD, ZAM also efficiently suppresses the cross term artifacts, still at the expense of the time-frequency resolution [100]. As the inherent characteristics of a real time signal not always known apriori, the proper kernel selection remains a critical issue in quadratic time-frequency analysis [83].

No single TFD produces equally good results for all types of signals [88,97]. Different decomposition approaches are possible for different types of signals. The focus of our work is on the medical percussion signals, a particular class of multi-component signals representing the transient response of a physical system to a single pulsed excitation event. This signal can be characterized by rapid simultaneous onset of all components and their gradual fadeout due to damping,

## **8.4 Proposed TFD Techniques**

The tradeoff between the time-frequency resolution and the suppression of cross terms remains a major challenge when dealing with non-stationary, multi-component signals. We already know the drawbacks of traditional TFDs for multi-component signals. In order to overcome those problems, we propose two time frequency distribution techniques.

- (1) First, we propose a time-frequency distribution that combines the Matrix Pencil Method (MPM) and the Wigner-Ville Distribution (WVD), called MPMWV distribution. The MPM decomposes the multi-component signal into a number of mono-component signals and then each mono-component signal will be sent to the WVD for presenting time-frequency analysis. At last, adding such elementary TFDs on a compound plot.
- (2) Another possible way to construct a time-frequency representation of the percussion signals would be by representing it as a linear superposition of elementary functions

with well-behaved TFDs and then assembling such elementary TFDs on a compound plot.

We proposed the clinical percussion signals as a linear combination of exponentially damped sinusoids (EDS). Such decomposition seems compatible with the underlying physics. Indeed, the percussed human body represents a passive viscoelastic system with multiple degrees of freedom. A percussion impact excites several such degrees at once, and then the oscillations fade out with their respective rates. If the impact is weak, the transient response can be considered linear, and the damping of all normal modes – exponential. In this work, the decomposition of medical percussion signals into damped harmonics was accomplished using Matrix Pencil Method (MPM). The MPM was chosen because it is reportedly the best performing of all damped harmonic analysis methods, especially in the presence of noise. The MPM decomposes the signal into a number of EDS components, detecting the exact location of the dominant frequencies and accurately distinguishing closely spaced frequency components [47, 48]. Each EDS is fully characterized by its amplitude, frequency, damping, and initial phase. The first two parameters can be visualized in the frequency domain as vertical line segments of certain height (amplitude). This representation allows for direct comparison with the Fourier amplitude spectrum [103,104]. However, without seeing the damping parameter it is difficult to judge about the relative contribution of individual EDS to the signal. Visualizing the damping parameter would help better capture the behavior of each EDS and show their time evolution in the time-frequency plane. We will demonstrate the proposed techniques and their performance analysis in the next section. First, we will use the simulated signals to verify the stability of the two proposed TFDs. The reason for using simulated signal is that the parameters of the signal are known, therefore, we will be able to verify the TFD accuracy. At last, we will apply these TFDs on medical percussion signals.

## 8.5 Proposed TFDs

### 8.5.1 First approach: MPMWV distribution

The proposed TFD is shown in figure 8.1 that includes MPM and WVD. In order to avoid cross term artifacts and achieve high time-frequency resolution, here we combine Matrix Pencil Method and Wigner-Ville distribution [47-51, 105]. MPM decompose the multi-component signal into a number of mono-component signals, then WVD is applied to the individual components, and the resulting distributions are reassembled to produce the composite time-frequency distribution of the original signal. As a result, the resulting TFD would be free from cross-terms.

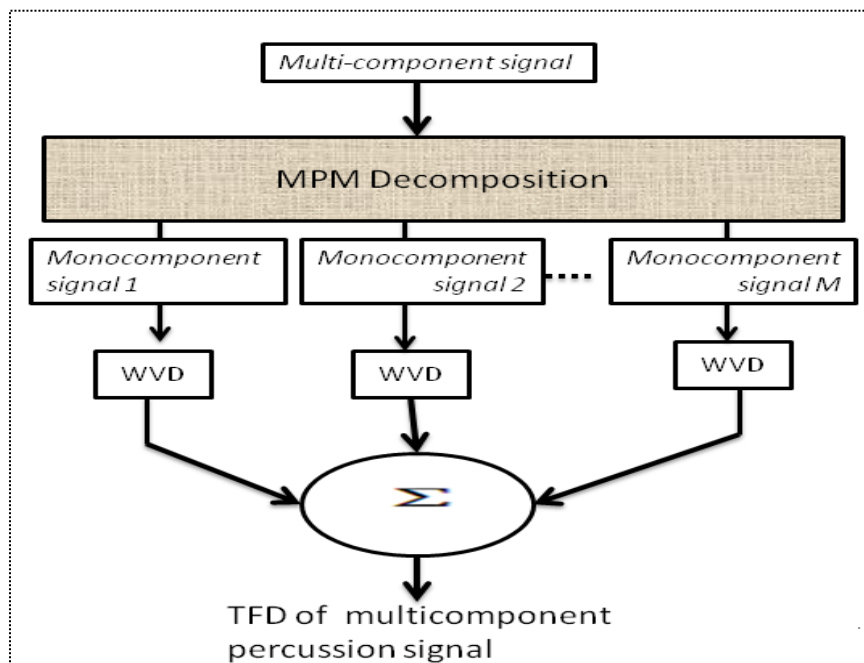


Figure 8.1 MPMWV algorithm diagram

The choice of the MPM to decompose percussion signals is not arbitrary. We have highlighted the advantages of MP method in chapter 5. Based on those merits, we can say that MPM would be a right tool for analyzing percussion signals in Time-Frequency domain. The WVD was selected due to its optimal time-frequency resolution characteristics [106]. This TFD does not need extra kernel function for achieving the optimal time-frequency resolution and it provides nearly exactly match of the theoretical energy distribution [102,105,106]. Mathematically, WVD can be define as

$$WVD(t, f) = \int_{-\infty}^{\infty} x(t + \frac{\tau}{2})x^*(t - \frac{\tau}{2})e^{-j2\pi f\tau} d\tau \quad (9.1)$$

Where,  $f$  is the frequency,  $x(t)$  is the time domain signal,  $\tau$  is the running time and  $x^*(t)$  is the complex conjugate of  $x(t)$ . Integration over time at each frequency gives the spectral density (instantaneous power) of the signal [83,84,97,105]. WVD belongs to the Cohen's class of distributions defined as [83,84,97,105]:

$$C(t, f, \varphi) = \frac{1}{2\pi} \iiint_{-\infty}^{\infty} \varphi(\xi, \tau, t, f) x(s + \frac{\tau}{2})x^*(s - \frac{\tau}{2})e^{-j2\pi[\zeta(t-s)-f\tau]} ds d\tau d\zeta \quad (9.2)$$

Where,  $\varphi(\xi, \tau, t, f)$  is the cohen's class filter (kernel) defining the distribution properties [84,87,102], In case of WVD,  $\varphi(\xi, \tau, t, f) = 1$ . When WVD is applied to a multi-component signal, the cross terms are produced by the product of  $x\left(s + \frac{\tau}{2}\right)x^*\left(s - \frac{\tau}{2}\right)$ . In order to suppress the cross terms it is common to introduce special kernel functions, such as  $\varphi(\xi, \tau) = e^{-\zeta^2 \tau^2 / \sigma}$  used in Choi-Williams distribution [94,105]. Here  $\sigma$  is a parameter that determines the tradeoff between the cross term suppression and the frequency resolution [84,87,94,105].

### 8.5.1.1 MPMWV distribution performance analysis

A damped sinusoidal signal is constructed by adding 4-EDS signals and the parameters of the individual EDS is shown as follows  $f=[100, 130, 170, 200]$  Hz,  $A=[1, 1.8, 1, 1.4]$  (arbitrary units),  $b=[7, 15, 9 \text{ and } 5] s^{-1}$ , and  $\varphi=30^\circ$  each. The signal contains 600 points and sampled by 1000 Hz. The resulting simulated signal and its spectrum are shown in figure 8.2 (a,b). The spectrum in the figure 8.2 (b) shows only the frequency contents of the signal, but does not show how the relative contribution of each component evolves with time. In that case, the time-frequency analysis would be able to show the signal in both domains. This simulated signal is a multi-component signal and the intension here to compare the proposed MPMWV distribution with two traditional TFDs. Our selected TFDs are WVD and CWD.

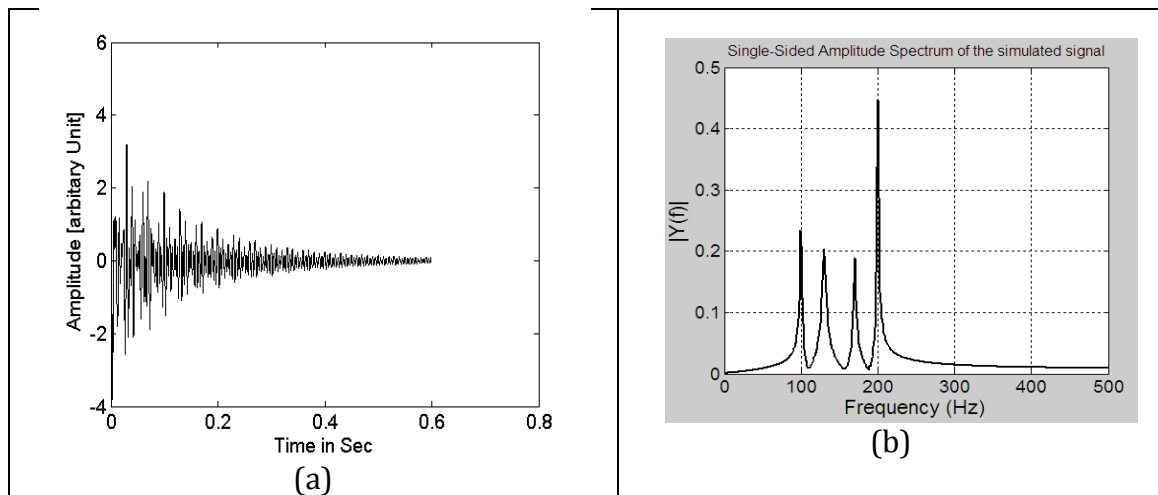
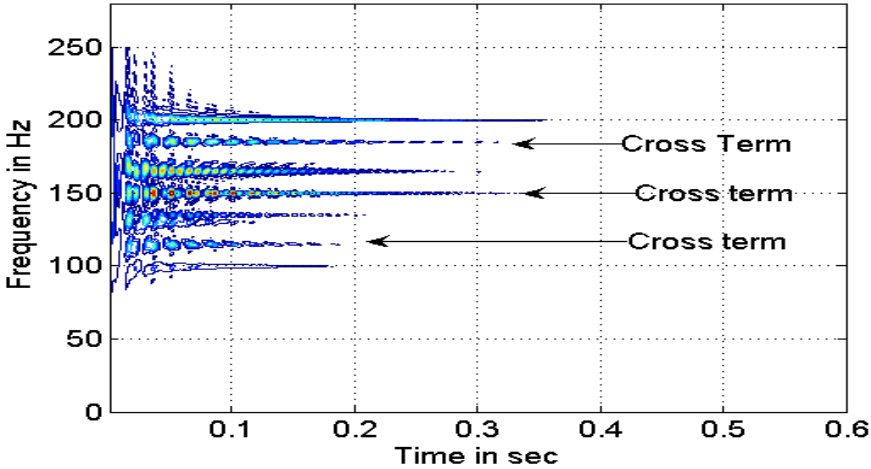


Figure 8.2 (a) A simulated signal generated by adding four exponentially damped sinusoidal

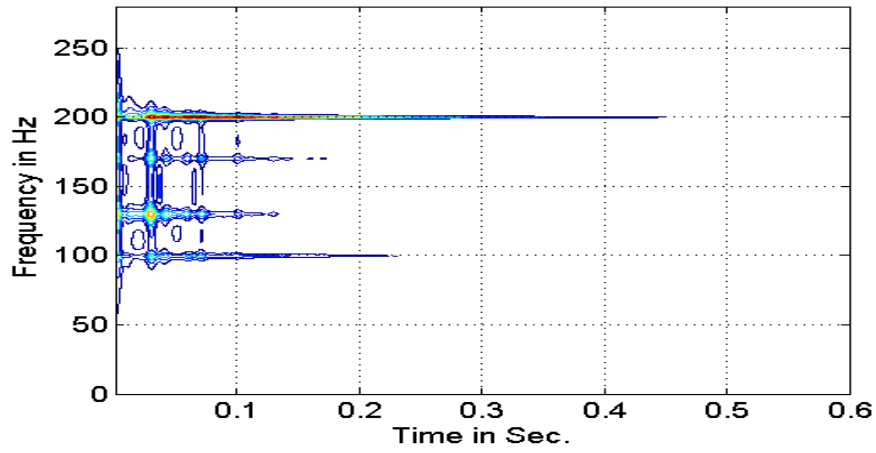
(b) Spectrum of the simulated signal

The rationale behind the choice of these particular distributions is that they are the most popular quadratic TFDs and because one of them uses a special kernel function for reducing the cross terms (CWD) and the other one does not (WVD) use such type of kernel function.

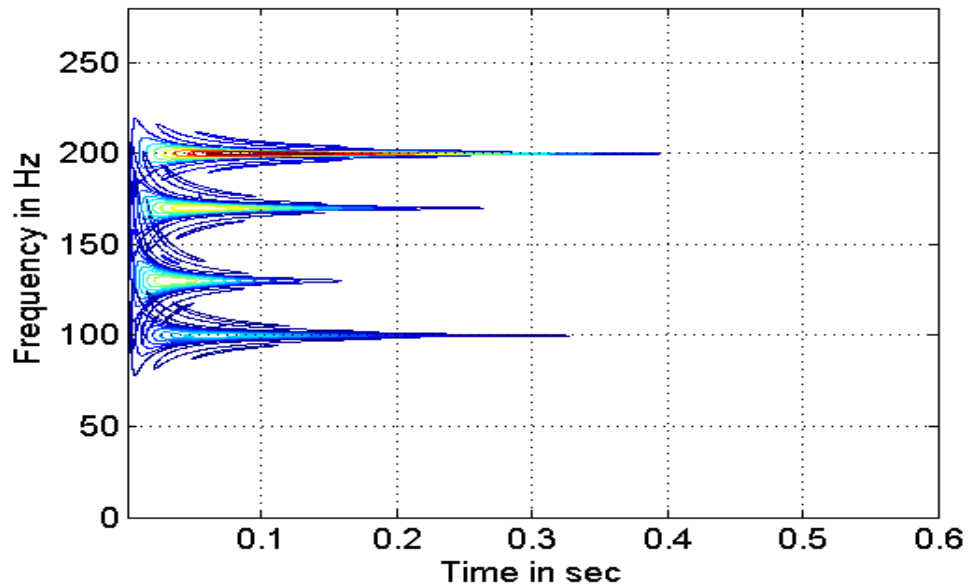
We can observe the WVD and CWD time-frequency distribution in figure 8.3 (a,b). It can be commented based on visual inspection that the four EDS TFDs are resolved efficiently with additional cross terms. The additional components are placed at 120, 150, and 160 Hz, which were not present in the original signal. These are undesirable cross-term artifacts produced by the WVD. The WVD's results may be improved by increasing the sampling rate of the original signal, but the cross terms cannot be avoided due to non-linearity. Figure 8.3(b) shows the results of applying CWD to the same signal. As expected, the cross terms are significantly reduced in the image. One can also notice that the frequency resolution is not satisfactory because CWD suppresses the cross terms at the expense of the resolution.



(a) WVD TFD presentation of simulated signal



(b) CWD TFD presentation of simulated signal



(c) MPMWV representation of simulated signal

Figure 8.3 Time-frequency representation of the simulated multi-component (four-component) signal by (a) WVD (b) CWD and (c) MPPMWV distribution. Notably, the MPPMWV is able to reduce the cross-terms completely, and the frequency resolution is higher than that of CWD.

Therefore, we can comment that even for this simplistic simulated signal neither the WVD nor the CWD are able to simultaneously resolve the cross terms problem and increase the resolution. This problem is exacerbated in practical applications as the multi-component signals are noisy, must be processed in real time, and are often of random character. In addition, it is impossible to know in advance the constituent components of a real signal. Hence, the cross-term artifacts will appear at random locations thus confusing the selection of the useful region of interest (ROI). We plot the TFD of MPMWV distribution in figure 8.3 (c). It can be seen from the figure 8.3 c that the proposed TFD detected all the four EDS clearly without cross terms. The frequency resolution is better than WVD and CWD for the same signal. It is clear that the MPMWV distribution produces superior result compared to the individual WVD and CWD when applied to a non-stationary multi-component signals.

We also evaluate the performance of MPMWV distribution for two close frequencies. The different parameters values were chosen as frequencies  $f=[80,110,120,125,150]$  Hz,  $A=[1.2, 1.1,1.0,1.0,1.0]$  (arbitrary units),  $d=[7, 10,10,10,10]$  s<sup>-1</sup>, and  $\varphi=30^\circ$  each. The signal contains 600 points sampled at 1000 Hz. Here, the two close frequencies are 120 and 125 Hz. It can be clearly observed from the figure 8.4 that the MPMWV identifies the two close frequency components with acceptable resolution.

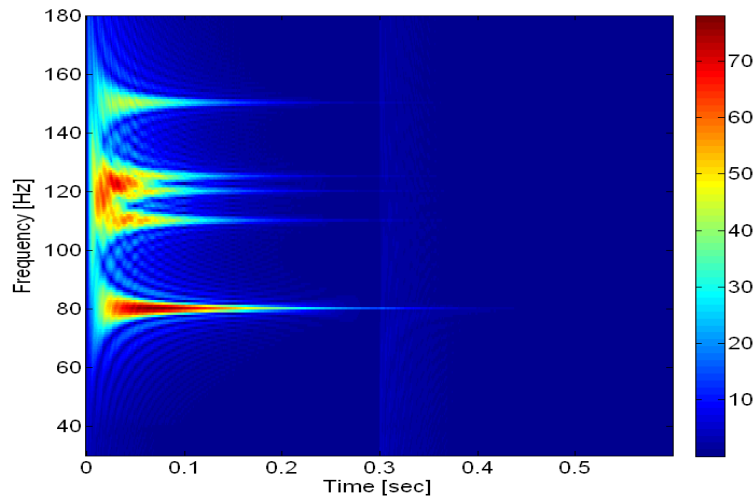


Figure 8.4 MPMWV TFD's for two close frequencies

These examples shows that the proposed TFD outperforms the WVD and the CWD in terms of time-frequency resolution and cross terms suppression for the non-stationary multi-component signals belonging to the transient impulse response class. In addition to WVD and CWD, we could have compared other quadratic TFD, but the result wouldn't be different as all of them are based on kernel functions. So the tradeoff between the cross terms suppression and time-frequency resolution would be an issue again for the multi-component signal.

### 8.5.2 Second approach: MPM based TFD

In the second approach, we thought that the WVD is an unnecessary addition for accomplishing TFD of multi-component signals. We decided to use only MPM for time-frequency analysis of multi-component signals showing energy of the individual component in the T-F domain. Here, Matrix Pencil Method (MPM) is used to decompose the signal into a set of EDS, which are then plotted in the time-frequency plane. This way we can specify the components by the property that their localized energies in the time-frequency plane. Such

representation provides better visualization of the signal structure than MPMWV distribution.

### 8.5.2.1 Performance analysis

We started the performance analysis of MPM TFD for a damped sinusoidal component that composed of four EDS and there parameters are listed below.

Table 8.1 PARAMETERS OF 6 EDS IN THE SIMULATED SIGNAL

Frequency $f_i$ [Hz]	100	130	170	200
Amplitude $A_i$ [a. u.]	1	1.8	1.0	1.4
Damping $d_i$ [ $s^{-1}$ ]	7	15	9	15
Initial phase $\varphi_i$ [deg]	30	30	30	30

The time-frequency analysis of the proposed second method for simulated signals is presented in Figure 8.5. The figure shows the time-frequency representations of the original EDS components of the signal.

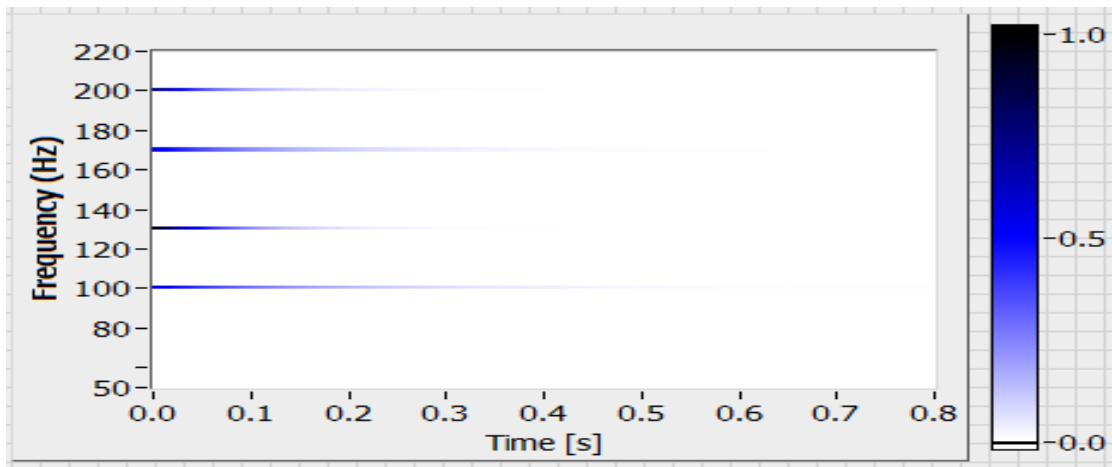


Figure 8.5 Time-frequency representation of the noise-free analytical signal based on only

MPM

This image has no cross term artifacts, infinite frequency resolution, and provides convenient visualization of damping. They adequately represent the noise-free simulated signal and are clearly superior to MPMWV, WVD, and CWD. For this case, the MPM TFR correctly identified the constituent EDS including weak and highly damped modes which is not resolvable by conventional distributions. Therefore, we choose the second option for analysis the percussion signals in time-frequency plane.

## 8.6. MPM TFR of medical percussion signals

The percussion signals (a. resonant and b.tympanic) waveforms are shown in Figure 8.6. The “resonant” signal (Fig 8.6.a) was acquired over the upper chest in the subclavicular area and the “tympanic” signal (Fig 8.6.b) was acquired over the left portion of the abdomen..

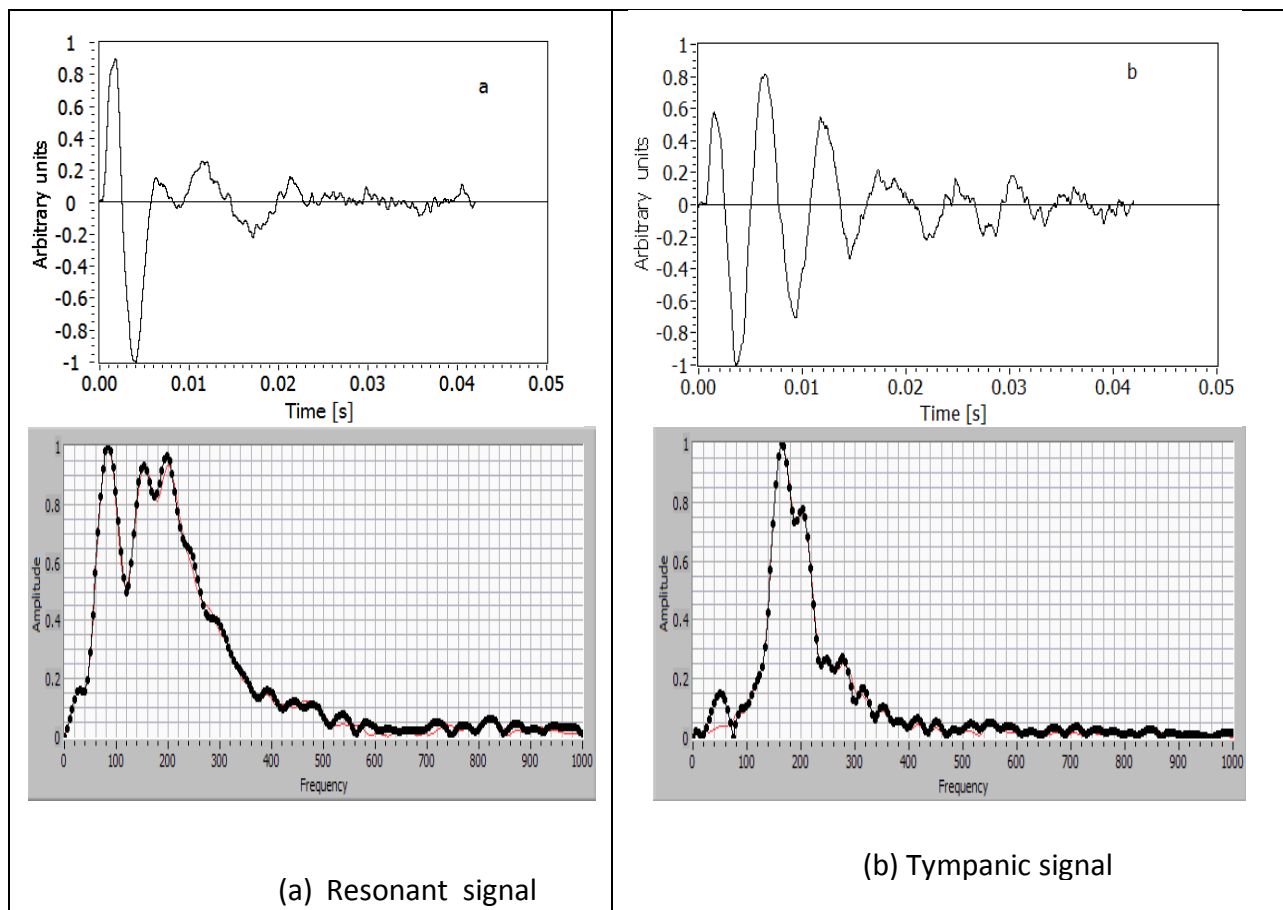


Figure 8.6 Medical percussion signals (a) Resonant (left) (b) Tympanic (right) and their

spectrums

The signals recorded in our experiments are quite repeatable, hardware-independent, and, in fact, similar in shape to those recorded by Murray and Neilson in 1975 [1]. The amplitude spectra of both signals are also shown in Fig. 8.6. Although the fine spectral structure may differ significantly from signal to signal, in general, “tympanic” spectra tend to be narrower and with fewer major sub-peaks than “resonant” ones. The first two parameters can be visualized in the frequency domain as vertical line segments of certain height (amplitude). This representation allows for direct comparison with the Fourier amplitude spectrum [26]. However, without seeing the damping parameter it is difficult to judge about the relative contribution of individual EDS to the signal. Visualizing the damping parameter would help better capture the behavior of each EDS and show their time evolution in the time-frequency plane. The time-frequency analysis of resonant and tympanic clinical percussion signals (Figure 8.6) is presented in figure 8.7.

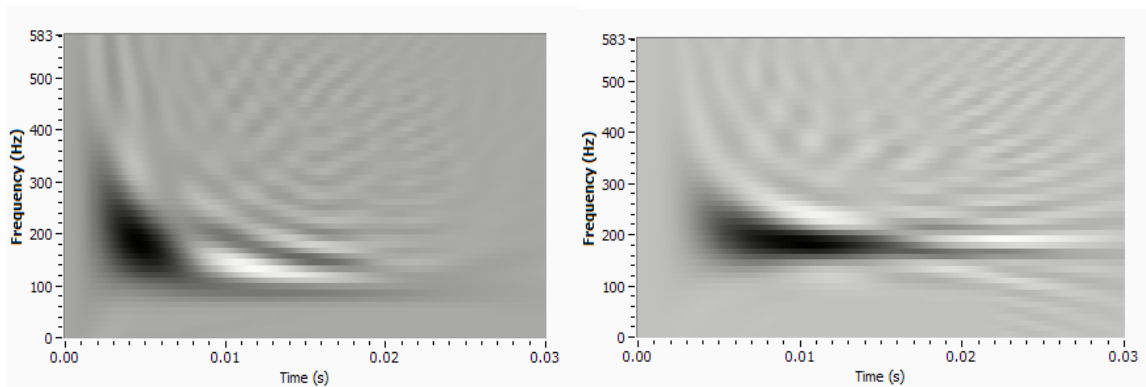
The resulting EDS (only those with positive frequency and damping values were selected) are shown in Tables 8.2 and 8.3. The EDS are sorted by the normalized amplitude. The Figure 8.7 (a,b,c) shows the T-F representation of the chest and abdominal percussion signals. Percussion signals that decay exponentially describes the rate of energy loss. As the percussion vibrates the chest or abdomen passing through a medium, it loses energy and therefore undergoes a reduction in amplitude and intensity. This loss of energy is determined by the characteristics of the medium. Since the EDS decomposition is performed using MPM, this representation is named MPM TFR. Each EDS (defined by its frequency  $f$ , amplitude  $A$ , damping  $d$ , and phase  $\varphi$ ) is plotted (fig.8.7 c) as a line parallel to the time axis, having ordinate value of  $f$  and colored according to the value of  $Ae^{-bt}$ .

Table 8.2 parameters of all EDS extracted by MPM from resonant signal

<b>A</b>	<b>f [Hz]</b>	<b>d [s<sup>-1</sup>]</b>	<b>φ [rad]</b>
1.0	197.39	226.164	-1.221
0.368	75.937	67.235	2.225
0.207	299.127	251.635	3.062
0.066	142.49	27.705	0.73
0.057	492.73	145.182	1.183
0.046	550.313	152.348	1.654
0.032	927.405	245.756	2.109
0.01	831.218	11.861	1.539
0.009	724.028	40.647	-2.372
0.007	358.181	58.512	1.24
0.003	642.492	38.446	-1.26
0.003	989.675	18.548	0.693

Table 8.3 parameters of all EDS extracted by MPM from tympanic signal

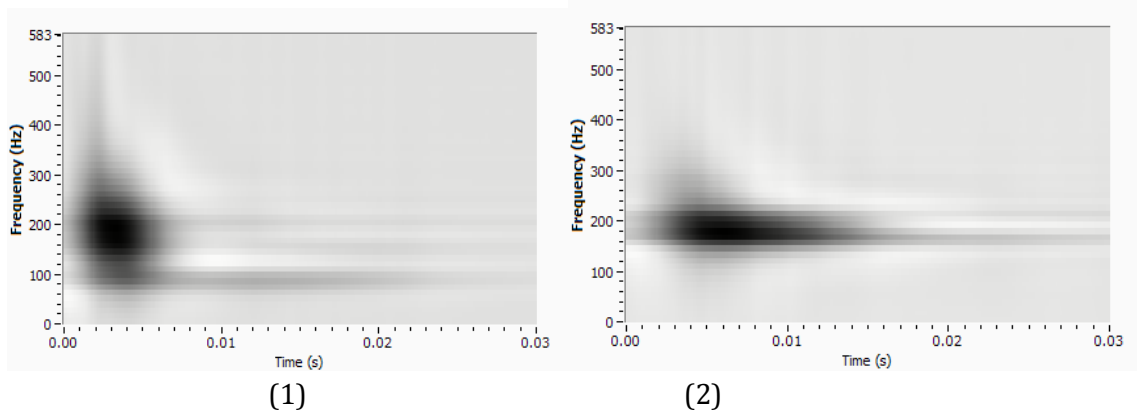
<b>A</b>	<b>f [Hz]</b>	<b>d [s<sup>-1</sup>]</b>	<b>φ [rad]</b>
1.0	159.629	79.883	0.167
0.586	210.907	86.856	-2.813
0.505	277.04	206.404	2.895
0.051	849.697	189.087	-0.921
0.02	370.45	74.406	1.742
0.018	552.295	6.767	2.383
0.008	486.105	13.611	2.98



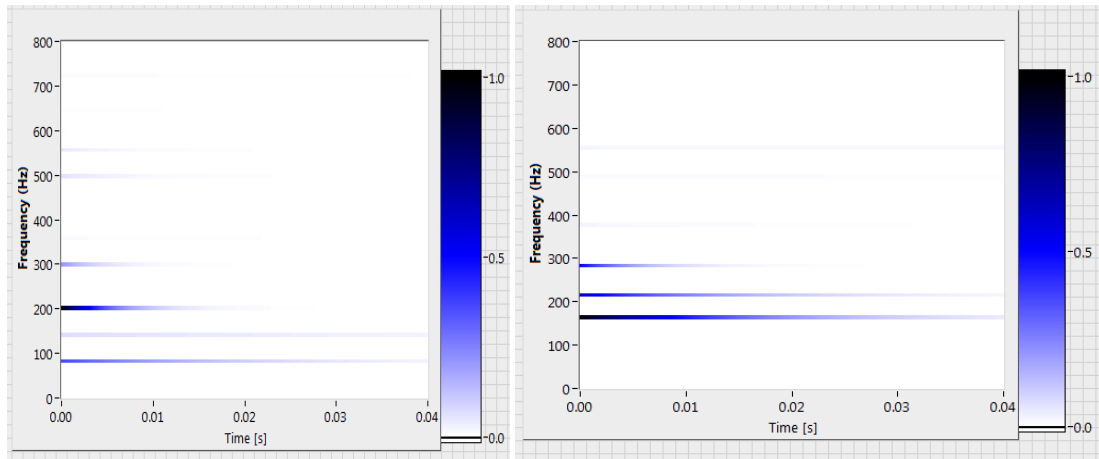
(1) Resonant signal TFD

(2) Tympanic signal TFD

(a) WVD representation of (1) resonant and (2) tympanic signal



(b) CWD representation of (1) Resonant and (2) Tympanic signal



(c) (1) Resonant Signal

(2) Tympanic signal

Figure 8.7 Time-Frequency representation of the percussion signals (fig 8.6) based on (a) WVD (b) CWD and (c) MPM TFR

This representation is very intuitive and readily reveals the main features of the signal. The damping of each EDS component can be estimated from its visible duration, while the color indicates the instantaneous amplitude (darker color means higher amplitude). Each component is associated with a particular frequency and experiences exponential decay with time. Components with high starting amplitude and low damping are dominant and determine the overall character of the signal. Weak components or those with very high damping are less important, as they often are artifacts produced by the MPM to fit the noise. It should be mentioned that the graphical representation of the MPM results is not

completely equivalent to these of the results obtained by the other methods. The frequencies on the vertical axis correspond to frequency of the EDS components and not to Fourier components. Even though they are represented by the same parameter, frequency, the set of EDS represents a different basis for the decomposition of the signals. The effect of damping on the harmonic components is a widening of the spectral peaks. This may result in overlapping of various components in the spectrum. In the EDS representation, the damping influences the apparent length of the horizontal lines. There is no overlapping on the frequency axis for the EDS representation, no matter how close in frequency and how damped are the components. This feature should be considered when one decides which representation is the most suitable for a specific application.

The MPM TFR images have no cross term artifacts, infinite frequency resolution, and provide convenient visualization of damping. However, MPM TFR follows from the EDS-based model, which is only an empirical suggestion and needs to be justified. Indeed, decomposition into a number of EDS is just one possible type of representing the signal. Other basis functions can be selected to fit the same signal, and the resulting TFR may look different than the MPM-based one.

One argument in favor of the EDS-based model comes from physical reasons, as described in the Introduction. Another independent proof could be obtained by demonstrating similarity of the time-frequency portraits produced by the MPM TFR and by non model-based distributions. Indeed, time-frequency portrait is the intrinsic property of the signal, and is independent of any particular analysis tool. Various TFDs can visualize this portrait only approximately, while introducing their specific artifacts. If certain TFDs introduce less severe artifacts than others for a given signal type, they are expected to produce more or less similar looking time-frequency portraits (approaching the actual portrait). On the other hand,

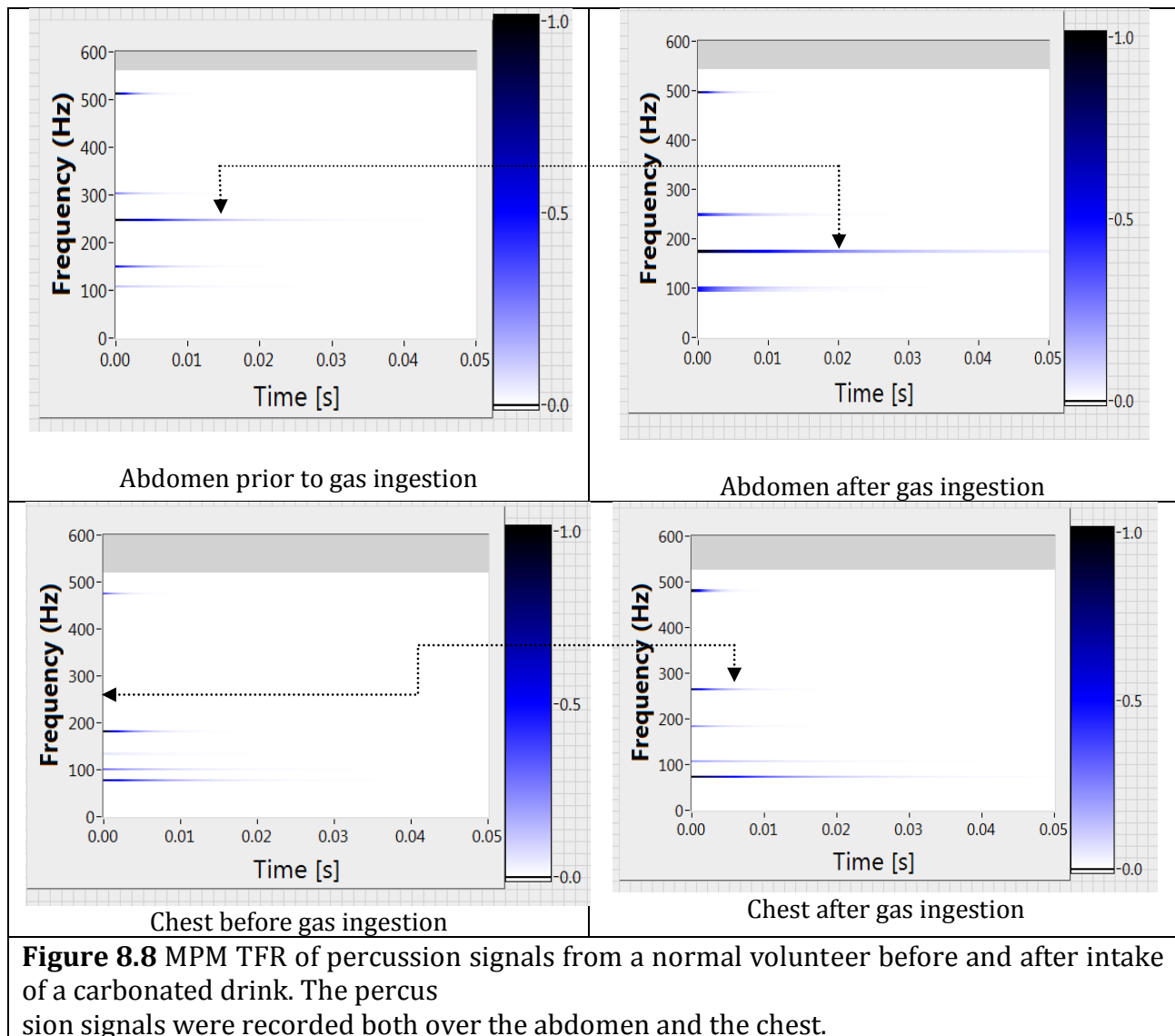
showing that a model-based distribution produces time-frequency portrait that looks similar to that produced by a non-model-based distribution could be considered as an argument in favor of the model. The WVD and CWD belong to different classes yet show very similar time-frequency portraits of the same clinical percussion signal. Notably, all dominant features present in the WVD and CWD are also present on the MPM TFR plot. Based on the above reasoning, this could be considered an independent proof of the validity of the EDS-based model of clinical percussion signals. On the other hand, MPM TFR reveals additional components, not resolved by the conventional distributions. Those components do not play critical role in the signal reconstruction as they have relatively low amplitudes and/or significantly higher damping compared to the dominant ones, determining the signal behavior. The physical origin of these minor components is unclear. The EDS with low-amplitude, too high-frequency, negative or excessive damping etc, could be artificially introduced by MPM to fit the noise or edge discontinuities in the signal. Alternatively, they may represent real (but weak) oscillation modes of the human body and be of practical importance. On the other hand, the noise (which is always present in percussion signals) could be the major cause of the poor resolution of the WVD, and CWD, reassigned spectrogram. Without the noise, these distributions could possibly show much better resolution. The dominant frequencies of medical percussion signal vary rapidly in time, reflecting pathophysiological changes under the percussed area. The energy density of the color image is represented by a color tone changing from white to blue as shown in the color bar, which is used for all the color images. Important variations are observed if we compare the resonant signal and the tympanic signal. The time-frequency representation clearly reveals the patterns of formants. The TFDs describe the signal energy distribution in the time-frequency domain.

The larger values of these spectra are displayed more darkly colored. The other regions represent values that are near zero in magnitude. It can be seen from Figure 8.7 (C) that the resonant signal has multiple energy concentration spots in the time-frequency space, while the tympanic signal has only one dominant energy concentration area. This information is new and cannot be derived from either the spectrum or the waveform alone. In general, we found that the percussion sound signal spectrum shape formed different kind in the different part of the body. Without considering the kind of pathology examined and doctors experienced, it is possible to classify the percussion sound signal in order diagnosis the disease/condition such as Pneumothorax . The damping of each EDS component can be estimated from its visible duration, while the color indicates the instantaneous amplitude (darker color means higher amplitude). Each component is associated with a particular frequency and experiences exponential decay with time. Components with high starting amplitude and low damping are dominant and determine the overall character of the signal. Weak components or those with very high damping are less important, as they often are artifacts produced by the MPM to fit the noise. The MPM TFR images have no cross term artifacts, infinite frequency resolution, and provide convenient visualization of damping. Various TFDs can visualize this portrait only approximately, while introducing their specific artifacts.

## **8.7 Using MPM TFR to detect changes in physical condition**

We have discussed the MPM TFR analysis for medical percussion signals in above section. In this section, we will discuss some of its practical applications. The rates of decay (damping), the frequencies, and the relative amplitudes of dominant EDS are important parameters, possibly reflecting pathophysiological properties of the percussed organ. An illustrative

example of how the MPM-based time frequency analysis can be practically deployed to detect changes in the signal is shown in Figure 8.8. In this experiment, a normal volunteer was withdrawn from food for 15 hours and then given a carbonated drink. The percussion signals were recorded over his abdomen and chest before and after consuming the drink. The MPM TFRs of these signals were constructed and compared. It can be seen that before consuming the drink, the least damped EDS at  $\sim 248\text{Hz}$  responsible for the overall tympanic character of the abdominal signal lasted for only  $\sim 20\text{ ms}$  (see Figure 8.8, top row, left).



After taking the drink, the intestinal gas pattern changed, so that the frequency of the least damped EDS shifted to  $\sim 171\text{Hz}$ , and its duration increased beyond 40 ms (see Figure 8.8, top row, right). Changes in the modal composition of the chest signal can be observed as well (see Figure 8.8, bottom row). For example, an additional strong but highly damped mode has appeared at  $\sim 263\text{Hz}$ , as marked by the dashed line. Other signal modes have remained almost unchanged (see Figure 8.8, bottom row, right). One possible explanation of this result is that gas-filled stomach has freed one of the chest vibration modes indirectly through diaphragm. It should be noted that none of the observed effects can be reliably detected using conventional TFRs examined due to their inferior resolution in the 0-5 or 0-12ms interval and due to their insensitivity to slight changes in the damping.

## 8.8 Summary

The proposed MPM TFR yields a clear and efficient graphical representation of both resonant and tympanic percussion signal types. The ability to resolve oscillation modes with closely spaced frequencies and high damping makes MPM TFR a preferable method for the analysis of clinical percussion signals. Its superiority becomes especially evident when analyzing the 5 ms interval following the signal onset, where such commonly used TFDs as WVD, and CWD all fail to resolve individual frequency components. This work describes an attempt to construct a TF representation specifically tailored to clinical percussion signals to achieve better resolution of individual components corresponding to physical oscillation modes. We have successfully demonstrated the usefulness of MPM TFR in detecting subtle percussion signal changes caused by physiological processes. We were able to detect the appearance of a new oscillation mode or slight changes in damping of an existing mode. Such effects cannot be reliably detected using conventional TFRs examined in this paper. Decomposing the signal

into a sum of elementary functions with known time-frequency representations and then combining those elementary TFRs produces the image free of cross terms and other common artifacts. MPM TFR is based on the EDS signal model, which can be justified both from physical principles and through direct comparison with CWD and WVD results. Besides clinical percussion, the proposed MPM TFR can be used in many other areas, including music and speech processing, where the EDS decomposition model is applicable.

# Chapter 9

## Medical Percussion Signals Classification and Recognition

---

### 9.1 Introduction

The main objective of this dissertation is to analyze, classify and recognize the medical percussion signals. Initially, our research focus was to find methodologies and algorithms for medical percussion signal analysis to provide efficient and effective ways of understanding the signal and its nature. The medical percussion signal acquired from the healthy volunteers is short and highly damped, as such; it requires advanced signal processing method for detection, processing and classification. Classification of medical percussion signals with powerful and advance signal processing techniques is an important requirement in accurate clinical diagnosis. We mentioned that tympanic sounds heard over the chest indicate PTX condition, which is a collapsed lung condition. In order to detect the PTX condition, the percussion signals needs to be classified accurately. For this purpose, we have proposed MP method for decomposing medical percussion signals in the chapter 5. Before using MP method, the percussion signals were preprocessed. The preprocessing algorithms and procedures were discussed in the chapter 4. The total process can be summarized as follows:

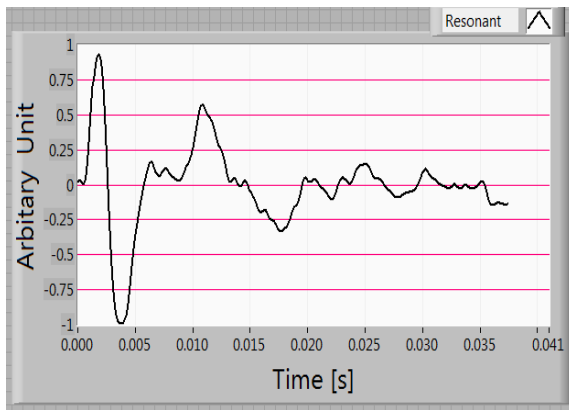
1. Formed Hankel Matrix using noisy percussion signal
2. Used hybrid filter (BP-HankelSVD) to cancel out noise.
- Found M (the signal part of the noisy percussion signal based on threshold criteria.)

3. Considered filtered matrix  $[V_s]$ , Considered so that it contains only M-dominant right singular vectors of  $[V]$ .
4. Decomposed percussion signals using Matrix pencil method
5. Computed the four parameters of the individual EDS
6. Obtained the complex poles of the percussion signals.

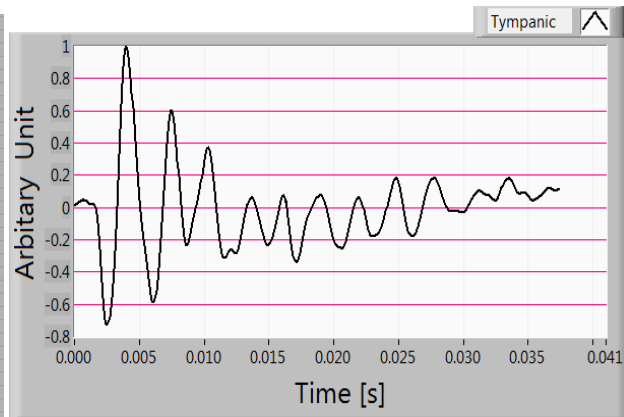
In this chapter, we will discuss the algorithms for classifying and recognizing medical percussion signals.

## 9.2 Minimum number of Pole modeling techniques

The MP method is an efficient and robust technique to fit noisy contaminated percussion signal with a sum of complex exponentials. It is a well-known pole extraction method. Based on the available poles, the minimum number of pole modeling technique is proposed to classify the medical percussion signals. We have discussed the reconstruction procedure of the percussion signals in chapter 6. We raised the issue of dominant EDS (in terms of poles) for reconstructing the percussion signals and said that the optimal number of the EDS can perfectly reconstruct the signal. The minimum number of pole-modeling algorithm originated from that idea. Figure 9.1 shows the resonant and tympanic signal those were collected from chest and abdomen using medical percussion technique. We have decomposed the percussion signals using MPM and collected all the poles of the percussion signals. The poles of the both signals are shown in table 9.1



(a) Resonant signal



(b) Tympanic signal

Fig.9.1. Percussion signals (a) Resonant collected from the chest (b) Tympanic collected from the abdomen of a healthy volunteer

Table 9.1 Percussion signals poles

SL#	Resonant signal Poles	Tympanic signal poles
1	-35.71945+44.42675j	-2.2926+32.877j
2	-76.42669+82.43888j	-54.8047+104.02j
3	-42.40236+165.6582j	-250.5971+193.47j
4	-102.7559+213.8655j	-5.5768+222.902j
5	-265.1824+322.5238j	-98.82+293.06j
6	-45.28041+485.0357j	-52.731 +341.14j
7	-282.4507+531.6088j	-26.18288+464.2309j
8	- 82.43388+663.279j	-79.121+508.14j
9	-49.2438138+732.023j	-150.39+962.2063j
10	-152.0485068+806.571j	
11	-73.87792+975.2665j	
12	-70.9023114+988.742j	

The location of the poles is shown in the figure 9.2. The complex plane contains the damping value in the x-direction and frequency value in the Y direction. Thus, each pole contains the information of the damping and the frequency of each individual EDS. As the poles are staying left half side of the complex plane; we can say that the poles are stable.

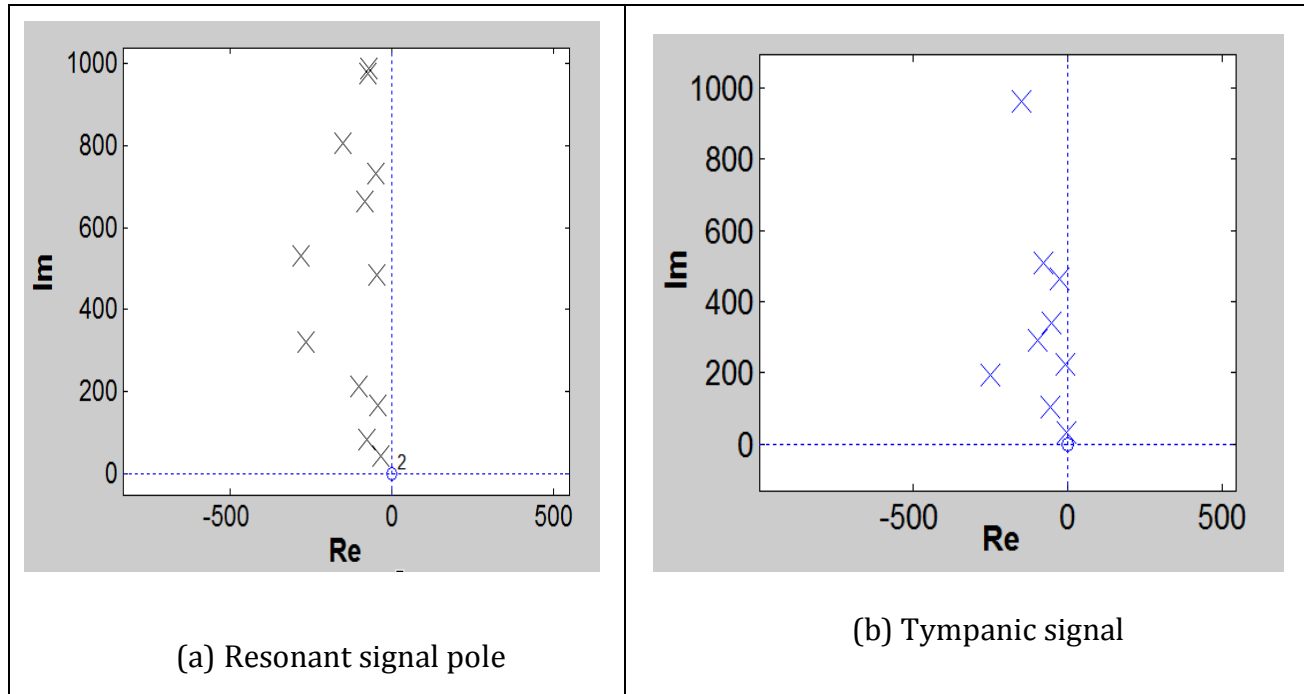


Figure 9.2 Pole structure of resonant and tympanic signal. The real part represents the damping and the imaginary part represents the frequency.

The location of the poles in the  $s$ -plane exhibits the nature of damped sinusoidal signal. A real pole in the left half of the  $s$ -plane defines an exponentially decaying component. The rate of the decay is determined by the pole location. Poles far from the origin in the left-half plane correspond to components that decay rapidly. On the other hand, poles near to the origin correspond to slowly decaying component. A pole at the origin defines a component that is constant amplitudes. The closer the pole moves to the frequency axis, the greater the

resonance. The complex conjugate pole pair  $-\sigma \pm j\omega$  in the left half of the s plane combine to generate the damped sinusoidal of the form  $Ae^{-\sigma t}\sin(\omega t + \varphi)$  where  $A$  is the amplitude and  $\varphi$  is the phase. A pole lying on the imaginary axis ( $\pm j\omega$ ) generate an oscillatory component. We can understand from the fig.9.2 that the decaying nature of the resonant signal poles is more than the tympanic signal poles. As because the increasing number of resonant signal poles are staying far from the imaginary axis. We also plot the pole/residue relationship in Figure 9.3.

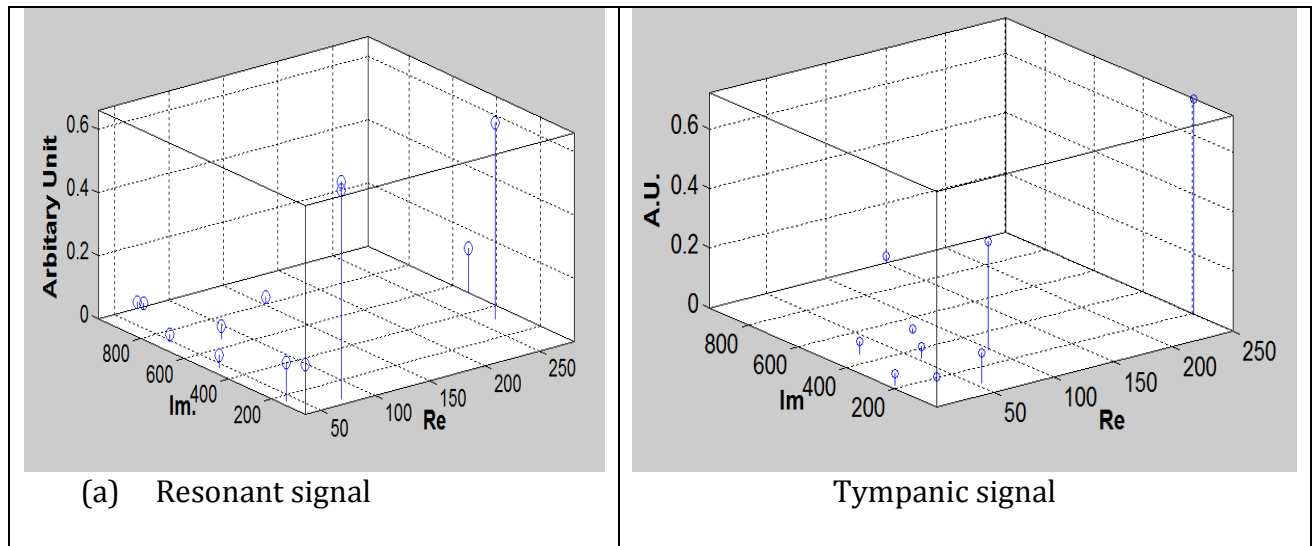


Figure 9.3 Resonant and Tympanic signal pole/residue relationship. The real part represents the damping and the imaginary part represents the frequency. A.U represents the arbitrary unit

It is possible to get very important information from the figure 9.3. The pole/residue plot indicates the comparable scenario of the dominant poles contains in the percussion signals. We can observe from the figure that the resonant signal contain six dominant poles (figure 9.3 a), whereas tympanic signal contains only three dominant poles (figure 9.3 b). Here consideration of the dominant poles is based on the residue of the each pole. It is also commendable that the dominant poles contain higher energy than the low amplitude poles.

The choice of discarding poles starts from the idea of dominant and less dominant poles. We can predict that the lowest amplitudes poles do not contribute much information in the percussion signal. In addition, these poles showed (described in chapter 6) less important compared to the dominant poles in signal reconstruction. Thus, by reducing those low amplitude poles from large number of poles bank, one can reduce the size of a pole set. These less important poles are more oscillatory in the percussion signal that decays with time. By comparing all the poles in both signals, it can be commented that resonant signal contains more dominant poles than tympanic signal. The low amplitude poles are high frequency by nature.

The idea of minimum pole modeling technique to recognize and classify the percussion a signal is depends on pole shedding criteria as described above. By discarding low amplitude poles one by one, we can get an optimal model for the percussion signals. The next section we will describe the implementation of the minimum number of pole modeling technique based on Percentage Root Means square difference (PRD) criteria.

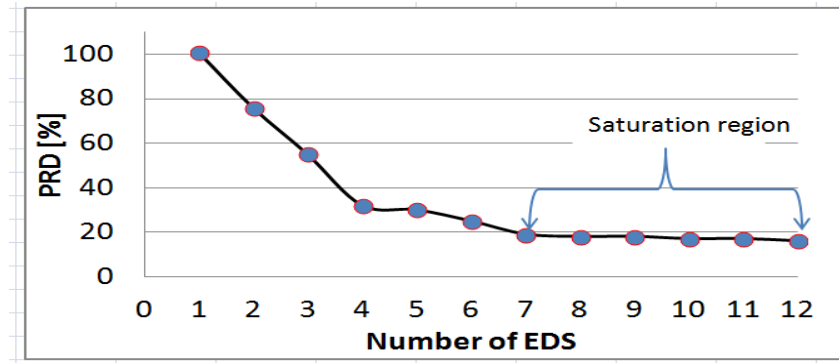
### **9.2.1 Medical percussion signals classification.**

The idea of minimum number of pole modeling technique is implemented in this section with the help of PRD. According to the PRD method, the percussion signal reconstruction starts from the largest dominant pole, then compared with the original percussion signal. In the second step, add the second largest pole with the previous selected poles and again compared with the original signal. In this process, the PRD values are calculated at every iteration. This process continues until hit the last pole of both signals. Basically, Percentage root mean difference (PRD) helps to measure distortion between the original signal and the reconstructed signal.

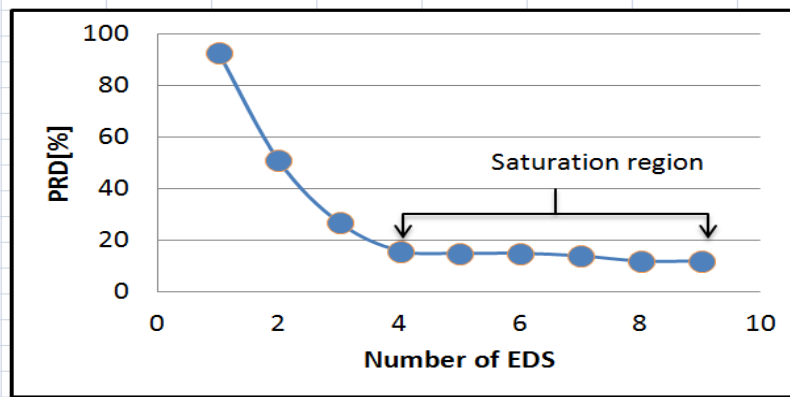
$$PRD = \sqrt{\left[ \frac{\sum_{i=1}^N (X_{orig} - X_{recons})^2}{\sum_{i=1}^N (X_{orig})^2} \right]} \times 100 \quad (9.1)$$

Here the PRD indicates reconstruction fidelity by point wise comparison with the original data. PRD value determines the deformation percent in the built signal. The PRD curves for the resonant signal and tympanic signal are shown in the figure 9.4. The error difference between the reconstructed signal and the original signal reduces at every time of the PRD calculation. After certain number of PRD calculation, the PRD curve shows the constant value curve .That means the error curve stays almost constant for the remaining PRD calculation. This constant portion of the PRD curve proposed to call the saturation stage. We have calculated the PRD values for both signals (resonant and tympanic).

We can compare the PRD curves (error curve) of the tympanic signal and resonant signal and find the differences between these two curves. It can be observed from the PRD curves that the resonant signal takes more dominant poles than tympanic signal for reaching the constant values. The saturation portion of the error is empirically chosen. It can be observed from the figure 9.4 that the saturation occurs after considering 7 EDS (dominant poles for the figure 9.1) for the resonant signal. However, the situation is different for the tympanic signal. Tympanic signal needs four dominant poles (applicable for the figure 9.1) for getting saturation state. At saturation state, if we add more EDS (dominant pole) the curve remain constant. This means that the addition of more EDS to the reconstructed signal has very little effect on the quality of the overall fit (which will never be better than less than 1% as we already truncated the signal at the SVD step).



(a) Resonant Signal



(b) Tympanic signal

Figure 9.4 PRD curve (error curve) for the resonant and tympanic signals

Hence, the number of EDS required to get prior to the saturation region would be a parameter for classifying the percussion signals. In order to count the number of “significant” EDS before the saturation occurs, one must sort them by the level of contribution to the signal. So far, we have shown the PRD calculation for a resonant signal and a tympanic signal. However, the scenario might change for signal to signal. As we considered the number of EDS (for the PRD curve) is a parameter for distinguishing the resonant and tympanic signal, we like see the overall scenario for the several percussion signals. As such, we calculated the number of EDS needed to get the saturation state of the error curve (PRD curve) for the percussion signals of 28 healthy volunteers. The results are plotted in figure 9.5.

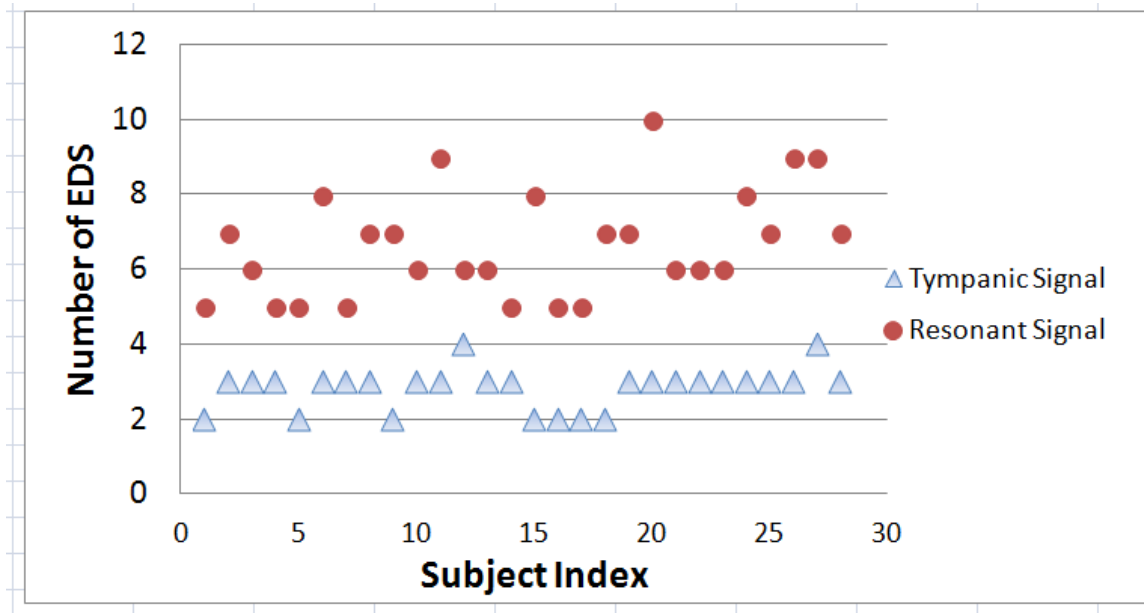


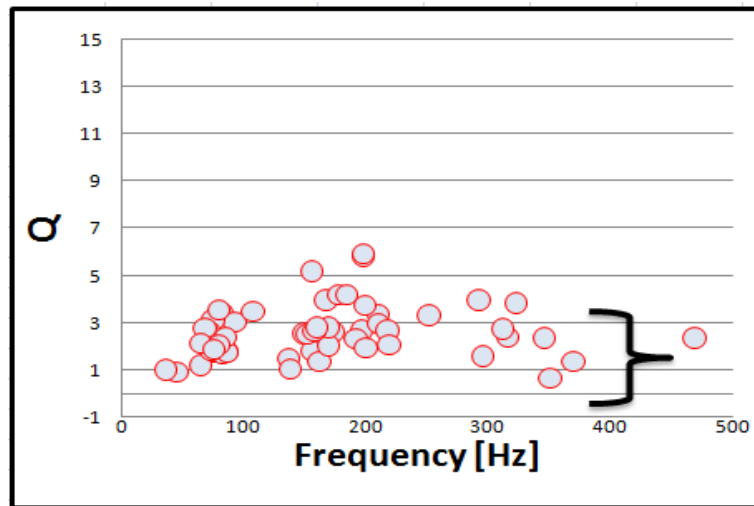
Figure 9.5 Number of EDS required reaching saturation region in PRD curve for the percussion signals of 28 healthy volunteers .

The figure 9.5 gives the overall idea of classification of percussion signals. By observing the figure, it is possible to make several comments for overall scenario of the percussion signals classification. The resonant signal takes more EDS than tympanic signal for reaching the saturation region. In that case, the resonant signals require five or more EDS whereas tympanic signals require two to four EDS to get the saturation state. So far, we have observed a criteria by which we can assure which is tympanic signal and which is resonant signal. It would be more informative if we can introduce more criteria for classifying percussion signals. We will discuss the quality factor of the percussion signals for getting another criterion for classifying these two kind of signals.

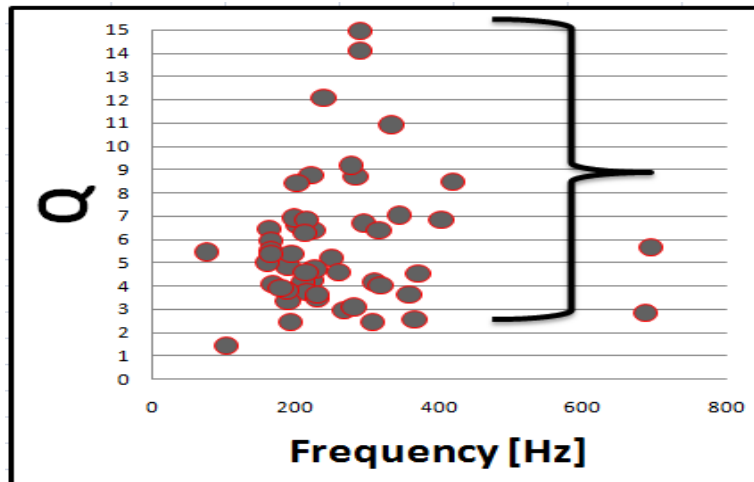
### 9.3 Medical Percussion signal classification based on Quality factor (Q factor)

Generally, the  $Q$  factor determines the qualitative behavior of damped oscillators. The EDS parameters used for statistical analysis are the frequency,  $f$ , and the damping factor,  $d$ , of the

dominant component. In order to allow an easier comparison with the results based on spectral parameters, the ratio  $Q = \pi f/d$  is analyzed rather than the damping factor  $d$  itself. In terms of energy of the EDS, this Q parameter is defined to be  $2\pi$  times the energy stored in the oscillator, divided by the energy lost in a single oscillation period. If the EDS are less damped then energy dissipation would be slow compare to highly damped signal. A 2D plot of the signal parameters  $(f,Q)$  (Figure 9.6 ) shows the Q factor variations for resonant and tympanic signals.



(a) Resonant signal Q factor



(a) Tympanic signal Q factor

Figure 9.6 Percussion signal classification based on Q-factor

It is clearly observe from the figure 9.6 that the Q factor for resonant signal is less prominent than tympanic one. Q factor values (based on dominant EDS) for the resonant signals are within five for the signals of 28 healthy volunteers. Here we picked the most dominant pole's and its corresponding frequency for the percussion signals. On the other hand, the tympanic signal Q factor values are more relaxed. The tympanic signal Q factor values concentrated more above 4 and maximum 15. Whereas the resonant signal Q factor values concentrated mostly below 4. The histogram of the  $Q$ -factors for the dominant EDS component is shown in Figure 9.7. This figure shows good separation between the two types of signals.

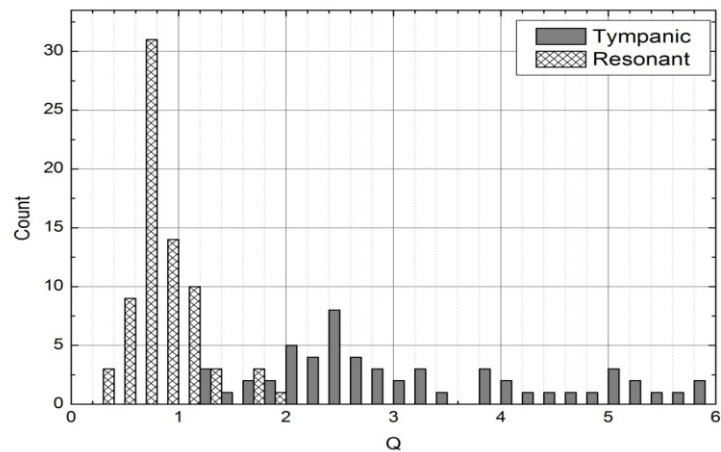


Figure 9.7: Distribution of the quality factor of the dominant EDS for resonant and tympanic signals

The lower  $Q$  factor of the resonant signals may be attributed to the high damping of the thoracic cavity by parenchyma and mediastinum. The few cases which fall in between these values are due to these signals with mixed character for which one of the higher frequency components became dominant, as mentioned above. For the purpose of the automatic classification and to reduce the frequency of false positive identification of tympanic signals

one can use a double condition, requesting that the signal parameters fall in one of the two range of Q factor values shown in Figure 9.6 a & b.

## 9.4 Classification of percussion signals based on dominant frequency

For the following analysis, the “dominant EDS” of the signal is defined as the component  $y_i(t) = A_i e^{-d_i t} \cos(2\pi f_i t + \varphi_i)$  having the highest value of the parameter  $B_i = A_i/d_i$ . The selection of this parameter is justified by the fact that  $B_i$  corresponds to the maximum of the amplitude frequency spectrum for the exponentially damped harmonic component and thus allows comparing the present results with similar analysis based on spectral parameters (figure 9.8).

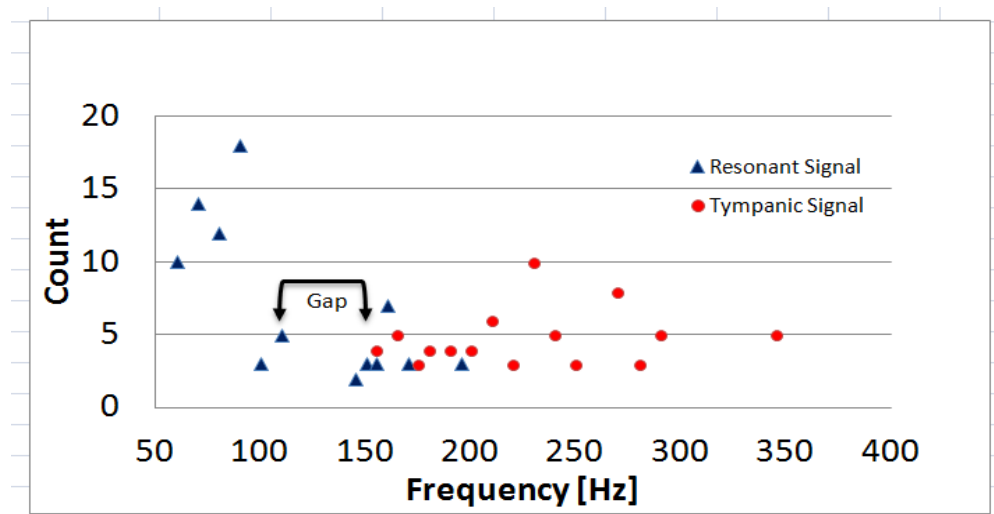


Figure 9.8 Frequency distribution of the dominant EDS for the resonant and tympanic signals

The Fourier transform (amplitude spectrum) of the exponentially damped harmonic signal  $y_i(t)$  is given by:

$$|\tilde{y}_i(\omega)| = \frac{A_i}{\sqrt{d_i^2 + (\omega - \Omega_i)^2}}$$

where  $\omega = 2\pi f$  and  $\Omega_i = \sqrt{4\pi^2 f_i^2 + d_i^2}$ . In general, the EDS with the largest value of the parameter  $B_i$  will correspond to the strongest peak in the frequency spectrum. Overlapping of components with frequency separation small compared to their damping factors may change this one-to-one correspondence, resulting either in a high spectral peak with a relatively low-amplitude matching EDS, or in several EDS with only one visible spectral peak. The normal volunteer data set includes signals obtained from 30 human subjects. Most of the subjects were percussed in three successive rounds. Chest signals analyzed here were obtained over the left subclavicular area. As already mentioned above, to collect signals of tympanic character, percussion was applied to the left abdominal area, on top of the upper colon. This location provides tympanic signals when gas pockets are present in the colon or stomach. Not all subjects were in the condition required to produce tympanic response at the time of the testing. For the statistical analysis we selected only the signals with clear tympanic character (based on visual inspection of the waveform). The frequency distribution of the dominant EDS for resonant and tympanic signals are shown in Figure 9.8. The figure shows good separation in frequency between the two types of signals. The resonant signals are characterized by lower dominant frequency, in the range 50-100 Hz. The tympanic signals have dominant frequencies above 150 Hz. A relatively small number of resonant signals (16 out of 90) have dominant frequencies in the range 100-200 Hz, entering the domain that may be attributed to the tympanic frequencies. Inspection of the spectra for these cases shows that they all have in common a spectrum with at least two peaks of comparable heights. As the relative heights are subject to variations even for the same subject (as observed by doing multiple rounds), it is not surprising that in some cases the

higher frequency peak becomes dominant, having the largest value of the parameter  $B$ . These possible origins of the higher frequency peaks in the spectrum of the resonant signals were discussed before. At least in some cases they show the same characteristic frequency as the signals obtained by directly percussing the abdominal or stomach areas.

## 9.5 Summary

We have discussed the percussion signals classification and recognition criteria in this chapter. We have introduced three criteria to classify the percussion signals. These three parameters are (1) The minimum number of the dominant poles needed to get the error curve constant (2) Q-factor and (3) the dominant frequency. The first one calculates the error between the original percussion signal and the reconstructed percussion signal. As a result, we have calculated the PRD values of the resonant signal and the tympanic signal based on minimum number of poles required to get the saturation point. The error between the original signal and the reconstructed signal are maximum if we use less number of poles. The error between the two signals became reduce once we added more number of poles. The analysis of the relative error between the original signal and the signal reconstructed from a subset of the EDS allows identifying the minimum number of significant components representing the signal with acceptable accuracy. After adding those components (sorted by their significance), the error curve comes to saturation. The second one was the quality factor calculation for the percussion signals. It has been demonstrated that the parameters of significant modes, in particular their frequencies and quality factors, can be used to differentiate between tympanic and resonant signals. Their plot shows the difference of two signal types in the  $(f, Q)$  space. The third one is the dominant frequencies collected from the various EDS of the percussion signals. Here we refer the analysis described in chapter 7 that the MPM decomposition readily identifies and fully characterizes all spectral peaks, including

closely spaced and overlapping ones. As a consequence, the entire analysis and classification process can be fully automated (and hence made objective), unlike the nonlinear fitting procedure described in the previous research. Based on these three criteria, we can classify the resonant signal and the tympanic signal, while one parameter alone may not be an efficient classifier.

One direct application of the presented approach is related to automatic detection of a tympanic signal in the upper chest area, which is often an indication of the pneumothorax condition. Other potential applications are related to diagnostics of less pronounced pulmonary pathologies as they might affect the parameters of individual damped harmonic modes. The computational efficiency of the MPM algorithm and the robustness of the damped harmonic analysis method allow for direct implementation of the signal classification algorithms on modern embedded platforms and can lead to the development of the handheld pulmonary diagnostic devices for rapid detection of the pneumothorax condition on the spot, especially in the battlefield or remote areas

# Chapter 10

## Conclusions and contributions

---

### 10.1 Conclusions

In this dissertation it was shown that the Matrix Pencil method can be applied to medical percussion processing problems. Although clinical percussion remains one of the most widespread traditional noninvasive methods for diagnosing pulmonary disease, the available analysis of physical characteristics of the percussion sound using modern signal processing techniques is still quite limited. Automation of this technique using modern signal processing involves the analysis of the signal to provide useful information upon which clinicians can make decisions. We have made an effort to process the medical percussion signals using a numerical based signal processing technique.

In chapter 1, the historical background of medical percussion was described. We proposed a mathematical model to the medical percussion signal. The proposed model and materials were discussed in chapter 2. In chapter 3, we have demonstrated the initial research ideas for the medical percussion signals. We have tried to recognize the medical percussion signals using cross correlation method. At last, we concluded that the cross correlation method is not suitable for analyzing the medical percussion signals. In chapter 4, we have talked about the noise cancellation procedures, preprocessing and signal preparation in details. We have suggested a hybrid (BP-Hankel SVD) noise reduction technique in this chapter. We have shown that the hybrid technique can cancel out the noises efficiently from the percussion signals. We presented a threshold technique to separate the signal part and the noise part from the percussion signals and also showed the ways of discarding those low amplitudes

singular values. This process is called low rank modeling of the original signal. In chapter 5, the mathematical theory of the Matrix Pencil method was described. We demonstrated the Matrix Pencil method and provided the mathematical equations in this chapter.

In chapter 6, the Matrix pencil method was applied to the medical percussion signals for estimating the parameters of EDS model. It was mentioned that the parameters estimation is an essential steps towards the development of automated classification of the medical percussion signals. We found the parameters of each individual EDS after decomposing the medical percussion signals. The individual EDS of a medical percussion signal was generated using the parameters. To check the accuracy of the parameters, the EDS was added one by one in order to get reconstructed signal. Then the reconstructed signal and the original signal were compared. It was found that the reconstructed signal is a good approximation of the original signal. It was also observed that only a subset of EDS components produced by the MPM algorithm is often enough to reconstruct the original signal with acceptable accuracy. The high-frequency and low-amplitude components can be discarded yielding computationally efficient reconstruction from a relatively small number of EDS. Based on the analysis, we found that the damped harmonic decomposition is potentially be useful to identify the main oscillating anatomical subsystems activated by the percussion event.

The majority of existing literature on the subject reports either time domain or spectral analysis methods. As Matrix Pencil Method is a super resolution technique, the modal analysis of the medical percussion signals was described in chapter 7. Therefore, the applicability of the Matrix Pencil Method to the analysis of the percussion signals was examined, and at the same time, the results were compared to conventional spectral analysis. In this chapter, we demonstrated that automatically decompose the percussion signals into a sum of exponentially damped harmonics would offer a more natural basis than the Fourier

harmonics and thus allow for a more robust representation of the percussion signal in the parametric space. The frequencies collected from the MPM decomposition were plotted with the amplitude spectra, and the proper normalization of the EDS amplitudes for such plotting was suggested. We observed that the EDS frequencies of the percussion signals agree well with the spectral analysis peak. However, the MPM decomposition readily identifies and fully characterizes all spectral peaks, including closely spaced and overlapping ones. As a consequence, the entire analysis and classification process can be fully automated (and hence made objective), unlike the nonlinear fitting procedure. Normally, MPM of clinical percussion signals produces relatively few EDS components (compared to Fourier harmonics) accurately representing the observed waveform, thus reducing the amount of information required for storage and processing.

We have introduced two new TFR for multi component signals those are also suitable for the medical percussion signals in chapter 8. These two ideas are based on MPM decomposition of the multi-component signals. The MPM-based time-frequency analysis is shown to be a better choice for clinical percussion signals than conventional TFDs, while its ability to visualize damping has immediate practical applications. The proposed MPM TFR yields a clear and efficient graphical representation of both resonant and tympanic percussion signal. Therefore, the ability to resolve oscillation modes with closely spaced frequencies and high damping makes MPM TFR a preferable method for the analysis of clinical percussion signals. Its superiority becomes especially evident when analyzing the 5 ms interval following the signal onset, where such commonly used TFDs as WVD and CWD all fail to resolve individual frequency components. We have successfully demonstrated the usefulness of MPM TFR in detecting subtle percussion signal changes caused by physiological processes. We were able to detect the appearance of a new oscillation mode or slight changes in damping of an

existing mode. Such effects cannot be reliably detected using conventional TFRs examined in this paper. Here, decomposing of a multi-component signal into a sum of elementary functions and then using known time-frequency distribution to represent the individual component TFR is the key idea. After doing, TFR of the individual EDS and then combining those elementary TFRs produces the image free of cross terms and other common artifacts.

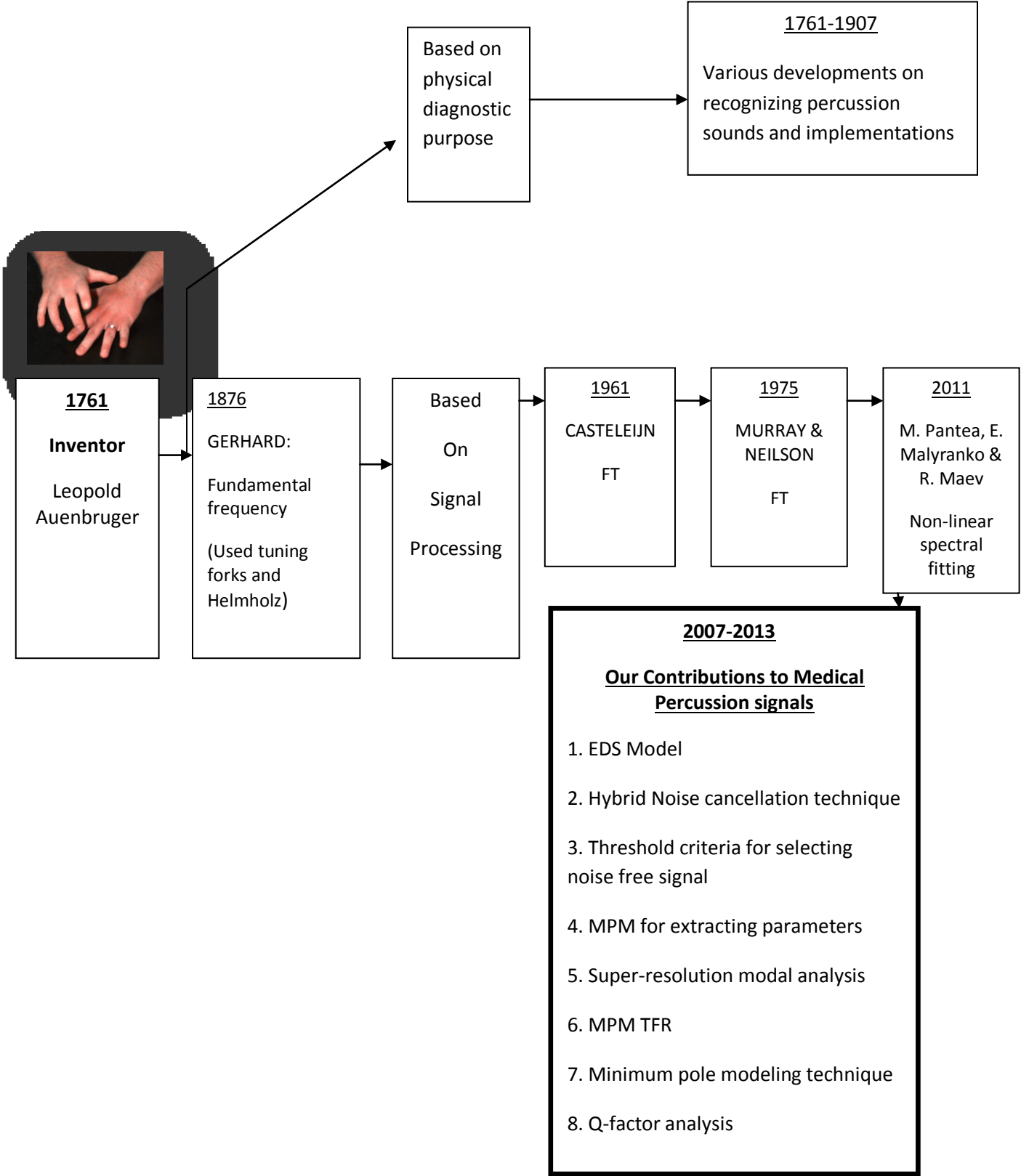
Medical percussion signals recognition and classification were discussed in the chapter 9. We introduced a minimum pole modeling technique for establishing a criterion, which was used for the classification of resonant and tympanic signal. The analysis of the relative error between the original signal and the signal reconstructed from a subset of the EDS allows identifying the minimum number of significant components representing the signal with acceptable accuracy. After adding those components (sorted by their significance) the error curve comes to saturation. It has been demonstrated that the parameters of significant modes, in particular their frequencies and quality factors, can be used to differentiate between tympanic and resonant signals. While one parameter alone may not be an efficient classifier, their combination allows for clear separation between two signal types in the  $(f, Q)$  space.

We have also demonstrated a possibility of efficient compression of percussion signals using only a few coefficients, which could be helpful when storing large amounts of percussion data or wirelessly transmitting data from the embedded controller to the remote host. One direct application of the presented approach is related to automatic detection of a tympanic signal in the upper chest area, which is often an indication of the pneumothorax condition. Other potential applications are related to diagnostics of less pronounced pulmonary pathologies as they might affect the parameters of individual damped harmonic modes. The damped harmonic decomposition can potentially be used to identify the main oscillating anatomical

subsystems activated by the percussion event. It can also be used for the signal classification purposes because it provides natural parameterization of the data and its mapping diagnostics. Each thorax oscillation mode excited by the percussion event and detected by the MPM is represented by four parameters, of which the frequency, damping and amplitude are the most informative. This is a very convenient representation, which allows direct comparison of individual modes, tracking their changes in time and from patient to patient, thus helping understand their physical nature. As a consequence, the entire analysis and classification process can be fully automated (and hence made objective), unlike the nonlinear fitting procedure. The computational efficiency of the MPM algorithm and the robustness of the damped harmonic analysis method allow for direct implementation of the signal classification algorithms on modern embedded platforms and can lead to the development of the handheld pulmonary diagnostic devices for rapid detection of the pneumothorax condition on the spot, especially in the battlefield or remote areas. As a general rule, the usefulness of MPM is limited when the SNR is low, or if the signal cannot be accurately represented as a combination of damped harmonics. However, such conditions can be automatically flagged by noticing a very large number of artificial EDS that MPM generates in an attempt to fit the “difficult” signal. If applied with due precautions, MPM correctly detects and accurately characterizes dominant oscillation modes present in the clinical percussion signal. The analysis of percussion data from 30 normal volunteers shows that the main “resonant” peak in the Fourier spectrum of the upper chest signals corresponds to several EDS components detected by MPM. The lowest-frequency component is common among different patients, while the behavior of the higher frequency components is affected by the amount and spatial distribution of abdominal gas. The lower frequency component could be attributed to the rib cage response, while the higher frequency ones could be

attributed to the oscillation of soft tissues (i.e. diaphragm, abdominal wall etc.) damped to various extents by the abdominal gas. In recent years, the development of modern diagnostic technologies has led to a decline in popularity of some traditional physical examination techniques, including percussion. This acoustical method offers many advantages including ease of administration, no reliance on bulky equipment, low cost, non-invasiveness, and the ability to acquire a large amount of information about both the physical condition and functionality of the respiratory system. At the same time, this technique has certain shortcomings, including limitations of the human ear, subjectivity of administrator, and low sensitivity. Furthermore, some sounds, which may be diagnostically important, may be overshadowed and lost due to the more intense background sounds produced by other chest functions. Digital signal processing techniques can be applied to perform objective analysis of lung sounds taking advantages of the inherent strengths of the method, while freeing it of its limitations

# 10.2 Contributions



# Bibliography

1. A. Murray and J.M.M. Neilson, "Diagnostic percussion sound: 1. A qualitative analysis," Medical and Biological Engineering, vol.13, pp.19-28, 1975.
2. A. Murray and J.M.M. Neilson, "Diagnostic percussion sound: 2. Computer-automated parameter measurement for quantitative analysis," Medical and Biological Engineering, vol. 13(1), pp.29-39, 1975.
3. A. Murray and J.M.M. Neilson "Diagnostic percussion: a study of chest-wall motion and the associated tactile sensation" Medical and Biological Engineering, vol. 16, pp.269-278, 1978.
4. J.C Yernault, A.B Bohadana, "Chest percussion," European Respiratory Journal, vol. 8, pp.1756-1760, 1995.
5. NK.Sethi, J Torgonick and PK. Sethi, "Chest percussion artifact," Clinical Neurophysiology, vol. 118, pp. 475-476, 2007.
6. Anit Mondal " Med easy" pp-3, chapter 5, Retrieved from :  
<http://medeasy.me/author/anu4bindu/page/3/>
7. E. D. Hudson, "A manual of the physical Diagnosis of thoracic Diseases," New York Willium Wood publishers , page-1887.
8. Frank L. Urbano, MD, Jaroslaw J. Fedorowski, "Medical Percussion," Hospital physician pp. 31-36, 2000.
9. J. Roddick Byers, "An Improved Method of Lung Percussion" The Canadian Medical Association journal, vol.14(7), pp. 580-581, 1924.
10. McGee SR, "Percussion and physical diagnosis: separating myth from science," Disease-a-month , v.41(10), pp.641-92, 1995.

11. H. J. Roberts, "Chest: In Defense of Percussion," The American College of Chest Physicians, v.49, pp.184-187, 1966.
12. Retrieval from :  
<http://health.rush.edu/healthinformation/hie%20multimedia/3/100150.aspx>

---

13. A. B. Bohadana, R. Patel and S. S. Kraman, "Contour maps of auscultatory percussion in healthy subjects and patients with large intrapulmonary lesions," J Lung, v.167, pp.359-372, 1989.
14. Pierre A, "Master of Percussion," Chest, v.60, pp.484-488, 1971.
15. Charles J. B. Williams, "On the Physical Examination of the Abdomen in Health and Disease," London Journal of Medicine, Vol. 4, No. 37, pp. 1-7, 1852
16. Saul Jarcho, "Some Notes on the Early History of Percussion and Auscultation," Medical History, vol.5 (2), pp-167-172, 1961.
17. Margot R. Roach, "Physical principles of Chest Auscultation," Canadian Society of Internal Medicine, vol.1, pp-xx-xx
18. D. Evan Bedford, "Auenbrugger's contribution to cardiology History of percussion of the heart," British Heart Journal, v.33, pp.817-821, 1971.
19. Bourke S, Nunes D, Stafford F, Hurley G and Graham I, "Percussion of the chest re-visited: a comparison of the diagnostic value of auscultatory and conventional chest percussion," Irish Journal of Medical Science, v.158(4), pp-82-4, 1989.
20. R. Cabot, "Physical diagnosis of diseases of the chest," New York: William Wood, pp. 66, 1900.
21. F. Dalmay, M.T Antonini, P. Marquet, and R. Menier, "Acoustic properties of the normal chest," EUR Respir J, vol. 8, pp.1761-1769, 1995.

22. V.I.Korenbaum and A. A. Tagil'tsv "Acoustic properties of a Human chest," Acoustical physics, vol.51(4), pp-410-413, 2005.
  23. S Y Tan, MD, JD and M Hu, "Josef Leopold Auenbrugger (1722-1809): father of percussion," Medicine in stamps, Singapore Med J, vol. 45(3), p103, 2004
  24. E. D. Hudson, "A manual of the physical diagnosis of thoracic disease," William Wood & Co. pp.19, 1887.
  25. Alice Jones, "A brief overview of the analysis of lung sounds," Physiotherapy, vol.81(1), pp.37-42, 1995.
  26. H.A. Mansy,T. J. Royston and R. H. Sandler, "Use of abdominal percussion for pneumoperitoneum detection," Medical and Biological Engineer comput. Vol. 40, pp. 439-446, 2002.

---

  27. Winter R, and Smethurst D, "Percussion -a new way to diagnose a pneumothorax," British Journal of Anesthesia, vol.83 (6), pp-960-1, 1999.

---

  28. H. A. Mansy,T. J. Royston, R. A. Balk and R. H. Sandler, "Pneumothorax detection using computerized analysis of breath sounds," Medical and Biological Engineering and Computing, vol. 40(5), pp-526-532, 2002.
  29. H. A. Mansy T. J. Royston, R. A. Balk and R. H. Sandler, "Pneumothorax detection using pulmonary acoustic transmission measurements," Medical and Biological Engineering and Computing, vol 40, Pp.520-525, 2002.
  30. G. P. Currie, R. Alluri, G. L. Christie, J. S. Legge, "Pneumothorax: an update," Postgrad. Med. J., vol.83 (981), pp.461-465, 2007.
  31. B. Abraham, Bohadana and S. S. Kraman, "Transmission of sound generated by sternal percussion," Journal of Applied Physiology, vol.66(1), pp. 273-277, 1989
-

32. Hussein A Mansy and Richard H. Sadler, "Methods and apparatus for detecting of air activities in the body," US patent 2003.
33. Mahagnah M, Gavriely N., "Gas density does not affect pulmonary acoustic transmission in normal men," J Appl Physiol, vol.78(3), pp.928-37, 1995
34. M. A. Pantea, E.V. Malyarenko, A. E. Baylor, and R. Gr. Maev, "A physical approach to the automated classification of clinical percussion sounds," J. Acoust. Soc. Am., Vol. 131(1), pp. 608-619, 2012.
35. I Trendafilova, "A Method for Vibration-Based Structural Interrogation and Health Monitoring Based on Signal Cross-Correlation," 9th International Conference on Damage Assessment of Structures, vol 305, 2011
- 
36. QU Guo-qin., Zang Bin, and Su Xiao-qing, " Wavelet Correlation Analysis of Geodetic Signals," Fifth International Conference on Natural Computation, vol.6 pp.585-590, 2009.
37. Laila, D.S. ; Larsson, M., Pal, B.C., Korba, P., "Nonlinear damping computation and envelope detection using Hilbert transform and its application to power systems wide area monitoring," IEEE Power & Energy Society General Meeting, pp 1-7, 2009
- 
38. Wim C. van Etten , "Introduction to Random Signals and Noise," John Wiley & Sons, Ltd  
ISBN: 0-470-02411-9, 2005. Retrived from:  
<http://doc.utwente.nl/65629/1/Etten05introduction.pdf>
39. M. Bhuiyan, E.V. Malyarenko, M. A. Pantea, F. Seviaryn, and R. Gr. Maev, "Advantages and limitations of using Matrix Pencil Method for the modal analysis of medical percussion signals," IEEE Trans Biomed Eng. Vol.60(2), pp. 417-26, 2013.
-

40. Hannu olkkonen, peitsa pesola, Juuso T. Olkkonen, Antti valjakka, Leena tuomisto, "EEG noise cancellation by a subspace method based on wavelet decomposition," *Med Sci Monit*, vol. 8(11), pp.99-204, 2002.
- 
41. Xuezhi Zhao , Bangyan Ye, "Similarity of signal processing effect between Hankel matrix-based SVD and wavelet transform and its mechanism analysis," *Mechanical Systems and Signal Processing* , ELSEVIER, vol. 23 pp.1062–1075, 2009.
42. K. Shin, J.K Hammond and P.R. white "Iterative SVD method for noise reduction of low-dimensional chaotic Time series," *mechanical systems and signal processing* , vol. 13(1), pp-115-124, 1999.
43. Lin Hu, Hong Ma ; Li Cheng, "Method of noise reduction based on SVD and its application in digital receiver front-end," *IEEE 18th Asia-Pacific conference on Communications (APCC)*, pp. 511 – 515, 2012
44. V. Stahl, A. Fischer, and R. Bippus, "Quantile based noise estimation for spectral subtraction and Wiener filtering", *Proceedings, IEEE Int. Conf. on Acoustics, Speech, and Signal Processing, ICASSP'00, Vol. 3*, pp. 1875 – 1878, 2000.
45. www.ni.com. Retrieval from  
[http://zone.ni.com/reference/en-XX/help/371988D-01/lvdfdtconcepts/dfd\\_decimation/](http://zone.ni.com/reference/en-XX/help/371988D-01/lvdfdtconcepts/dfd_decimation/)
46. K.Y Sanliurk and O,Cakar, " A new method for noise elimination from measure frequency response functions," *Istabil Tech. university, Faculty of Mechanical engineering, APCC IEEE* , 2012
47. T. K. Sarkar and O. Pereira, "Using the Matrix Pencil Method to estimate the parameters of a sum of complex exponentials," *Antennas and Propagation Magazine, IEEE*, vol.37 (1), pp.48-55, 1995.

48. J. Laroche, "The use of the Matrix Pencil Method for the spectrum analysis of musical signals," *J. Acoust. Soc. Am.*, vol.94(4), pp.1958-1965,1993.
49. A. J. Mackay and A. Mccowen, "An improved pencil-of-function method and comparisons with traditional methods of pole extraction," *IEEE trans. Antennas propagation*, vol.35(4), pp. 435-441, 1987.
50. M. L. Van blaricum and R. Mittra, "A technique for extracting the poles and residues of a system directly from its transient response," *IEEE Trans. Antennas propagat.*, vol. 23(6), pp. 777-781, 1975.
51. Raviraj S. Adve, Tapan kumar Sarkar, Odilon Maroja C. Pereira-filho, and sadsiva M. Rao, "Extrapolation of time-domain responses from three-dimensional conducting objects utilizing the matrix pencil technique," *IEEE transactions on antennas and propagation*, vol 45,(1), pp.147-156, 1997.
52. Tapan kumar sarkar, Sheeyun Park, Jinhwan Koh, and Sadasiva M. Rao, "Application of the matrix pencil method for estimating the SEM (singularity expansion method) poles of source-free transient responses from multiple look directions," *IEEE transactions on antennas and propagation*, vol. 48( 4), pp.612-618, 2000.
53. Jain, Vijay k., Sarkar Tapan k., Weiner, Donald D, "Rational modeling by pencil-of-function method," *IEEE transactions on acoustics, speech, and signal processing*, vol. 31, no. 3, pp.54-573, 1983.
54. Ramdas Kumaresan and Donald W. Tufts, "Estimating the parameters of exponentially damped sinusoids and pole-zero modeling in noise," *IEEE transactions on acoustics, speech, and signal processing*, vol. 30, no. 6, pp.833-840,1982.

55. Weidong Wang, Haizhou Li and Youan ke, "Generalized eigenvector decomposition method for pole extraction and GPOF method," TENCON, IEEE conference proceedings, Computer, Communication, Control and Power Engineering, pp.601-604, 1993
56. [http://en.wikipedia.org/wiki/Matrix\\_pencil](http://en.wikipedia.org/wiki/Matrix_pencil)
57. Fengduo Hu, Sarkar TK, Yingbo Hua, "The spectral parameter estimation by using prefiltering and matrix pencil method," IEEE Fifth ASSP Workshop on Spectrum Estimation and Modeling (Cat. No.90TH0331-9). pp.45-9. New York, NY, USA., 1990.
58. S.K. Tapan, and J. E. Fernández del Río., "Comparison between the Matrix Pencil Method and the Discrete-Fourier Transform Technique for High-Resolution Spectral Estimation," Digital Signal Processing , Science Direct, Vol. 6(2), pp.108-125, 1996.
59. M. Kitamura, J. Takada and K. ARAKI, "A Model Order Estimation in the Matrix Pencil Method for the Transient Response of a Microwave Circuit Discontinuity," IEICE Trans Electron, vol. E82-C (11), pp.2081-2086, 1999.
60. B. Kokanos and G.Karady, "Associate Hermite Expansion Small Signal Mode Estimation," IEEE Trans. Power Systems, vol. 25(2), pp.999-1006, 2010.
61. Li. Shiyong, Lv. Xin., S. Houjun, & Hu Weidong, "Scattering Centers Measurements Using a Modified Matrix Pencil Method," 8th International Conference on Signal Processing. Beijing, vol.4, 2006.
62. Yingbo Hua, Tapan K. Sharkar, "Generalized Pencil-of-Function Method for Extracting Poles of an EM System from Its Transient Response," IEEE transactions on antennas and propagation, vol. 37, no. 2, pp.229-234, 1989.
63. Y. Liu Q. H. Liu, and Z. Nie, "Reducing the Number of Elements in the Synthesis of Shaped-Beam Patterns by the Forward-Backward Matrix Pencil Method," Antennas and Propagation, IEEE Transactions, vol.58(2), pp.604-608, 2010.

64. K. Uros and B. Grega, "Matrix Pencil for Early Detection of Low Frequency Oscillations," International Review of Electrical Engineering (I.R.E.E), vol.4(4), pp.654-659,2009
65. Y. Hua and T. K. Sarkar, "Matrix Pencil Method for estimating parameters of exponentially damped/undamped sinusoids in noise", Acoustics, Speech and Signal Processing, IEEE Transactions, 38(5), pp.814 - 824 ,1990.
66. T. K. Sarkar, F. Hu, Y. Hu,a and M. Wicks, "A real-time signal processing technique for approximating a function by a sum of complex exponentials utilizing the Matrix Pencil Method," Digital Signal Processing, vol. 2(2), pp.127-140, 1994.
67. Darren M.Haddad, "the application of the matrix Pencil to speech processing," Syracuse university, 2007.
68. D. El-Hadi and T. Marc, "Statistical analysis of the Kumaresan-Tufts and Matrix Pencil Methods in estimating a damped sinusoid," In proc. European Signal Processing Conference, EUSIPCO, pp.6-10, 2004.
69. Ping Fan, Zhanrong Jing, "Scattering Center Estimation of UWB Radar Target with Improved MP Method," IEEE international Knowledge Acquisition and Modeling, pp.767-770, 2008.
70. Guohua Liu, Guangxin Zhang, Tongjun Zhang, Zekui Zhou, "The Improved Signal Processing Method Based on Matrix Pencil Algorithm," The sixth world congress on Intelligent Control and Automation, Vol. 2, pp-5981 - 5984, 2006.

71. Feng Cheng and Quanrang Yang, "On the use of the matrix-pencil technique to improve the computational efficiency of the FDTD method," *Microwave and Optical Technology Letters*, Vol.27(3),pp.213–216, 2000.
72. Licul, S. and Davis, William A., "Unified frequency and time-domain antenna modeling and characterization," *IEEE Transactions on Antennas and Propagation*, Vol. 53(9), pp.2882 – 2888, 2005
73. M. Bhuiyan, E.V. Malyarenko, M. A. Pantea, R. Gr. Maev, and Alfred E. Baylor, "Estimating the parameters of audible clinical percussion signals by fitting exponentially damped harmonics", *Journal of the Acoustical Society of America* 131: 4690-4698, 2012;
- 
74. Hua, Y. and Sarkar, T.K., "On SVD for estimating generalized eigenvalues of singular matrix pencil in noise" *IEEE Transactions on Signal Processing*, I Vol. 39(4), 1991.
75. Khaled Chahine, Vincent Baltazart, Yide Wang, "Interpolation-based matrix pencil method for parameter estimation of dispersive media in civil engineering" *Signal processing*, Elsevier, vol. 90(8), pp-2567-2580, 2010
76. Li, Y., Liu, K.J.R. ; Razavilar, J., " A parameter estimation scheme for damped sinusoidal signals based on low-rank Hankel approximation" *IEEE Transactions on Signal Processing*, Vol.45(2), 481 – 486, 1997
77. L. Zbigniew, T. Lobos and J. Rezmer; "Spectrum Estimation Methods for Signal Analysis in the Supply System of a DC Arc Furnace," *Xiii international symposium on theoretical electrical engineering ISTET*, pp. 161-164, Jul. 2005.
78. G.W.Chang, C.I.Chen, and Y.C. Chin, "Modified high-resolution Singular Value Decomposition method for power signal analysis by using down-sampling technique," *IEEE Harmonics and Quality of Power ICHQP 13th International Conference*, pp. 1 – 6, Sept. 2008.

79. L. Zhenmei, L. Shen, T.Boxue, and L.Yin, "Power System Interharmonics Monitoring Based on Wavelet Transform and AR Model," Computational Intelligence and Industrial Application, Pacific-Asia Workshop , pp.612 - 616, 2008 .
80. Li.Hong, Li. Zhong, A. wolfgang, and C. Guanrong, "Analyzing chaotic spectra of DC-DC converters using the Prony method," IEEE Trans. Circuits and Systems II: Express Briefs, vol. 54,(1), pp.61-65, Jan. 2007.
81. H.J. Kogkin, Z. Leonowicz, T. Lobos, "High-resolution spectrum-estimation methods for signal analysis in power systems," IEEE Trans. Instrumentation and Measurement, vol. 55(1), Feb. 2006.
82. Kay, and S.L. Marple, " Spectrum Analysis-A Modern Perspective," Proceedings of the IEEE, vol. 69,(11), pp.1380-1419, Nov. 1981
83. Hlawatsch F, Boudreaux-Bartels G F "Linear and quadratic time-frequency signal representations," IEEE signals processing Magazine, vol. 9(2), 1992
- 
84. Choi H , Williams W.J, "Improved time-frequency representation of multi-component signal using exponential kernels," IEEE trans. on acoust., Speech, and Signal Processing. Vol.37(8), pp. 862-871, 1989
85. Sattar F, Salomonsson G, "The use of a filter bank and the Wigner-Ville distribution for time-frequency representation," IEEE transaction on Signal Processing, vol.47(6),pp. 1776 – 178, 1999
- 
86. Zhang L, Xiong2 G, Liu H, zou H, Guo W, "Time-frequency representation based on time-varying autoregressive model with applications to non-stationary rotor vibration analysis," vol.35(2), pp. 215–232, 2010

87. Davidović, Milos D, Davidović Milena D, Vojisavljevic V, " Time-Frequency Analysis of Non-stationary Optical Signals Using Husimi Type Function," Proceedings of the international school and conference on Photonics, vol. 116(4), pp. 675, 2009.
88. Hussain Z.M , "Frequency estimation of mono and multi-component FM signals using the T – Distributions," IEEE conference on TENCON, 2005
- 
89. A. Kacha, F. Grenez , and K. Benmahammed, "Time-Frequency Analysis of Multicomponent Signals Using Two-Sided Linear Prediction, " Circuits, Systems & Signal Processing , Springer, Vol. 27(3), pp.309-330, 2008
- 
90. Fortunato E, Rix H, Suisse G, Meste O, "Combining time frequency representation and parametric analysis for the enhancement of transients in sleep EEG signal," IEEE 23rd annual EMBS international conference, vol. 2, pp.1800 – 1803, 2008.
- 
91. Leon A, Escobar-Moreira, "Ultrasonic fault machinery monitoring by using the Wigner-Ville and Choi-Williams distributions," IEEE international conference on Electrical Machines and Systems, pp.741-745, 2008.
92. Goli A, McNamara D.M, Ziarani A.K. "A novel method for decomposition of multi-component non-stationary Signals," IEEE workshop on applications of Signal Processing to Audio and Acoustics, pp. 255 – 258, 2007
93. Barkat B, Boashash B "A high-resolution quadratic time-frequency distribution for multi-component signals analysis," IEEE transactions Signal Processing, vol.49(10), pp.2232 – 2239, 2001
-

94. Boutana D, Barkat B, Marir F, "A proposed high-resolution time-frequency distribution for the analysis of multi-component and speech signals," World Academy of Science, Engg and Technology, vol.2, 2005
95. Chen D, Durand LG, Lee H.C., "Time-frequency analysis of the first heart sound. Part1: simulation and analysis," Med Biol Eng Computing, vol.35(4), pp.306-310, 1996.
- 
96. A. Kacha, F. Grenez , and K. Benmahammed, "Time-Frequency Analysis of Multicomponent Signals Using Two-Sided Linear Prediction, " Circuits, Systems & Signal Processing , Springer, Vol. 27(3), pp.309-330, 2008
- 
97. Griffin C, "A comparison study on the Wigner and Choi-Williams Distributions for detection," IEEE international conference on acoustics, Speech, and Signal Processing, Vol.2, pp. 1485-1488, 1991.
98. Dian-Fa Ping, Xian-Zhong Liu, Bing Deng, "Cross-Term Suppression in the Wigner-Ville Distribution Using beamforming," IEEE conference on industrial electronics and applications, pp.1103-1105, 2009.
99. Tang S.K, "On the time-frequency analysis of signals that decay exponentially with time," Journal of sound and vibration, vol.234(1), pp.241-258, 2000
100. Wang Yong, Jiang Yi-cheng "Generalized time-frequency distributions for multicomponent polynomial phase signals," ELSEVIER, Signal Processing vol.88, pp.984-1001, 2008
101. Zhuang Li, Crocker M J, "A study of joint time-frequency analysis-based modal analysis" IEEE transactions on instrumentation and measurement, vol. 55(6), 2006.
-

102. Noguchi Y, Watanabe K, Kashiwagi E, Hamada T, Mariko E, Matsumoto F, Sugimoto S  
“Time-frequency analysis with eight-figure kernel ,” IEEE Proceedings of the 19th Annual International Conference, Engineering in Medicine and Biology Society, vol.3,pp. 1324 – 1327, 1997
103. T. Lobos. Z. Leonowicz, J.Rezmer., H.J. Koglin, “Advanced signal processing methods of harmonics and interharmonics estimation,” IEEE seventh international conference on developments in Power System Protection, vol.50, pp-514-519, Apr.2001.
104. R.B. Pachori, P.Sircar, “Analysis of multi-component non-stationary signals using Fourier-Bessel transform and wigner Distribution,” European Signal processing conference EUSIPCO, 2006
105. Leon A, Escobar-Moreira, “Ultrasonic fault machinery monitoring by using the Wigner-Ville and Choi-Williams distributions,” IEEE international conference on Electrical Machines and Systems, pp.741-745, 2008
106. Ryusuke Imai, Yasuhiro Hashimoto, Ken Kikuchi, and Shoji Fujii, *Member, IEEE*,” High-Resolution Beamforming by the Wigner–Ville Distribution Method,” IEEE Journal of Oceanic Engineering, vol. 25, no. 1, pp. 499 – 503, 2000

# Vita Auctoris

**Doctor of Philosophy (Ph.D.)**

2007 –August, 2013

Department of Electrical and Computer Engineering

University of Windsor, ON, Canada

*Dissertation: Automated classification of medical percussion signals for the diagnosis of pulmonary injuries*

**Professional Engineer,** Province of Ontario, Canada,

2012

**Master of Applied Science (M.A.Sc.) in Electrical & Computer Engineering**

2006

Ryerson University, Toronto, ON.

*Thesis: Congestion Aware Overlay Network*

**Bachelor of Applied Science (B.A.Sc.) in Electrical & Electronic Engineering**

1994

Chittagong University of Engineering and Technology, Bangladesh.

*Thesis: Design and develop a bangla word processor*